

**Global OZone Chemistry And Related Datasets for the
Stratosphere (GOZCARDS): methodology and sample results
with a focus on HCl, H₂O, and O₃**

**L. Froidevaux¹, J. Anderson², H.-J. Wang³, R. A. Fuller¹, M. J. Schwartz¹,
M. L. Santee¹, N. J. Livesey¹, H. C. Pumphrey⁴, P. F. Bernath⁵,
J. M. Russell III², and M. P. McCormick²**

¹Jet Propulsion Laboratory, California Institute of Technology, Pasadena, CA, USA

²Hampton University, Hampton, VA, USA

³Georgia Institute of Technology, Atlanta, GA, USA

⁴The University of Edinburgh, Edinburgh, UK

⁵Old Dominion University, Norfolk, VA, USA

Correspondence to: L. Froidevaux (lucienf@jpl.nasa.gov)

Abstract

We describe the publicly available data from the Global OZone Chemistry And Related Datasets for the Stratosphere (GOZCARDS) project, and provide some results, with a focus on hydrogen chloride (HCl), water vapor (H₂O), and ozone (O₃). This dataset is a global long-term stratospheric Earth System Data Record, consisting of monthly zonal mean time series starting as early as 1979. The data records are based on high quality measurements from several NASA satellite instruments and ACE-FTS on SCISAT. We examine consistency aspects between the various datasets. To merge ozone records, the time series are debiased relative to SAGE II values by calculating average offsets versus SAGE II during measurement overlap periods, whereas for other species, the merging derives from an averaging procedure during overlap periods. The GOZCARDS files contain mixing ratios on a common pressure/latitude grid, as well as standard errors and other diagnostics; we also present estimates of systematic uncertainties in the merged products. Monthly mean temperatures for GOZCARDS were also produced, based directly on data from the Modern-Era Retrospective analysis for Research and Applications.

The GOZCARDS HCl merged product comes from HALOE, ACE-FTS and lower stratospheric Aura MLS data. After a rapid rise in upper stratospheric HCl in the early 1990s, the rate of decrease in this region for 1997-2010 was between 0.4 and 0.7%/yr. On 6-8 yr timescales, the rate of decrease peaked in 2004-2005 at about 1%/yr, and has since levelled off, at ~0.5%/yr. With a delay of 6-7 years, these changes roughly follow total surface chlorine, whose behavior versus time arises from inhomogeneous changes in the source gases. Since the late 1990s, HCl decreases in the lower stratosphere have occurred with pronounced latitudinal variability at rates sometimes exceeding 1-2%/yr. Recent short-term tendencies of lower stratospheric and column HCl vary substantially, with increases from 2005-2010 for northern mid-latitudes and deep tropics, but decreases (increases) after 2011 at northern (southern) mid-latitudes.

For H₂O, the GOZCARDS product covers both stratosphere and mesosphere, and the same instruments as for HCl are used, along with UARS MLS stratospheric H₂O data (1991-1993). We display seasonal to decadal-type variability in H₂O from 22 years of data. In the upper mesosphere, the anti-correlation between H₂O and solar flux is now clearly visible over two full solar cycles. Lower stratospheric tropical H₂O has exhibited two periods of increasing values,

followed by fairly sharp drops (the well-documented 2000-2001 decrease and a recent drop in 2011-2013). Tropical decadal variability peaks just above the tropopause. Between 1991 and 2013, both in the tropics and on a near-global basis, H₂O has decreased by ~5-10% in the lower stratosphere, but about a 10% increase is observed in the upper stratosphere and lower mesosphere. However, such tendencies may not represent longer-term trends.

For ozone, we used SAGE I, SAGE II, HALOE, UARS and Aura MLS, and ACE-FTS data to produce a merged record from late 1979 onward, using SAGE II as the primary reference. Unlike the 2 to 3% increase in near-global column ozone after the late 1990s reported by some, GOZCARDS stratospheric column O₃ values do not show a recent upturn of more than 0.5 to 1%; long-term interannual column ozone variations from GOZCARDS are generally in very good agreement with interannual changes in merged total column ozone (Version 8.6) data from SBUV instruments.

A brief mention is also made of other currently available, commonly-formatted GOZCARDS satellite data records for stratospheric composition, namely those for N₂O and HNO₃.

1 Introduction

The negative impact of anthropogenic chlorofluorocarbon emissions on the ozone layer, following the early predictions of Molina and Rowland (1974), stimulated interest in the trends and variability of stratospheric ozone, a key absorber of harmful ultraviolet radiation. The discovery of the ozone hole in ground-based data records (Farman et al., 1985) and the associated dramatic ozone changes during southern hemisphere winter and spring raised the level of research and understanding regarding the existence of new photochemical processes (see Solomon, 1999). This research was corroborated by analyses of aircraft and satellite data (e.g., Anderson et al., 1989; Waters et al., 1993), and of independent ground-based data. Global total column ozone averages in 2006-2009 were measured to be smaller than during 1964-1980 by ~3%, and larger more localized decreases over the same periods reached ~6% in the southern hemisphere midlatitudes (WMO, 2011). Halogen source gas emissions have continued to decrease as a result of the Montreal Protocol and its amendments. Surface loading of total chlorine peaked in the early 1990s and subsequent decreases in global stratospheric HCl and ClO have been measured from satellite-based sensors (Anderson et al., 2000; Froidevaux et al., 2006;

Jones et al., 2011) as well as from the ground (e.g., Solomon et al., 2006, Kohlhepp et al., 2012). A slow recovery of the ozone layer towards pre-1985 levels is expected (WMO, 2011; 2014). High quality long-term datasets for ozone and related stratospheric species are needed to document past variability and to constrain global atmospheric models. The history of global stratospheric observations includes a large suite of satellite-based instruments, generally well-suited for the elucidation of long-term global change. A review of differences between past and ongoing satellite measurements of atmospheric composition has been the focus of the Stratosphere-troposphere Processes And their Role in Climate (SPARC) Data Initiative; results for stratospheric H₂O and O₃ intercomparisons have been described by Hegglin et al. (2013) and Tegtmeier et al. (2013), respectively, to be followed by a report on many other species. Systematic biases reported in these papers mirror past validation work.

Under the Global OZone Chemistry And Related Datasets for the Stratosphere (GOZCARDS) project, we have created monthly zonally averaged datasets of stratospheric composition on a common latitude/pressure grid, using high quality data from the following satellite instruments: the Stratospheric Aerosol and Gas Experiments (SAGE I and SAGE II), the Halogen Occultation Experiment (HALOE) which flew aboard the Upper Atmosphere Research Satellite (UARS), the UARS Microwave Limb Sounder (MLS), the Atmospheric Chemistry Experiment Fourier Transform Spectrometer (ACE-FTS) on SCISAT, and Aura MLS. Table 1 provides characteristics of the original datasets; validation papers from the instrument teams and other related studies give a certain degree of confidence in these data. However, the existence of validation references does not imply that there are no caveats or issues with a particular measurement suite. In this project, we have strived to optimize data screening and mitigate some undesirable features, such as the impact of outlier values or the effects of clouds or aerosols. All source data sets still have imperfections, but in creating the GOZCARDS Earth System Data Record (ESDR) we maintain the integrity of the original data and do not arbitrarily disregard data, nor do we typically attempt to fill in spatial or temporal gaps in the record.

Based on original profiles from the various instruments, GOZCARDS “source” monthly zonal mean values were derived. After data screening, monthly average profiles were created by vertical interpolation onto the GOZCARDS pressure levels, followed by binning and averaging

into monthly sets. In order to accomodate the lower vertical resolution of some limb viewers, such as UARS MLS, the GOZCARDS pressure grid was chosen as

$$p(i) = 1000 \times 10^{-\frac{i}{6}} (\text{hPa}) \quad (1)$$

with i varying from 0 to a product-dependent top; this grid width corresponds to ~ 2.7 km. The high resolution SAGE O₃ profiles were converted to mixing ratio versus pressure using their associated NCEP temperature profiles, and smoothed vertically onto this grid. Given the sampling of solar occultation instruments, which usually provide 15 sunrise and 15 sunset profiles in two narrow latitude bands every day (versus the denser sampling from MLS, with almost 3500 profiles/day), we used 10°-wide latitude bins (18 bins from 80°S-90°S to 80°N-90°N) to construct monthly zonal means. Next, we merged the GOZCARDS source data by computing average relative biases between source datasets during periods of overlap, and then adjusting each source dataset to a common reference to remove relative biases. Non-zero biases always exist between data from different instruments for various reasons, such as systematic errors arising from the signals or the retrieved values, different vertical resolutions, or sampling effects. Toohey et al. (2013) studied sampling biases from a large suite of satellite-based stratospheric profiling instruments, based on simulations using fully-sampled model abundance averages versus averages of output sampled at sub-orbital locations. Larger sampling errors arise from occultation than from emission measurements, which often sample thousands of profiles per day. Toohey et al. (2013) found that sampling biases reach 10-15%, notably at high latitudes with larger atmospheric variability. Sofieva et al. (2014) have also discussed sampling uncertainty issues for satellite ozone datasets.

We have observed very good correlations between GOZCARDS and other long-term ozone data, such as the Stratospheric Water vapor and OzOne Satellite Homogenized (SWOOSH) data (S. Davis, personal communication, 2012) and homogenized Solar Backscatter Ultraviolet (SBUV) data. Dissemination of trend results arising from analyses of GOZCARDS and other merged ozone datasets was planned as part of WMO (2014) and the SI²N (Stratospheric Processes And their Role in Climate (SPARC), International Ozone Commission (IOC), Integrated Global Atmospheric Chemistry Observations (IGACO-O₃), and the Network for the Detection of Atmospheric Composition Change (NDACC)) initiative. Profile trend results have been provided by Tummon et al. (2015), Harris et al. (2015), as well as Nair et al. (2013, 2015).

This paper starts with a discussion of data screening issues (Sect. 2 and Appendix A), and then describes the GOZCARDS data production methodology, followed by some atmospheric results for HCl (Sect. 3), H₂O (Sect. 4), and O₃ (Sect. 5). We provide specific diagnostics that indicate generally good correlations and small relative drifts between the source datasets used to create the longer-term GOZCARDS merged time series. Section 6 briefly mentions GOZCARDS N₂O and HNO₃, as well as temperatures derived from Modern-Era Retrospective analysis for Research and Applications (MERRA) fields. The version of GOZCARDS described here is referred to as ESDR version 1.01 or ev1.01.

2 GOZCARDS source data and data screening

Data provenance information regarding the various measurements used as inputs for GOZCARDS is provided in Appendix A (Sect. A.1).

2.1 GOZCARDS data screening and binning

The screening of profiles for GOZCARDS has largely followed guidelines recommended by the various instrument teams and/or relevant publications, and we have documented these issues and procedures in Appendix A (Table A1). Unless otherwise noted, we only provide monthly means constructed from 15 or more (good) values in a given latitude/pressure bin. For ACE-FTS data, we also found it necessary to remove occasional large outlier values that could significantly impact the monthly zonal means. Our outlier screening removed values outside 2.5 times the standard deviation, as measured from the medians in each latitude/pressure bin, for each year of data. This was deemed close to optimum by comparing results to Aura MLS time series, which typically are not impacted by large outliers, and to ACE-FTS zonal means screened (in a slightly different way) by the ACE-FTS instrument team. Up to 5% of the profile values in each bin in any given month were typically discarded as a result, but the maximum percentage of discarded values can be close to 10% for a few months of ACE-FTS data, depending on year and species. Moreover, because of poor ACE-FTS sampling, the threshold for minimum number of good ACE-FTS values determining a monthly zonal mean was allowed to be as low as 10 for mid- to high latitudes, and as low as 6 for low latitudes (bins centered from 25°S to 25°N). Zonal mean data from ACE-FTS become too sparse in some years if such lower threshold values are not

used. Finally, no v2.2 ACE-FTS data are used after September 2010 (or after December 2009 for ozone) because of a data processing problem that affected this data version; a newly reprocessed ACE-FTS dataset was not available before we made the GOZCARDS data public.

Placing profiles on a common pressure grid is straightforward when pressures are present in the original files, as is the case for most data used here. Also, the vertical resolutions are similar for most of the instruments used for GOZCARDS. The UARS MLS, HALOE, and Aura MLS native pressure grids are either the same as or a superset of the GOZCARDS pressure grid, so these datasets were readily sampled for the construction of monthly means. For ACE-FTS, pressures are provided along with the fixed altitude grid, and we used linear interpolation versus $\log(\text{pressure})$ to convert profiles to the GOZCARDS grid. More details are provided later for SAGE I and SAGE II O_3 , for which density versus altitude is the native representation.

The binning of profiles occurs after the screened values are averaged (in each latitude/pressure bin). Note that for the species discussed here, sunset and sunrise occultation values in the same latitude bin during a given month are averaged together. Negative monthly means are set to -999.0 in the GOZCARDS files; while negative mixing ratios smaller (in absolute value) than the associated standard errors can in theory be meaningful, negative monthly means are unlikely to be very useful scientifically. Quantities other than mixing ratios are provided in the netCDF GOZCARDS files, which are composed of one set of individual yearly files for all source datasets, and one set of yearly files for the merged products. The main quantities are monthly averages, plus standard deviations and standard errors. The GOZCARDS source files also provide the number of days sampled each month as well as minimum and maximum values for the source datasets. Other information includes average solar zenith angles and local solar times for individual sources. Finally, formulae for monthly standard deviations of the merged data are given in Appendix A, where sample time series of the standard deviations and standard errors (not systematic errors) for both source and merged data are also shown.

3 GOZCARDS HCl

3.1 GOZCARDS HCl source data records

We used HCl datasets from HALOE, ACE-FTS and Aura MLS to generate the monthly zonal mean source products for GOZCARDS HCl. In addition to the procedures mentioned before, a first-order aerosol screening was applied to the HALOE HCl profiles: all HCl values at and below a level where the 5.26 μm aerosol extinction exceeds 10^{-3} km^{-1} were excluded. Regarding Aura MLS HCl, Froidevaux et al. (2008a) found anomalously high values versus aircraft data at 147 hPa at low latitudes; these values are not used in the production of the merged HCl product. Also, the ongoing standard MLS HCl product is retrieved using band 14 rather than band 13, which targeted HCl for the first 1.5 years after launch, but started deteriorating rapidly after Feb. 2006. As the remaining lifetime for band 13 is expected to be short, this band has been turned on only for a few days since Feb. 2006. MLS HCl data are not recommended for trend analyses at pressures < 10 hPa. However, for pressures ≥ 10 hPa, band 14 HCl is deemed robust, because of the broader emission line in this region, in comparison to the measurement bandwidth.

Past validation studies have compared MLS HCl (v2.2), ACE-FTS (v2.2) and HALOE (v19) datasets using coincident pairs of profiles; such work was described by Froidevaux et al. (2008a) for MLS HCl validation and by Mahieu et al. (2008) for ACE-FTS HCl validation. The MLS version 3.3/3.4 HCl data used here (see Livesey et al., 2013) compare quite well with v2.2 HCl (average relative biases are within 5%). HALOE HCl values were found to be biased low by $\sim 10\text{-}15\%$ relative to both MLS and ACE-FTS, especially in the upper stratosphere; this low bias versus other (balloon- and space-based) measurements had been noted in past HALOE validation studies (Russell et al., 1996). Also, HALOE (v19) and ACE-FTS (v2.2) HCl data tend to lose sensitivity and reliability for pressures less than ~ 0.4 hPa.

3.2 GOZCARDS HCl merged data records

Although Aura MLS HCl data for pressures less than 10 hPa do not contribute to the time dependence of the merged HCl product, the 2004-2005 absolute Aura HCl measurements in this region are used to compute the offsets for the ACE-FTS and HALOE zonal mean source data in a consistent manner versus pressure. Figure 1 illustrates the merging process for HCl at 32 hPa

for the 45°S latitude bin (covering 40°S-50°S). Given that there exists very little overlap between the three sets of measurements in the same months in 2004 and 2005, especially in the tropics, a simple 3-way averaging of the datasets would lead to significant data gaps. Our methodology is basically equivalent to averaging all three datasets during this period, and we use Aura MLS as a transfer dataset. This was done by first averaging ACE-FTS and Aura MLS data, where the datasets overlap, and then including the third dataset (HALOE) into the merging process with the temporary merged data. As the HALOE HCl values are generally lower than both the MLS and ACE-FTS values, the merged HCl dataset is generally further away from HALOE than it is from either ACE-FTS or Aura MLS. The top left panel in Fig. 1 shows GOZCARDS source data for HALOE, ACE-FTS, and Aura MLS during the overlap period, from August 2004 (MLS data start) through November 2005 (HALOE data end). The top right panel illustrates the result of step 1 in the merging procedure, with the temporary merged data values (orange) resulting from the adjustment of ACE-FTS and Aura MLS values to the mean reference (black dashed line); this reference is simply the average of the two series for all months when both values exist. The middle left panel shows step 2, namely the values (brown) obtained from merging HALOE values with the temporary merged values from step 1; the temporary merged values are weighted by 2/3 and HALOE values by 1/3 (giving the black dashed line as mean reference), so this is equivalent to averaging the three datasets with a weight of 1/3 each. A simple mathematical description of the above procedure is provided in Appendix A. The middle right panel shows the source data along with the final merged values during the overlap period, whereas the bottom panel shows the full time period, after the additive offsets are applied to the whole source series, thus removing relative biases; the three adjusted series are then averaged together wherever overlap exists, to obtain the final merged dataset. We tested this procedure by using one or the other of the two occultation data as the initial one (for step 1) and the results were not found to differ appreciably. We also found that the use of multiplicative adjustments generally produces very similar results as additive offsets. Some issues were found on occasion with multiplicative offsets, when combining very low mixing ratios, but additive offsets can also have drawbacks if the merged values end up being slightly negative, notably as a result of changes that modify the already low HCl values during Antarctic polar winter. This occurs on occasion as additive offsets tend to be weighted more heavily by larger mixing ratios found during non-winter seasons; as a

result, we decided not to offset lower stratospheric HCl source datasets in the polar winter at high latitudes for any of the years. Further specifics and procedural details regarding the merging of HCl data are summarized in Appendix A.

In Fig. 2, we display the offsets that were applied to the three HCl source datasets as a result of the merging process in each latitude/pressure bin; a positive value means that a dataset is biased low relative to the reference mean and needs to be increased by the offset value. These offsets show that in general, ACE-FTS and Aura MLS HCl values were adjusted down by 0.1-0.2 ppbv (a decrease of about 2-10%), while HALOE HCl was adjusted upward by 0.2-0.4 ppbv. Offset values tend to be fairly constant with latitude and the sum of the offsets equals zero. The generally homogeneous behaviour versus latitude is a good sign, as large discontinuities would signal potential issues in the merging (e.g., arising from large variability or lack of sufficient statistics). Figure S1 provides more detailed examples of upper and lower stratospheric offsets versus latitude, including standard errors based on the variability in the offsets during the overlap period (error bars provide an indication of robustness). Another indication of compatibility between datasets is provided by a comparison of annual cycles. Figure S2 provides average annual cycle amplitudes obtained from simple regression model fits to HALOE, ACE-FTS, and Aura MLS series over their respective periods. While there are a few regions where noise or spikes exist (mainly for ACE-FTS), large annual amplitudes in the polar regions occur in all time series; this arises from HCl decreases in polar winter, followed by springtime increases.

A more detailed analysis of interannual variability and trend consistency is provided from results in Fig. 3, which shows an example of ACE-FTS and Aura MLS time series. We have used coincident points from these time series to compare the deseasonalized anomalies (middle panel in Fig. 3) from both instrument series; correlation coefficient values (R values) are also computed. Very good correlations are obtained and no significant trend difference between the anomalies (bottom panel in Fig. 3) exists for ACE-FTS versus Aura MLS HCl. A view of these correlations and drifts at all latitudes/pressures is provided in Fig. 4, where the top panel gives R values for deseasonalized anomalies, and the bottom panel gives the ratio of the difference trends over the error in these trends. The results in Fig. 4 confirm that there are significant trend differences between the upper stratospheric HCl time series from ACE-FTS and Aura MLS (as a reminder, we did not use Aura MLS HCl for pressures less than 10 hPa). Fig. 4 also shows very

low correlation coefficients from the deseasonalized HCl series in the uppermost stratosphere, because Aura MLS HCl exhibits unrealistically flat temporal behavior, whereas ACE-FTS HCl varies more. In the lower stratosphere, there is generally good agreement between the ACE-FTS and Aura MLS HCl time series, with R values typically larger than 0.7 and difference trend to error ratios smaller than 1.5. The few low R values for 100 hPa at low latitudes likely reflect more infrequent ACE-FTS sampling and some (possibly related) outlier data screening issues.

Figure S3 illustrates GOZCARDS merged 46 hPa HCl variations versus time; there is clearly a much more complete global view (with no monthly gaps) after the launch of Aura MLS. Gaps at low latitudes in 1991 and 1992 are caused by post-Pinatubo aerosol-related issues in the HALOE record, and gaps in later years arise from the decrease in coverage from UARS. In the upper stratosphere, there are more gaps compared to 10 hPa and below, as a result of the much poorer tropical coverage from ACE-FTS and the elimination of MLS data in this region.

An indication of systematic errors in the merged values is given by the range of available monthly mean source data. For each bin, we compute the ranges of monthly means above and below the merged values that include 95% of the available source data monthly means. These error bars are not usually symmetric about the merged values, especially if one dataset is biased significantly more than others, in a relative sense. We did not have enough datasets here to consider a more statistical approach (such as the standard deviations among source datasets). Figure 5 shows the result of such a systematic error calculation at 46 hPa for the 35°S latitude bin. The lower shaded region range gives the lower bound, determined by HALOE data, and the upper limit of the grey shading originates from ACE-FTS data. Figure 6 shows contour plots of these estimated systematic errors in HCl. These are fairly conservative error bars; however, even the source data averages at the 95% boundaries have their own systematic errors (rarely smaller than 5%), so our estimates do not really encompass all error sources. Error bars representing a range within which 95% of the source data values reside (see Figs. 5 and 6) can be a useful guide for data users or model comparisons; although this is not an official product, users can readily calculate such ranges (or we can provide these values).

3.3 GOZCARDS HCl sample results and discussion

Stratospheric HCl is important because it is the main reservoir of gaseous chlorine and it can be used to follow the chlorine budget evolution over the past decades. This includes a significant increase before the mid-1990s as a result of anthropogenic chlorofluorocarbon (CFC) production, followed by a slower decrease as a result of the Montreal Protocol and subsequent international agreements to limit surface emissions that were correctly predicted to be harmful to the ozone layer (Molina and Rowland, 1974; Farman et al., 1985).

In Fig. 7, we provide an overview of the HCl evolution since 1991, based on GOZCARDS average merged HCl for 3 different latitude regions at 4 pressure levels, from the upper stratosphere to the lower stratosphere. In the upper stratosphere (at 0.7 hPa shown here), the rapid early rise in HCl was followed by a period of stabilization (1997-2000) and subsequent decreases. Rates of decrease for stratospheric HCl and total chlorine have been documented using satellite-based upper stratospheric abundances, which tend to follow tropospheric source gas trends with a time delay of order 6 years, with some uncertainties in the modeling of this time delay and related age of air issues (Waugh et al., 2001; Engel et al., 2002; Froidevaux et al., 2006). As summarized in WMO (2011), the average rate of decrease in stratospheric HCl has typically been measured at -0.6 %/yr to -0.9 %/yr, in reasonable agreement with estimated rates of change in surface total chlorine; see also the HCl upper stratospheric results provided by Anderson et al. (2000) for HALOE, Froidevaux et al. (2006) for the one and a half year band 13 Aura MLS data record, and Jones et al. (2011) and Brown et al. (2011) for a combination of HALOE and ACE-FTS datasets. The WMO (2011) summary of trends also includes results from column HCl data at various NDACC Fourier transform infrared (FTIR) measurement sites; see Kohlhepp et al. (2012) for a comprehensive discussion of ground-based results, showing some scatter as a function of latitude. Figure 7 demonstrates that a global-scale decline in mid- to lower stratospheric HCl is visible since about 1997. We also notice that at 68 hPa in the tropics, the long-term rate of change appears to be near-zero or slightly positive. In addition, there are shorter-term periods in recent years when an average increasing “trend” would be inferred rather than a decrease; in particular, see the northern hemisphere from 2005 through 2012 at 32 hPa.

We created deseasonalized GOZCARDS merged monthly zonal mean HCl data at different latitudes and we show in Fig. 8 the linear rate of change that results from simple fits through

such series. The long-term trends (1997 - 2013 for lower and 1997 - 2010 for upper stratosphere) are generally negative and between about -0.5%/yr (upper stratosphere) and -1%/yr (lower stratosphere). Some separation between northern and southern hemisphere results is observed in the lower stratosphere, with less negative trends in the northern hemisphere. Also, the scatter increases from 68 hPa to 100 hPa, where some positive trends occur at low latitudes; however, we have less confidence in the 100 hPa results, given the larger scatter and errors (and smaller abundances) in that region. Without trying to assign exact linear trends from these simple analyses, we observe considerable latitudinal variability in lower stratospheric HCl short-term behavior, especially after 2005. Such lower stratospheric changes in HCl have been captured in column HCl FTIR data (Mahieu et al., 2013, 2014). The latter reference shows that total column (FTIR) results and GOZCARDS lower stratospheric HCl trends agree quite well, and the authors imply that a relative slowdown in the northern hemispheric circulation is responsible for observed recent changes in the lower stratosphere. However, we note (Fig. 7) that changes in lower stratospheric HCl appear to be fairly short-term in nature, with an apparent reversal in behavior occurring at both northern and southern midlatitudes since 2011 (e.g., at 32 hPa). Lower stratospheric changes are distinct from the upper stratospheric long-term decrease, which we expect to continue, as long as the Montreal Protocol and its amendments are followed and total surface chlorine keeps decreasing.

In Figure 9, we provide simple rates of upper and lower stratospheric change in HCl for 6-yr sliding time periods (e.g., a 2004 value means a 2001-2006 average) for various latitudes. These results indicate that there has been an acceleration in the rate of decrease of upper stratospheric HCl between 2000 and 2004, followed by a period with somewhat smaller rates of change. This is roughly in agreement with curves showing the rates of change for surface total chlorine based on National Oceanic and Atmospheric Administration (NOAA) surface data (Montzka et al., 1999), as shown in Fig. 9 (top panel) with the Earth System Research Laboratory Global Monitoring Division data, time shifted by 6 or 7 years to account for transport delays into the upper stratosphere. Chlorine source gases have indeed shown a reduction in their rate of decrease during the second half of the past decade, as discussed by Montzka et al. (1999) and summarized in WMO (2011, 2014). Reasons include the initial rapid decrease in methyl chloroform, slower rates of decrease from the sum of CFCs in recent years, and increases in

hydrochlorofluorocarbons (HCFCs). The lower stratospheric HCl behavior in Fig. 9 (bottom panel) shows rates of change in partial column density between 68 hPa and 10 hPa. These changes show more variability with latitude than in the upper stratosphere for short (6-yr) time periods, and a hemispheric asymmetry exists, peaking in 2009, when positive tendencies are seen in the northern hemisphere, as opposed to decreases in the south (Mahieu et al., 2014). These results do not depend much on whether 6-yr or 8-yr periods (not shown) are used, but longer periods smooth out the rates of change; interannual variations, such as those arising from the quasi-biennial oscillation (QBO), will affect short-term results. Temporal patterns in the upper and lower stratosphere are qualitatively similar, and rates of change in surface emissions will impact both regions, but carefully disentangling this from changes in dynamics or in other species (e.g., CH₄) that can affect chlorine partitioning will require more analyses and modeling.

4 GOZCARDS H₂O

4.1 GOZCARDS H₂O source data records

We used water vapor datasets from HALOE, UARS MLS, ACE-FTS, and Aura MLS to generate the monthly zonal mean source products for GOZCARDS H₂O. In addition to the data screening procedures mentioned in Appendix A, we screened HALOE H₂O data for high aerosol extinction values, closely following the screening used for merged H₂O in the Stratospheric Water vapor and OzOne Satellite Homogenized (SWOOSH) dataset (S. Davis, personal communication, 2012). This method (see Fig. S4) screens out anomalous HALOE H₂O values that occurred mainly in 1991-1992, when the aerosol extinction near 22 hPa exceeded $5 \times 10^{-4} \text{ km}^{-1}$; for pressure levels at and below 22 hPa, we have excluded the corresponding H₂O values. While this method may exclude some good data points, the lowest values (< 3 ppmv) do get screened out; such outliers are not corroborated by 22 hPa UARS MLS data (with most values > 3 ppmv). Also, for upper mesospheric HALOE data, care should be taken during high latitude summer months, as no screening was applied for the effect of polar mesospheric clouds (PMCs). High biases (by tens of percent) in H₂O above ~70 km have been shown to occur as a result of PMCs in the HALOE field of view (McHugh et al., 2003). Indeed, monthly means larger than 8-10 ppmv are observed in GOZCARDS H₂O merged data and in HALOE source data for pressures less than ~0.03 hPa. A more recent HALOE data version (V20 or VPMC) could be used to

largely correct such PMC-related effects, although this was not implemented for GOZCARDS H₂O. Aura MLS and ACE-FTS measurements, obtained at longer wavelengths than those from HALOE, do not yield such large H₂O values; a rough threshold of 8.5 ppmv could also be used (by GOZCARDS data users) to flag the pre-2005 merged dataset.

UARS MLS stratospheric H₂O for GOZCARDS was obtained from V6 (or V600) H₂O data. This data version is identical to the original prototype (named V0104) from Pumphrey (1999), who noted that UARS MLS H₂O often exhibits drier values (by 5-10%) than HALOE H₂O (see also Pumphrey et al., 2000). The resulting UARS MLS H₂O source data span the period from Sep. 1991 through April, 1993; a significant fraction of this dataset in the tropics at 100 hPa is flagged bad, as a result of diminishing sensitivity.

Summarizing past validation results, SPARC WAVAS (2000) analyses pointed out the existence of a small low bias in HALOE stratospheric H₂O versus most other measurements, except for UARS MLS. Lambert et al. (2007) showed agreement within 5-10% between Aura MLS version 2.2 H₂O and other data, including ACE-FTS H₂O. From the mid-stratosphere to the upper mesosphere, excellent agreement between ground-based data from the Water Vapor Millimeter-wave Spectrometer and H₂O profiles from Aura MLS and ACE-FTS has been demonstrated by Nedoluha et al. (2007, 2009, 2011). Changes from MLS v2.2 to v3.3 led to an increase of 0.2-0.3 ppmv in stratospheric H₂O (Livesey et al., 2013). Recent comparisons by Hurst et al. (2014) of MLS v3.3 H₂O data versus Cryogenic Frost point Hygrometer time series above Boulder show excellent overall agreement, indicating that systematic uncertainties for lower stratospheric MLS data may be as low as ~5%; this reinforces MLS H₂O validation work by Read et al. (2007) and Voemel et al. (2007). Aura MLS stratospheric H₂O v3.3 values are slightly larger (by up to ~5%) than the multi-instrument average from a number of satellite datasets, as discussed in satellite intercomparisons by Hegglin et al. (2013), who observed only small disagreements in interannual variations from various series for pressures less than 150 hPa.

4.2 GOZCARDS H₂O merged data records

The merging process for H₂O is nearly identical to the method used for HCl. The main difference is an additional step that merges UARS MLS data with the already combined datasets from HALOE, ACE-FTS, and Aura MLS, by simply adjusting UARS MLS values to the average of

the previously merged series during the early (1991-1993) overlap period; see Fig. S5 for an illustration. Typically, this requires an upward adjustment of UARS MLS H₂O data, as these values are biased low versus most other datasets; nevertheless, the short but global record from UARS MLS helps to fill the time series. After considering the channel drift issues for SAGE II H₂O (and following past advice from the SAGE II team itself), we decided to use caution and did not include that dataset for GOZCARDS, as trend results could be affected. Other minor procedural merging details or issues for H₂O are included in the Supplement. Also, data users should be aware of anomalous effects arising in merged average series from non-uniform latitudinal sampling when no MLS data exist, in regions with large latitudinal gradients, as for H₂O at 147 hPa, the largest pressure for merged GOZCARDS H₂O. Latitudinal averages can be biased in certain months and month-to-month variability is increased because of relatively poor global sampling (in this region) prior to Aug. 2004, after which Aura MLS data are used.

In Fig. 10, we display the average offsets that were applied to the four H₂O source datasets; these offsets follow previously known relative data biases. For example, low biases in UARS MLS H₂O, especially in the mesosphere, were discussed by Pumphrey (1999) and the UARS MLS offsets (see Fig. 10) correct that dataset upward. The application of offsets derived for HALOE and UARS MLS raises the H₂O time series from these instruments, whereas negative offsets lower the H₂O source data from ACE-FTS and Aura MLS. As we found for HCl, the offset values generally display small variations versus latitude and are therefore fairly stable systematic adjustments to the time series. Figure S6 displays the amplitudes of the fitted annual cycles for HALOE, ACE-FTS, and Aura MLS. As for HCl, similar patterns emerge for these datasets. Wintertime descent into the polar vortex regions is responsible for large annual cycles at high latitudes, especially in the mesosphere; also, the seasonal impact of dehydration in the lower stratospheric Antarctic region causes a large annual cycle in Aura MLS high southern latitude data. Figure 11 provides some statistical information, as done for HCl in Sect. 3.2, regarding the correlations and trend differences between ACE-FTS and Aura MLS. There are a few regions with noisier relationships. While slow increases in H₂O are generally observed by both instruments in the stratosphere and mesosphere, the tropical region near 0.1 hPa shows a slight decreasing trend for the ACE-FTS points, thus leading to larger discrepancies; it is not clear what the source of these discrepancies is. While the tropical ACE-FTS data are generally

sampled with a significantly lower temporal frequency, the same applies for all pressure levels; however, a few outlier points can have a much larger impact when sampling is poorer. There are also a few other spots, such as near 65°S and 65°N and near 5 hPa, with a large drift in the difference time series; this may be caused by a combination of poorer sampling by ACE-FTS and higher atmospheric variability, which can lead to more scatter. At the highest latitudes in the lower stratosphere, the observed slope differences are more within error bars, but the larger variability means that a longer record is needed to determine if the time series trend differently. The merged dataset tends to be much closer to Aura MLS in terms of trends because there are many more months of Aura MLS than ACE-FTS data; the overall impact of ACE-FTS data on the merged H₂O series is fairly small.

Figure S7 provides a visual representation of the merged GOZCARDS H₂O fields at 3 hPa and 68 hPa, respectively. Well-known features are displayed in these plots, given the good global coverage in the post-2004 period in particular. In the upper stratosphere, descent at high latitudes during the winter months leads to larger H₂O values, and low latitude QBO features are also observed. In the lower stratosphere, one observes dehydration evidence at high southern latitudes in the winter months, as well as a low latitude seasonal “tape recorder” signal; this phenomenon is driven by tropopause temperatures and has been measured in satellite data since the early 1990s (Mote et al., 1996; Pumphrey, 1999). A vertical cross-section of this lower stratospheric tropical (20°S to 20°N) tape recorder in GOZCARDS merged H₂O for 1991-2013 is shown in Fig. 12; periods of positive anomalies alternate with negative anomalies, including the post-2000 lows, as well as the most recent decreases in 2012-2013 (see also next section).

As we discussed for HCl, we have estimated systematic errors for the merged H₂O product. This is illustrated by the contour plots in Fig. 13; these ranges encompass at least 95% of the monthly mean source data values from HALOE, UARS MLS, ACE-FTS, and Aura MLS above or below the merged series. These errors typically span 5 to 15% of the mean between 100 and 0.1 hPa; errors larger than 30% exist in the tropical upper troposphere (147 hPa), and large values in the upper mesosphere arise from the low bias in UARS MLS H₂O.

4.3 GOZCARDS H₂O sample results and discussion

Stratospheric H₂O variations have garnered attention because of the radiative impacts of water vapor in the UTLS and the connection to climate change (Solomon et al., 2010), as well as the stratospheric chemical significance of H₂O oxidation products. Individual water vapor datasets have been used here to produce a merged stratospheric H₂O record spanning more than two decades. We do not attempt here to characterize trends or to imply that recent tendencies will carry into the next decade or two. Rather, as variability is also of interest to climate modelers, we focus here on observed decadal-type (longer-term) variability in stratospheric water vapor.

Figure 14 illustrates monthly, annual, and longer-term changes in stratospheric water vapor, based on GOZCARDS merged H₂O; this shows the well-known H₂O minimum in the lower tropical stratosphere as well as an increase in the upper stratosphere (as a result of methane oxidation). As we know from past studies (e.g., Randel et al., 2004), medium- to long-term changes in H₂O are large-scale in nature. However, lower stratospheric H₂O variations are more accentuated at low latitudes, in comparison to near-global (60°S-60°N) results. It has long been known (e.g., from the *in situ* balloon-borne measurements of Kley et al., 1979) that the hygropause is typically located a few km higher than the thermal tropopause. We observe that the tropical stratosphere is drier at 68 hPa than at 100 hPa (near the tropopause). According to the 22-year GOZCARDS data record, annually-averaged H₂O values in the tropics (20°S-20°N) have varied between about 3.2 and 4.2 ppmv at 68 hPa. The rapid drop between 2000 and 2001 is observed at 100 and 68 hPa, with some dilution of this effect at higher altitudes. There is a clear difference in long-term behavior between the upper stratosphere, where changes in methane should have the clearest influence, and the lower stratosphere, where cold point temperatures and dynamical changes have a significant impact. To first-order, the last few years show ~10% larger values in the upper stratosphere than in the early 1990s, while the opposite holds in the lowest stratospheric region, where a decrease of order 10% is observed over the same period. Figure 14 also shows that month-to-month and seasonal variations are usually somewhat larger than the long-term changes in the lower stratosphere, most notably at 100 hPa.

In order to provide longer-term variability diagnostics for water vapor, we show in Fig. 15 the minimum to maximum spread in annual averages (tropics and mid-latitudes) from Fig. 14 for the 22-yr period. We observe that the tropical variability is largest just above the tropopause (here

this means at the 68 hPa GOZCARDS level), where it reaches ~27% (1 ppmv). Such diagnostics of variability should be useful for comparisons to various chemistry climate models.

The longer-term variability in water vapor increases above the stratopause and reaches close to 30% in the uppermost mesosphere, as seen in Fig. 16(a); this plot shows the monthly and annual near-global (60°S-60°N) H₂O variations at 0.01 hPa. Large seasonal changes in this region are driven by vertical advection associated with the mesospheric circulation, with each hemisphere's summertime peaks contributing to the maxima (two per year) in these near-global averages; such seasonal variations were compared to model results by Chandra et al. (1997), based on the first few years of HALOE H₂O data. The strong upper mesospheric variability in annual-mean H₂O is known from previous studies of ground-based and satellite H₂O data (Chandra et al., 1997; Nedoluha et al., 2009; Remsberg, 2010), and this region is where the solar (Lyman α) influence on H₂O is strongest. Figure 16(b) displays the near-global variations in annual upper mesospheric H₂O from 0.1 to 0.01 hPa. We clearly see increased variability in the uppermost mesosphere, and decreases in the mixing ratios as a result of H₂O photodissociation.

5 GOZCARDS ozone

A number of discussions relating to signs of ozone recovery have been presented before (Newchurch et al., 2003; Wohltmann et al., 2007; Yang et al., 2008; Jones et al., 2009; Hassler et al., 2011; Salby et al., 2011, 2012; Ziemke and Chandra, 2012; Gebhardt et al., 2014; Kuttipurath et al., 2013; Kirgis et al., 2013; Nair et al., 2013, 2015; Shepherd et al., 2014, Frith et al., 2014). While there are some indications of small increases in O₃ in the past 10-15 years, further confirmation of an increase in global O₃ and its correlation with column increases is needed in order to more clearly distinguish between long-term forcings, notably from the 11-yr solar cycle, slow changes in halogen source gases, temperature changes, and shorter-term variability. Continuing, good long-term ozone datasets are clearly needed for such studies.

5.1 GOZCARDS ozone source data records

We used ozone datasets from SAGE I, SAGE II, HALOE, UARS MLS, ACE-FTS, and Aura MLS to generate the monthly zonal mean source products for GOZCARDS. Due to time constraints, we did not use the newer SAGE II version 7 ozone (see Damadeo et al., 2013) as part of the GOZCARDS merged dataset. Our studies indicate that there are systematic

differences of only a few percent between SAGE II V6.2 and V7 O₃ on their native coordinates (number density versus altitude). However, these 2 versions exhibit some differences if the data are converted to mixing ratios on pressure surfaces. These differences result mainly from different temperatures (and their trends) between MERRA and analyses from the National Centers for Environmental Prediction (NCEP), used by SAGE II V7 and V6.2 retrievals, respectively. The main differences between MERRA and NCEP temperatures occur in the upper stratosphere for time periods before 1989 and after mid-2000 (see further details in Sect. 5.2).

5.1.1 Treatment of SAGE ozone profiles

Both SAGE I and SAGE II used solar occultations during satellite sunrise and sunset to measure vertical profiles of ozone, along with other composition data and aerosol extinction (McCormick et al., 1989; Cunnold et al., 1989). It takes about 1 month for SAGE I and II to provide near global coverage (about 80°N to 80°S), with some dependence on season. The SAGE I measurements started in February 1979 and stopped in November 1981, while SAGE II provided data between October 1984 and August 2005. In the middle of July 2000, SAGE II had a problem in its azimuth gimbal system. Although this was corrected by November 2000, the instrument operation was switched to a 50% duty cycle, with either sunrise or sunset occultations occurring in monthly alternating periods, until the end of the mission.

It is known that there were altitude registration errors in SAGE I (V5.9) data (Veiga et al., 1995; Wang et al., 1996). To correct this problem, an empirical altitude correction method based on Wang et al. (1996) had been applied to SAGE I (V5.9) data; these corrected SAGE I V5.9 profiles, which had been evaluated in previous trend studies (e.g. SPARC, 1998; WMO, 2003), were used to create the GOZCARDS SAGE I product (denoted as version V5.9_rev). We did not use reprocessed version 6.1 SAGE I data (L. W. Thomason, personal communication, 2012) because the altitude registration problems had not been completely fixed and new altitude correction criteria should be derived and validated.

Ozone data screening details for the original SAGE I and SAGE II datasets are provided in Appendix A. The number density profiles were converted to mixing ratios on pressure levels by using NCEP temperature and pressure data provided with each profile. Derived ozone profiles were then interpolated to fixed pressure levels on the following grid:

$$p(i) = 1000 \times 10^{-\frac{i}{30}} \text{ (hPa)} \quad i = 0, 1, 2, \dots \quad (2)$$

Ozone values at each of the 5 levels centered on every GOZCARDS pressure level were then averaged (weighted by pressure) to derive mixing ratios at each GOZCARDS pressure level. By doing this, the SAGE profiles were smoothed to a vertical resolution comparable to that of the other satellite instruments used in this GOZCARDS work. Monthly zonal means were then computed for the SAGE ozone datasets on the GOZCARDS-compatible grid.

5.1.2 Comparisons of ozone zonal means

Ozone differences between SAGE II and other satellite data are shown in Fig. S8. Zonal mean differences between SAGE II and HALOE are generally within 5% for 1.5 to 68 hPa at mid-latitudes, and for 1.5 to 46 hPa in the tropics; relative biases are larger outside those ranges and increase to ~10% near the tropopause and also near 1 hPa. This good level of agreement was demonstrated in the past (e.g., SPARC, 1998). SAGE II data show better agreement with UARS and Aura MLS in the upper stratosphere and lower mesosphere, within 5% up to 0.68 hPa and for latitudes outside the polar regions. Aura MLS O₃ compares better with SAGE II data than does UARS MLS in the tropics for pressures larger than 68 hPa; the high bias in UARS MLS O₃ at 100 hPa has been discussed previously (Livesey et al., 2003). There are no months that include both SAGE II and ACE-FTS data in the northern hemisphere tropics (see the gap in Fig. S8, bottom right panel), largely due to the poorer coverage from ACE-FTS in the tropics. ACE-FTS O₃ shows the largest positive bias (greater than 10%) with respect to SAGE II, for pressures less than 1.5 hPa. The high bias in upper stratospheric ACE-FTS ozone has been mentioned in past validation work using ACE-FTS data (e.g., Froidevaux et al., 2008b; Dupuy et al., 2009). The biases shown here are also consistent with recent O₃ intercomparison studies from a comprehensive array of satellite instruments by Tegtmeier et al. (2013). It has been known for some time that the HALOE and SAGE II ozone datasets, which govern the main variations of the GOZCARDS merged ozone values before 2005, agree quite well (within 5%) in absolute value, and also in terms of temporal trends (Nazaryan et al., 2005), and versus ozonesondes (mostly above ~20 km or ~50 hPa). Larger percentage differences occur in the lowest region of the stratosphere at low latitudes, and especially in the upper troposphere, where HALOE values become significantly smaller than SAGE II data, which are already biased low (by ~50%) versus

sondes (Wang et al., 2002); see also Morris et al. (2002), as well as results of SAGE II and HALOE comparisons versus solar occultation UV-Visible spectrometer measurements from long duration balloons (Borchi et al., 2005). We should note here that in this GOZCARDS merging work, we have largely avoided the upper tropospheric region.

Zonal mean differences between SAGE II and Aura MLS show some latitudinal structure between 1 and 3 hPa, with larger (5-10%) biases in the southern hemisphere, especially for 0 to 30°S (see Fig. S8). There are no such features between SAGE II and HALOE or UARS MLS. We found that this results from anomalous NCEP temperatures after 2000, which affect SAGE II data converted from number density/altitude to GOZCARDS VMR/pressure coordinates. Figure 17 shows an example of the ozone series from SAGE II and other satellite data for 10°S to 20°S from 1 to 6.8 hPa. At 1 hPa, the SAGE II ozone values (converted to mixing ratios) drift relative to HALOE and are elevated after mid-2000; this can be attributed to abnormal NCEP temperature trends compared to MERRA and HALOE during the same time period (for detailed views, see Figs. S9 and S10). Similar features are found down to pressures near 3 hPa. These issues relating to anomalous upper stratospheric NCEP temperature trends were noted by McLinden et al. (2009). Because such artifacts are confirmed by using either MERRA or HALOE temperatures, we decided not to include in the merging process any SAGE II O₃ values after June 30, 2000 for pressures equal to or less than 3.2 hPa. SAGE II ozone is not significantly affected by the conversion to mixing ratio/pressure coordinates at 4.6 and 6.8 hPa (Fig. 17).

5.2 GOZCARDS ozone merged data records

5.2.1 Methodology for GOZCARDS merged ozone

Ozone measurements from SAGE I, SAGE II, HALOE, UARS MLS, Aura MLS and ACE-FTS, were used to establish a near-continuous monthly zonal mean record from late 1979 through 2012 for the GOZCARDS merged O₃ product (ESDR version 1.01). The SAGE II dataset was used as a reference standard, since it has the longest period of measurements and has been extensively validated. A GOZCARDS ozone merged data record is constructed by combining these measurements after removing systematic biases with respect to SAGE II. This is done by applying additive offsets to all other instrument series, as determined from average differences

between monthly zonal means and SAGE II during overlap time periods. The merged data are then derived by averaging all available adjusted datasets. Because there are gaps in overlap between SAGE II and ACE-FTS monthly mean data in some latitudes (Fig. S7), and as SAGE II ozone VMRs obtained from the vertical grid transformation were affected by anomalous NCEP temperatures after mid-2000 for pressures smaller than or equal to 3.2 hPa, a two-step approach is used to generate the merged product. First, SAGE II data are used as reference for pressures larger than 3.2 hPa to adjust HALOE, UARS MLS and Aura MLS based on overlapping months between 1991 and Nov. 2005; see the method overview schematic in Fig. 18. For $p \leq 3.2$ hPa, SAGE II O₃ is still used as a reference through June 2000, and HALOE and UARS MLS data are adjusted accordingly. This eliminates the effect of anomalous NCEP temperatures on SAGE II ozone and leads to more accurate offsets based on HALOE values, after they have been adjusted to SAGE II. Adjusted HALOE data (HALOE* in Fig. 18) are then used as a reference to derive estimated offsets for Aura MLS O₃, using the overlap period with HALOE from Aug. 2004 to Nov. 2005. In step 2, a new reference value is derived by averaging all available data from SAGE II, HALOE*, UARS MLS* and Aura MLS*. This value is used to adjust ACE-FTS ozone based on all overlapping months between March 2004 and Nov. 2005. By including Aura MLS in the dataset created in step 1, we obtain more complete spatial and temporal coverage than possible with SAGE II and HALOE, and ensure that there are overlapping months between this combined dataset and ACE-FTS source data. At the end of step 2, the final merged ozone is derived by averaging the temporary merged dataset from step 1 with the adjusted ACE-FTS data.

5.2.2 Further considerations regarding GOZCARDS merged ozone data

Even in the absence of diurnal variations, measurements from occultation sensors can yield larger sampling errors than those from densely-sampled emission measurements (Toohey et al., 2013). Diurnal changes in ozone can affect data comparisons and could impact data merging. Recently, Sakazaki et al. (2013) presented diurnal changes measured by the Superconducting Submillimeter-Wave Limb-Emission Sounder (SMILES) and Parrish et al. (2014) analyzed ground-based microwave O₃ profile variations versus local time in conjunction with satellite data. Ozone diurnal variations range from a few percent in the lower stratosphere to more than 10% in the upper stratosphere and lower mesosphere (see also Ricaud et al., 1996; Haefele et al., 2008; Huang et al., 2010). SAGE II and other occultation instruments observe ozone at local

sunrise or sunset, and the retrieved values are generally closer to nighttime values in the upper stratosphere and mesosphere. To characterize systematic differences between satellite data, coincident profiles with small differences in space and time are most often used; an example of mean differences and standard deviations between SAGE II and Aura MLS using both coincident profile and zonal mean methods is provided in Fig. S11. SAGE II and coincident Aura MLS nighttime O₃ values agree within ~5% between 0.46 and 100 hPa, except in the tropical lower stratosphere where comparisons are noisier. Differences between zonal mean SAGE II and Aura MLS data are very close to differences from averaged coincident values, except for pressures less than 2 hPa, where differences increase from a few to ~10% at 0.3 hPa, consistent with what one expects from the diurnal cycle. Although zonal mean differences are likely to be less representative of “true” differences, by combining SAGE II with Aura MLS data adjusted by zonal mean biases, we provide a series adjusted to the average of sunrise and sunset, as measured by SAGE II. If Aura MLS data were adjusted by biases obtained using the coincident method, an upper stratospheric offset of more than several percent and artificial trends due to such a diurnal cycle effect could be introduced. The use of long-term datasets with consistent sampling should be an advantage for trend detection, even in a region with diurnal changes. Also, our avoidance of SAGE II upper stratospheric O₃ after mid-2000 mitigates potential artifacts arising from changing SAGE II sunrise/sunset sampling patterns over time.

Figure 19 displays the average ozone offsets obtained from the biases relative to SAGE II. A high bias in upper stratospheric ACE-FTS O₃ relative to other datasets is evident from the negative ACE-FTS offsets (as large as 25%). Most of the other instrument offsets are in the 5-10% range; lowering O₃ from UARS MLS, HALOE, and Aura MLS in the lower mesosphere is required to match SAGE II. Sampling differences and data sparseness may be mostly responsible for larger offsets at high latitudes; in these regions, the merged data are less amenable to long-term analyses because of data gaps and larger variability (especially prior to 2004).

As shown in the Supplement (Fig. S12), we observe strong similarities (e.g., peaks at midlatitudes near 10 and 1.5 hPa) in the O₃ annual cycle amplitude patterns from SAGE II, HALOE, ACE-FTS, and Aura MLS over their respective measurement periods. Middle stratospheric peaks are a result of the annual cycle in oxygen photolysis, whereas temperature variations drive the annual cycle in the upper stratosphere (Perliski et al., 1989). This sort of

comparison provides some reassurance regarding the consistency of various datasets. Figure 20 provides diagnostics similar to those given for HCl and H₂O, namely correlation coefficients and significance ratios for the slopes of the deseasonalized anomaly time series from SAGE II versus HALOE as well as from ACE-FTS versus Aura MLS (for 1992 through 1999, and 2005 through 2009, respectively). These diagnostic results for ACE-FTS and Aura MLS are of a quality that is comparable to the HALOE/SAGE II results; poorer fits occur mostly at high latitudes and in the upper stratosphere. Poorer correlations at upper altitude appear largely tied to a decrease in the amount of valid data in this region (especially at high latitudes), coupled with a relatively small variability. For regions with poorer agreement between ACE-FTS and Aura MLS, we often see small variability in the series from Aura MLS but larger changes (scatter) in the ACE-FTS series. Larger differences in trends between SAGE II and HALOE were noted by Nazaryan et al. (2005) at low latitudes near 50 km; this is also indicated by our simple linear fits (not shown here) to the GOZCARDS source datasets from these two instruments and the existence of poorer agreements in Fig. 20 for the slope of the difference series in that region. The existence of good correlations in interannual ozone variations between a large number of satellite measurements was discussed by Tegtmeier et al. (2013). Regarding temporal drifts, Nair et al. (2012) have shown that small drifts (mostly within about $\pm 0.5\%/yr$ for the 20-35 km region) exist between most of the datasets from six ozone lidar sites and coincident HALOE, SAGE II, and Aura MLS measurements; similar results were obtained by Kirgis et al. (2013). Other recent studies (in particular, by Hubert et al., 2015) corroborate the very good stability of the datasets used for GOZCARDS, which relies most heavily on O₃ data from SAGE II and Aura MLS. While we feel justified in the use of the longer-term time series chosen for GOZCARDS O₃, data users should still note the existence of a few regions with poorer correlations or trend agreement (and, therefore, larger uncertainties) between different satellite ozone datasets, as indicated in Fig. 20. Long-term merged datasets from GOZCARDS and other sources should undergo continued scrutiny from the community, as done recently for trends by Tummon et al. (2015) and Harris et al. (2015). Sample cross-sectional views of two slices through the GOZCARDS merged O₃ field are provided in the Supplement (Fig. S13). Figure 21 shows estimated systematic errors from our calculation of the 95% ranges for the monthly mean source data used here, both above and below the merged values. In this case, as SAGE II is used as a reference dataset, the applied offsets

(Fig. 20) correlate quite well with this plot depicting the ranges about SAGE II values. Minimum error bars can be slightly lower than 5% for the middle stratosphere at low latitudes, where ozone values are largest. This view of systematic error bars is consistent with results by Tegtmeier et al. (2013), based on the larger set of data analyzed for the SPARC Data Initiative. They also found that the regions with lowest errors (scatter) are in the middle stratosphere at low to mid-latitudes, where most monthly mean satellite data fit within $\pm 5\%$ of the multi-instrument mean.

5.3 GOZCARDS ozone sample results and discussion

Nair et al. (2013) used regression analyses to compare profile trend results from GOZCARDS merged O_3 at northern midlatitudes versus a combined O_3 dataset from lidar and coincident satellite data at the Observatoire de Haute Provence (OHP), France. They showed that good consistency exists for the decreasing ozone time period, from the early 1980s to 1997, and for the upper stratospheric increase since 1997, but some differences exist in the lower stratosphere during this second time period, when the GOZCARDS results show a near-zero trend in comparison to small positive trends from the combined (and more localized) dataset. The above results for the declining time period agree broadly with earlier work (for the 1979-1997 period) by Jones et al. (2009). Gebhardt et al. (2014) analyzed ozone profile trends from SCIAMACHY on ENVISAT, and compared this to trends from Aura MLS, Optical Spectrograph and InfraRed Imager System (OSIRIS) on the Odin satellite, and sondes; their results include the detection of localized ozone increases in the mid-stratosphere at low latitudes; see also Bourassa et al. (2014), who analyzed merged SAGE II and (OSIRIS) observations for 1984-2013, as well as results from Kyrölä et al. (2013) on combined SAGE II and Global Ozone Monitoring by Occultation of Stars (GOMOS) records for 1984-2012, and Eckert et al. (2014), who investigated ENVISAT MIPAS trends for 2002-2012. The shortness of data records since 1997, coupled with relative variability and potential drifts between various measurements may explain some differences in recent trend results, notably for the post-1997 period. More comprehensive analyses from the SI²N initiative have focused on an intercomparison of profile changes from a variety of datasets, including GOZCARDS and other merged records (Tummon et al., 2015; Harris et al., 2015).

Here, we investigate ozone column results for the stratosphere, based on the global GOZCARDS data, in light of other column ozone datasets, including the work by Ziemke and

Chandra (2012), hereafter referenced as ZC12. These authors analyzed total column and stratospheric column data from satellites, and their analyses yielded a rather strong near-global (60°S-60°N) average ozone increase since 1998. Their stratospheric columns depend on the convective-cloud differential (CCD) method and use Total Ozone Mapping Spectrometer (TOMS) and Ozone Monitoring Instrument (OMI) column data over convective clouds near the tropopause (see also Ziemke et al., 2005). In Fig. 22, we compare changes in 60°S-60°N ZC12 column ozone data (J. Ziemke, personal communication, 2013) to changes in GOZCARDS O₃ columns above 68 hPa for that region; note that GOZCARDS values do not provide for a continuous long-term time series down to pressures of 100 hPa or more in the SAGE I years (1979-1981). To eliminate biases between stratospheric columns as calculated using the CCD methodology and the GOZCARDS fixed bottom pressure approach, we reference all stratospheric columns to the 1980 total column value. These column series include SAGE I data and are linearly interpolated between 1981 and 1984, when no GOZCARDS source datasets exist. We observe that relative changes in GOZCARDS columns follow the ZC12 curves within a few DU in the downward phase until about 1992, but the 1992-1997 decrease in total columns does not compare very well. Some of this discrepancy may occur because total columns capture a stronger decrease from levels below 68 hPa, not fully represented in GOZCARDS. Focusing on the late period (from Aura MLS and ACE-FTS), we also show the GOZCARDS columns above 68 hPa, referenced to 2007 instead of 1980. There is a good match in the variations between GOZCARDS and ZC12 columns during 2005-2010, in agreement with the fact that very good correlations were obtained by ZC12 between Aura MLS columns and stratospheric column data from the CCD technique. ZC12 values for stratospheric and total columns are in good agreement, although the stratospheric values have gaps when not enough data were present for near-global estimates. The increase in ZC12 data from 1997 to 1998 is not matched very well by GOZCARDS; this is also true if we remove the 11-yr solar cycle from both datasets (not shown here), as done by ZC12. However, the interannual changes in GOZCARDS columns are in better agreement with near-global total column variations in the Merged Ozone (Version 8.6) Dataset obtained from the suite of SBUV instruments (McPeters et al., 2013, Frith et al., 2014), as shown in Fig. 22. Discrepancies between the GOZCARDS and SBUV column data are largest between 1992 and 1997; this could be related to the somewhat less robust SBUV datasets in this period

(resulting from SBUV satellite orbits closer to the terminator, e.g., see Frith et al., 2014), and/or to some issues in this portion of the GOZCARDS ozone data record. Discrepancies between the various column results in Fig. 22 could also arise from differences in ozone column calculations or coverage because of different methodologies, grids, or sampling to properly determine near-global results. We note that recent analyses by Shepherd et al. (2014), who used a chemistry-climate model constrained by meteorology to investigate causes of long-term total column O_3 variations, show a partial return, in 2010, towards 1980 ozone column values, but not nearly as much as implied by ZC12. Long-term halogen source gas reductions that have occurred since the mid-1990s should only lead to column ozone increases of a few DU since 1997 (Steinbrecht et al., 2011).

6 Other GOZCARDS data records

We now briefly mention the N_2O , HNO_3 , and temperature GOZCARDS records that were part of the delivery for public dissemination in 2013. For N_2O and HNO_3 , the somewhat simpler merging procedure consisted of averaging the source datasets from ACE-FTS and Aura MLS over the overlap time period (Aug. 2004 through Sep. 2010) to obtain the additive offsets for each of the two individual records. We then simply used the correspondingly-adjusted and averaged series to create the merged results; this procedure is the same as we described for the first step in the HCl (or H_2O) merging process.

6.1 N_2O

This data set starts in August 2004, when the Aura MLS data record began; the only dataset after Sep. 2010 is the Aura MLS N_2O (version 3.3) data record. Because of degradation in the main target MLS N_2O band (near 640 GHz) after the first few months of 2013, the N_2O standard MLS product is being reprocessed for the whole Aura MLS period using an alternate measurement band; currently, there are no official GOZCARDS N_2O data after 2012.

Excellent agreement (mostly within 5%) exists between stratospheric ACE-FTS and Aura MLS N_2O profiles (see Lambert et al., 2007; Strong et al., 2008; Livesey et al., 2013). Plots showing the average offsets applied to both MLS and ACE-FTS N_2O series as a function of latitude and pressure are provided in Fig. S14. These plots are in agreement (in magnitude and in

sign) with the above-referenced studies; the two datasets yield typical offsets (one half of the average differences) of less than 5%. Also, very good temporal agreement between these two time series (for 2004-2010) is illustrated by the quality of the N₂O diagnostic information displayed in Fig. S15, showing generally highly correlated fields and insignificant drifts.

Figure 23 shows sample contour plots for the N₂O merged field (2004-2012); as seen from the bottom panel (100 hPa), wintertime descent brings low N₂O values down at high latitudes inside the polar vortices. N₂O is a conserved tracer in the lower stratosphere and its variations near the tropopause have implications regarding age of air. Variations in upper stratospheric N₂O are clearly affected by seasonal and dynamical effects; this is evident from the striking semi-annual, annual and QBO-related patterns displayed in Fig. 23 for the 6.8 hPa level (top panel).

6.2 HNO₃

As for N₂O, we merged the HNO₃ data from ACE-FTS (version 2.2) and Aura MLS (version 3.3) from Aug. 2004 onward, and included only the adjusted MLS dataset after Sep. 2010. The average offsets applied to MLS and ACE-FTS time series as a function of latitude and pressure for HNO₃ are provided in Fig. S16. The typical offsets (one half of the average differences) for HNO₃ are less than ~10% (and less than 0.5 ppbv). Despite somewhat larger percent absolute differences than for N₂O between Aura MLS and ACE-FTS HNO₃, there is very good agreement as a function of time between these two datasets in the stratosphere. This is illustrated by the HNO₃ diagnostic information provided in Fig. S17; the poorest correlations are obtained at or below the tropical tropopause.

Comparisons of v3.3 Aura MLS and v2.2 ACE-FTS nitric acid profiles have shown good agreement (see also Livesey et al., 2013), as the MLS HNO₃ v3.3 values are now generally larger than in v2.2, for which validation results were provided by Santee et al. (2007). Wolff et al. (2008) also compared MLS (v2.2) and ACE-FTS (v2.2) coincident profiles, and obtained similar results; in addition, they demonstrated that very good agreement exists between the HNO₃ profiles from ACE-FTS and coincident profiles from MIPAS on Envisat. Also, comparisons between Aura MLS HNO₃ (v3.3) profiles and wintertime HNO₃ profiles retrieved by a Ground-based Millimeter-wave Spectrometer (GBMS) in Thule, Greenland, during the first 3 months of 2010, 2011, and 2012 show agreement mostly within 10-15% (Fiorucci et al., 2013).

Figure 24 (top two panels) displays the HNO_3 fields at 46 hPa from the UARS MLS period (1991-1997) as well as from the 2004-2013 period, for which a merged GOZCARDS product was produced, based on Aura MLS and ACE-FTS source datasets. Also shown (bottom two panels) are time series for 45°N and 32 hPa from both these periods; the bottom right panel includes the source and merged time series. We have performed additional investigations (not shown here) which lead us to believe that small upward adjustments to the UARS MLS HNO_3 values (by about 10%) are needed to better cross-correlate these datasets across the two distinct time periods; such relative biases are within the expected systematic errors. This is based on a consideration of ground-based Fourier Transform infrared column HNO_3 data covering the full time period, as well as past GBMS HNO_3 profile retrievals. Also, Aura MLS and ACE-FTS HNO_3 data match ground-based and other correlative data quite well, and typically better than the intrinsically poorer quality UARS MLS HNO_3 data. However, obtaining an optimum global set of adjustments for the UARS MLS nitric acid field will be limited by the number of sites with such ground-based data as well as by the different vertical resolutions for these datasets versus MLS. More collaborative work regarding such analyses is needed in order to find the optimum adjustments to help tie together these two time periods for this species. Although we did not deliver the UARS MLS HNO_3 source data files for GOZCARDS, we could provide these monthly zonal mean series upon request, keeping the above caveats in mind.

6.3 Temperature

Finally, in terms of the initial set of delivered GOZCARDS products, and for the convenience of stratospheric composition data users, we have used temperatures (T) from the Modern-Era Retrospective Analysis for Research and Applications (MERRA) to produce a monthly mean GOZCARDS temperature data set from 1979 onward. MERRA is a NASA Goddard reanalysis (Rienecker et al., 2011) for the satellite era using Goddard Earth Observing System Data Assimilation System version 5 (GEOS-5); T is from the DAS 3d analyzed state MAI6NVANA, version 5.2 files (such as MERRA300.prod.assim.inst6_3d_ana_Nv.20110227.hdf). Data from four daily MERRA files (for 00, 06, 12, and 18 hr UT) were averaged to provide daily mean temperature fields (appropriate for a mean time of 09 hr). Vertical interpolation was performed onto the GOZCARDS pressure grid, which, for temperature, covers 30 pressures levels from

1000 hPa to 0.0147 hPa. Averaged values were stored for the 10° GOZCARDS latitude bins, and daily results were binned to create the GOZCARDS monthly temperature data set (version 1.0).

7 Summary and conclusions

We have reviewed the GOZCARDS project's production of merged data records of stratospheric composition, mainly for HCl, H₂O, and O₃, using carefully screened satellite data, starting in 1979 with SAGE I and continuing through Aura MLS and ACE-FTS data periods. The source data have a high degree of maturity and we have reinforced our confidence in their usefulness through investigations of various diagnostics (offsets, annual cycles, correlations and trend differences of deseasonalized series). These records are publicly available as GOZCARDS ESDR version 1.01 and can be referenced using DOI numbers (Froidevaux et al., 2013b, Anderson et al., 2013, and Wang et al., 2013, for the above species, respectively). The other GOZCARDS data records also have references, namely Schwartz et al. (2013) for the MERRA-based temperature records, and Froidevaux et al. (2013c, 2013d) for N₂O and HNO₃, respectively. Table 2 provides a summary of the GOZCARDS monthly mean datasets. Yearly netCDF files are available for public access (<http://mirador.gsfc.nasa.gov>). The merging methodology follows from a determination of mean biases (for each pressure level and 10° latitude bin) between monthly mean series, based on the overlap periods. For ozone, SAGE II data are the chosen reference, whereas for other species, the merging basis is equivalent to an average of the datasets during the periods of overlap. The merged data files contain the average offset values applied to each source data time series, along with standard deviations and standard errors. The GOZCARDS README document (Froidevaux et al., 2013a) provides more details about data file quantities, including local time and solar zenith angle information, and a list of days with available data. We also display here estimated systematic errors about the merged values; we find that mixing ratio errors are typically within 5% to 15% and are consistent with the magnitude of observed relative biases.

The GOZCARDS HCl merged record in the upper stratosphere enables long-term tracking of changes in total stratospheric chlorine. The long-term increase in HCl prior to the late 1990s, and the subsequent gentler decrease in the 21st century, are delayed manifestations of changes in the sum of the surface source gas abundances as a result of regulations from the Montreal Protocol

and its amendments. From 1997 to 2010, the average rate of change in upper stratospheric HCl (50°S to 50°N) was about -0.4 to -0.7%/yr (with the smaller rates of decrease after 2003). In the lower stratosphere, where Aura MLS data are weighted heavily, recent short-term variations have shown a flattening out and, in particular for northern midlatitudes and at 50-70 hPa for the deep tropics, a significant reversal and increasing trend (see also Mahieu et al., 2014), compared to the decrease from the late 1990s to about 2004. However, lower stratospheric HCl tendencies appear to be reversing again in recent years (2011-2014), with decreases at northern midlatitudes and some increasing tendencies at southern midlatitudes. In the future, we expect to see long-term global HCl decreases in both the upper and lower stratosphere.

For water vapor, we have used data from the same instruments as for HCl, with the same methodology, except for the addition of 1991-1993 UARS MLS data. The H₂O data record shows large mesospheric variations that are anti-correlated with the solar flux over the past two 11-yr solar cycles. Net long-term trends in lower stratospheric H₂O are quite small if one considers the past 22 years, but there has been considerable interannual variability, including the steep drop from 2000 to 2001, as mentioned in past work. While H₂O tendencies have been generally positive after 2001, the 68 and 100 hPa levels show some steep decreases (by 0.5-0.8 ppmv) from 2011 to 2013 (see also Urban et al., 2014). Over the past 22 years, long-term global H₂O increases of order 10% are observed in the upper stratosphere and lower mesosphere, whereas a decrease of nearly 10% has occurred in the lower stratosphere (near 70-100 hPa). However, there is no regular monotonic change on decadal timescales, especially in the tropical lower stratosphere, where fairly sharp decreases followed by steadier increases may be a recurrent pattern (see also Fueglistaler, 2012); this complicates the detection of any small underlying trend. As one might expect from the well-documented temperature influence on the tropical lower stratosphere, H₂O variability (based on maximum minus minimum yearly averages) is largest in the tropics and just above the tropopause. More accurate studies of seasonal to decadal water vapor variability will be enabled by continuing such merged H₂O datasets in the future. A reduction in model spread for stratospheric H₂O is likely easier to achieve than tighter upper tropospheric model results; for the upper troposphere, see the data/model comparisons (H₂O and ice water content) by Jiang et al. (2012).

For ozone, we have used measurements from SAGE I, SAGE II, HALOE, UARS MLS, Aura MLS and ACE-FTS to produce a merged record starting in 1979, after adjusting the series to SAGE II. We observed temporal drifts in the SAGE II series, after conversion to the GOZCARDS mixing ratio/pressure grid, as a result of the NCEP temperature data used in this conversion, mostly in the upper stratosphere after June 2000 (see also McLinden et al., 2009). To mitigate this issue, we used HALOE upper stratospheric O₃ as a reference for July 2000 to November 2005, after adjusting the HALOE series to SAGE II. The resulting GOZCARDS merged O₃ data for northern midlatitudes have been used in regression analyses (Nair et al., 2013) to reveal decreases in the whole stratosphere for 1984-1996. Nair et al. (2015) extended this work and found increasing trends in upper stratospheric GOZCARDS O₃ since 1997, but no significant positive trends in the lower stratosphere. Other studies of GOZCARDS O₃ profile trends have been discussed as part of the WMO (2014) and SI²N assessments (Tummon et al., 2015; Harris et al., 2015). Here, we looked at the consistency of column data between stratospheric GOZCARDS O₃ and work by Ziemke and Chandra (2012), who noted that a fairly rapid change (“recovery”) in near-global ozone columns from TOMS and OMI could be inferred since the mid-1990s. We show that the similarly analyzed GOZCARDS column data does not show an upturn of more than 0.5-1% since that period. Reasons for these differences could include data coverage or merging-related issues in either dataset, or inaccuracies in globally-averaged stratospheric columns. A recent global total ozone study (Shepherd et al., 2014) also points to less of a return towards 1980 levels than implied by ZC12.

We also briefly described the creation of N₂O and HNO₃ GOZCARDS data records, based on Aura MLS and ACE-FTS. The agreement between these two instruments’ datasets for these species was shown to be generally very good. For HNO₃, UARS MLS HNO₃ source datasets in the GOZCARDS format are available from the authors. However, a small upward adjustment (of order 10%) to the UARS MLS values is likely needed based on our preliminary work comparing these series to HNO₃ column results from FTIR measurements. More detailed work should help determine if global adjustments can indeed be made to UARS MLS HNO₃ data; lacking this, one should ensure that error bars reflect likely biases that can affect the continuity between HNO₃ datasets before and after 2000, given the multi-year gap in satellite coverage for this species.

There is a Supplement related to this article.

Acknowledgements. Work at JPL was performed under contract with the National Aeronautics and Space Administration (NASA). We dedicate this work to the memory of Professor Derek Cunnold (Georgia Institute of Technology) who was a member of the original NASA MEaSUREs (Making Earth System Data Records for Use in Research Environments) GOZCARDS proposal. The GOZCARDS data generation could not have been possible without the past work from instrument teams for SAGE I, SAGE II, HALOE, UARS MLS, Aura MLS, and ACE-FTS, and related data usage documentation. At JPL, we thank Joe Waters for his leadership role in making MLS instruments and datasets possible and Bill Read for his key role; thanks to Vince Perun for MERRA-related work, and to Brian Knosp and Robert Thurstans for database and computer management assistance. We also thank Kaley Walker and Ashley Jones for comments regarding ACE-FTS data, Gloria Manney and William Daffer for help in making the original ACE-FTS data profiles available, and Joe Zawodny and Larry Thomason for their contributions and comments regarding SAGE data. We acknowledge the work of the GMAO team responsible for MERRA data used to generate the GOZCARDS temperatures, specifically, Steven Pawson and Jianjun Jin for discussions and cross-checks regarding temperature data. We acknowledge Jerry Ziemke for the ozone column data (from Ziemke and Chandra, 2012), and Sean Davis for discussions on data usage and screening, and the creation of long-term series. For early HNO₃-related work connecting ground-based data to MLS datasets, we thank Giovanni Muscari and Irene Fiorucci. We are thankful for the NOAA Earth System Research Laboratory (ESRL) Global Monitoring Division (GMD) website information and data on total surface chlorine. We obtained solar flux data for the Ottawa/Penticton sites from the NOAA National Geophysical Data Center (NGDC) website (www.ngdc.noaa.gov), for which we also acknowledge the National Research Council of Canada.

References

- Anderson, J. G., Brune, W. H., and Proffitt, M. H.: Ozone destruction by chlorine radicals within the Antarctic vortex: The spatial and temporal evolution of ClO–O₃ anticorrelation based on in situ ER-2 data, *J. Geophys. Res.*, 94, 11,465-11,479, 1989.
- Anderson, J., Russell, J. M., Solomon, S., and Deaver, L. E.: HALOE confirmation of stratospheric chlorine decreases in accordance with the Montreal Protocol, *J. Geophys. Res.*, 105, 4483-4490, 2000.
- Anderson, J., Froidevaux, L., Fuller, R. A., Bernath, P. F., Livesey, N. J., Pumphrey, H. C., Read, W. G., and Walker, K. A.: GOZCARDS Merged Data for Water Vapor Monthly Zonal Means on a Geodetic Latitude and Pressure Grid, version 1.01, Greenbelt, MD, USA: NASA Goddard Earth Science Data and Information Services Center, accessible from doi:10.5067/MEASURES/GOZCARDS/DATA3003, 2013.
- Barath, F., Chavez, M. C., Cofield, R. E., Flower, D. A., Frerking, M. A., Gram, M. B., Harris, W. M., Holden, J. R., Jarnot, R. F., Kloeze, W. G., Klose, G. J., Lau, G. K., Loo, M. S., Maddison, B. J., Mattauch, R. J., McKinney, R. P., Peckham, G. E., Pickett, H. M., Siebes, G., Soltis, F. S., Suttie, R. A., Tarsala, J. A., Waters, J. W., and Wilson, W. J.: The Upper Atmosphere Research Satellite Microwave Limb Sounder Experiment, *J. Geophys. Res.*, 98, 10751-10762, 1993.
- Bernath, P. F., McElroy, C. T., Abrams, M. C., Boone, D., Butler, M., Camy-Peyret, C., Carleer, M., Clerbaux, C., Coheur, P.-F., Colin, R., DeCola, P., DeMaziere, M., Drummond, J. R., Dufour, D., Evans, W. F. J., Fast, H., Fussen, D., Gilbert, K., Jennings, D. E., Llewellyn, E. J., Lowe, R. P., Mahieu, E., McConnell, J. C., McHugh, M., McLeod, S. D., Michaud, R., Midwinter, C., Nassar, R., Nichitiu, F., Nowlan, C., Rinsland, C. P., Rochon, Y. J., Rowlands, N., Semeniuk, K., Simon, P., Skelton, R., Sloan, J. J., Soucy, M.-A., Strong, K., Tremblay, P., Turnbull, D., Walker, K. A., Walkty, I., Wardle, D. A., Wehrle, V., Zander, R., and Zou, J.: Atmospheric Chemistry Experiment (ACE): Mission overview, *Geophys. Res. Lett.*, 32, L15S01, doi:10.1029/2005GL022386, 2005.
- Bhatt, P. P., Remsberg, E. E., Gordley, L. L., McInerney, J. M., Brackett, V. G., and Russell, III, J. M.: An evaluation of the quality of Halogen Occultation Experiment ozone profiles in the lower stratosphere, *J. Geophys. Res.*, 104 (D8), 9261-9275, 1999.
- Borchi, F., Pommereau, J.-P., Garnier, A., and Pinharanda, M.: Evaluation of SHADOZ sondes, HALOE and SAGE II ozone profiles at the tropics from SAOZ UV-Vis remote measurements onboard long duration balloons, *Atmos. Chem. Phys.*, 5, 1381-1397, 2005.

1007 Bourassa, A. E., Degenstein, D. A., Randel, W. J., Zawodny, J. M., Kyrölä, E., McLinden, C. A., Sioris,
 1008 C. E., and Roth, C. Z., Trends in stratospheric ozone derived from merged SAGE II and Odin-OSIRIS
 1009 satellite observations, *Atmos. Chem. Phys.*, 14, 6983-6994, doi:10.5194/acp-14-6983-2014, 2014.

1010 Brown, A. T., Chipperfield, M. P., Boone, C., Wilson, C., Walker, K. A., and Bernath, P.: Trends in
 1011 atmospheric halogen containing gases since 2004, *J. Quant. Spec. Rad. Trans.*, 112, 2552-2566, 2011.

1012 Chandra, S., Jackman, C. H., Fleming, E. L., and Russell, J. M.: The seasonal and long term changes in
 1013 mesospheric water vapor, *Geophys. Res. Lett.*, 24, No. 6, 639-642, 1997.

1014 Chu, W. P., and McCormick, M. P.: Inversion of Stratospheric Aerosol and Gaseous Constituents From
 1015 Spacecraft Solar Extinction Data in the 0.38-1.0 μm Wavelength Region, *Appl. Opt.*, 18, No. 9, 1404-
 1016 1413, 1979.

1017 Cunnold, D. M., Chu, W. P., Barnes, R. A., McCormick, M. P., and Veiga, R. E.: Validation of SAGE II
 1018 ozone measurements, *J. Geophys. Res.*, 94, 8447-8460, 1989.

1019 Damadeo, R. P., Zawodny, J. M., Thomason, L. W., and Iyer, N.: SAGE version 7.0 algorithm:
 1020 application to SAGE II, *Atmos. Meas. Tech.*, 6, 3539-3561, doi:10.5194/amt-6-3539-2013, 2013.

1021 Dupuy, E., Walker, K. A., Kar, J., Boone, C. D., McElroy, C. T., Bernath, P. F.,
 1022 Drummond, J. R., Skelton, R., McLeod, S. D., Hughes, R. C., Nowlan, C. R., Dufour, D. G., Zou, J.,
 1023 Nichitiu, F., Strong, K., Baron, P., Bevilacqua, R. M., Blumenstock, T., Bodeker, G. E., Borsdorff, T.,
 1024 Bourassa, A. E., Bovensmann, H., Boyd, I. S., Bracher, A., Brogniez, C., Burrows, J. P., Catoire, V.,
 1025 Ceccherini, S., Chabrillat, S., Christensen, T., Coffey, M. T., Cortesi, U., Davies, J., De Clercq, C.,
 1026 Degenstein, D. A., De Maziere, M., Demoulin, P., Dodion, J., Firanski, B., Fischer, H., Forbes, G.,
 1027 Froidevaux, L., Fussen, D., Gerard, P., Godin-Beekmann, S., Goutail, F., Granville, J., Griffith, D.,
 1028 Haley, C. S., Hannigan, J. W., Hopfner, M., Jin, J. J., Jones, A., Jones, N. B., Jucks, K., Kagawa, A.,
 1029 Kasai, Y., Kerzenmacher, T. E., Kleinbohl, A., Klekociuk, A. R., Kramer, I., Kullmann, H.,
 1030 Kuttippurath, J., Kyrölä, E., Lambert, J.-C., Livesey, N. J., Llewellyn, E. J., Lloyd, N. D., Mahieu, E.,
 1031 Manney, G. L., Marshall, B. T., McConnell, J. C., McCormick, M. P., McDermid, I. S., McHugh, M.,
 1032 McLinden, C. A., Mellqvist, J., Mizutani, K., Murayama, Y., Murtagh, D. P., Oelhaf, H., Parrish, A.,
 1033 Petelina, S. V., Piccolo, C., Pommereau, J.-P., Randall, C. E., Robert, C., Roth, C., Schneider, M., Senten,
 1034 C., Steck, T., Strandberg, A., Strawbridge, K. B., Sussmann, R., Swart, D. P. J., Tarasick, D. W., Taylor,
 1035 J. R., Tetard, C., Thomason, L. W., Thompson, A. M., Tully, M. B., Urban, J., Vanhellemon, F.,

1036 Vigouroux, C., von Clarmann, T., von der Gathen, P., von Savigny, C., Waters, J. W., Witte, J. C., Wolff,
 1037 M., and Zawodny, J. M.: Validation of ozone measurements from the Atmospheric Chemistry Experiment
 1038 (ACE), *Atmos. Chem. Phys.*, 9, 287–343, doi:10.5194/acp-9-287-2009, 2009.

1039 Eckert, E., von Clarmann, T., Kiefer, M., Stiller, G. P., Lossow, S., Glatthor, N., Degenstein, D. A.,
 1040 Froidevaux, L., Godin-Beekmann, S., Leblanc, T., McDermid, S., Pastel, M., Steinbrecht, W., Swart, D.
 1041 P. J., Walker, K. A., and Bernath, P. F.: Drif-corrected trends and periodic variations in MIPAS IMK/IAA
 1042 ozone measurements, *Atmos. Chem. Phys.*, 14, 2571–2589, doi:10.5194/acp-14-2571-2014, 2014.

1043 Engel, A., Strunk, M., Muller, M., Haase, H.-P., Poss, C., Levin, I., and Schmidt, U.: The temporal
 1044 development of total chlorine in the high latitude stratosphere based on reference distributions of mean
 1045 age derived from CO₂ and SF₆, *J. Geophys. Res.*, 107, 4136, doi:10.1029/2001JD000584, 2002.

1046 Farman, J. C., Gardiner, B. G., and Shanklin, J. D.: Large losses of total ozone in Antarctica reveal
 1047 seasonal ClO_x/NO_x interaction, *Nature*, 315, 207–210, 1985.

1048 Fiorucci, I., Muscari, G., Froidevaux, L., and Santee, M. L.: Ground-based stratospheric O₃ and HNO₃
 1049 measurements at Thule, Greenland: an intercomparison with Aura MLS observations, *Atmos. Meas.*
 1050 *Tech.*, 6, 2441–2453, doi:10.5194/amt-6-2441-2013, 2013.

1051 Frith, S. M., Kramarova, N. A., Stolarski, R. S., McPeters, R. D., Bhartia, P. K., and Labow, G. J.: Recent
 1052 changes in total column ozone based on the SBUV Version 8.6 Merged Ozone Data Set, *J. Geophys.*
 1053 *Res.*, 119, 9735–9751, doi:10.1029/2014JD021889, 2014.

1054 Froidevaux, L., Livesey, N. J., Read, W. G., Salawitch, R. J., Waters, J. W., Drouin, B., MacKenzie, I. A.,
 1055 Pumphrey, H. C., Bernath, P., Boone, C., Nassar, R., Montzka, S., Elkins, J., Cunnold, D., and
 1056 Waugh, D.: Temporal decrease in upper atmospheric chlorine, *Geophys. Res. Lett.*, 33, L23813,
 1057 doi:10.1029/2006GL027600, 2006.

1058 Froidevaux, L., Jiang, Y. B., Lambert, A., Livesey, N. J., Read, W. G., Waters, J. W., Fuller, R. A.,
 1059 Marcy, T. P., Popp, P. J., Gao, R. S., Fahey, D. W., Jucks, K. W., Stachnik, R. A., Toon, G. C.,
 1060 Christensen, L. E., Webster, C. R., Bernath, P. F., Boone, C. D., Walker, K. A., Pumphrey, H. C.,
 1061 Harwood, R. S., Manney, G. L., Schwartz, M. J., Daffer, W. H., Drouin, B. J., Cofield, R. E., Cuddy, D. T.,
 1062 Jarnot, R. F., Knosp, B. W., Perun, V. S., Snyder, W. V., Stek, P. C., Thurstans, R. P., and Wagner, P. A.:
 1063 Validation of Aura Microwave Limb Sounder HCl measurements, *J. Geophys. Res.*, 113,
 1064 doi:10.1029/2007JD009025, D15S25, 2008a.

1065 Froidevaux, L., Jiang, Y. B., Lambert, A., Livesey, N. J., Read, W. G., Waters, J. W.,
 1066 Browell, E. V., Hair, J. W., Avery, M. A., McGee, T. J., Twigg, L. W., Sumnicht, G. K., Jucks, K. W.,
 1067 Margitan, J. J., Sen, B., Stachnik, R. A., Toon, G. C., Bernath, P. F., Boone, C. D., Walker, K. A.,
 1068 Filipiak, M. J., Harwood, R. S., Fuller, R. A., Manney, G. L., Schwartz, M. J., Daffer, W. H., Drouin, B. J.,
 1069 Cofield, R. E., Cuddy, D. T., Jarnot, R. F., Knosp, B. W., Perun, V. S., Snyder, W. V., Stek, P. C.,
 1070 Thurstans, R. P., and Wagner, P. A.: Validation of Aura Microwave Limb Sounder stratospheric and
 1071 mesospheric ozone measurements, *J. Geophys. Res.*, 113, doi:10.1029/2007JD008771, D15S20, 2008b.
 1072
 1073 Froidevaux, L., Fuller, R., Schwartz, M., Anderson, J., and Wang, R.: README Document for the
 1074 Global OZoneChemistry And Related trace gas Data records for the Stratosphere (GOZCARDS) project,
 1075 Goddard Earth Sciences Data and Information Services Center (GES DISC), <http://disc.gsfc.nasa.gov>,
 1076 NASA Goddard Space Flight Center, Code 610.2, Greenbelt, MD 20771 USA, 2013a.
 1077 Froidevaux, L., Anderson, J., Fuller, R. A., Bernath, P. F., Livesey, N. J., Russell III, J. M., and
 1078 Walker, K. A.: GOZCARDS Merged Data for Hydrogen Chloride Monthly Zonal Means on a Geodetic
 1079 Latitude and Pressure Grid, version 1.01, Greenbelt, MD, USA: NASA Goddard Earth Science Data and
 1080 Information Services Center, accessible from doi:10.5067/MEASURES/GOZCARDS/DATA3002,
 1081 2013b.
 1082 Froidevaux, L., Fuller, R. A., Lambert, A., Livesey, N. J., Bernath, P. F., Livesey, N. J., and Walker,
 1083 K. A.: GOZCARDS Merged Data for Nitrous Oxide Monthly Zonal Means on a Geodetic Latitude and
 1084 Pressure Grid, version 1.01, Greenbelt, MD, USA: NASA Goddard Earth Science Data and Information
 1085 Services Center, accessible from doi:10.5067/MEASURES/GOZCARDS/DATA3013, 2013c.
 1086 Froidevaux, L., Fuller, R. A., Santee, M. L., Manney, G. L., Livesey, N. J., Bernath, P. F., and Walker,
 1087 K. A.: GOZCARDS Merged Data for Nitric Acid Monthly Zonal Means on a Geodetic Latitude and
 1088 Pressure Grid, version 1.01, Greenbelt, MD, USA: NASA Goddard
 1089 Earth Science Data and Information Services Center, accessible from
 1090 doi:10.5067/MEASURES/GOZCARDS/DATA3008, 2013d.
 1091 Fueglistaler, S.: Step-wise changes in stratospheric water vapor? *J. Geophys. Res.*, 117, D13302,
 1092 doi:10.1029/2012JD017582, 2012.
 1093 Gebhardt, C., Rozanov, A., Hommel, R., Weber, M., Bovensmann, H., Burrows, J. P., Degenstein, D.,
 1094 Froidevaux, L., and Thompson, A. M.: Stratospheric ozone trends and variability as seen by

1095 SCIAMACHY from 2002 to 2012, *Atmos. Chem. Phys.*, 14, 831–846, doi:10.5194/acp-14-831-2014,
 1096 2014.
 1097
 1098 Haefele, A., Hocke, K., Kampfer, N., Keckhut, P., Marchand, M., Bekki, S., Morel, B.,
 1099 Egorova, T., and Rozanov, E.: Diurnal changes in middle atmospheric H₂O and O₃: Observations in the
 1100 Alpine region and climate models, *J. Geophys. Res.*, 113, D17303, doi:10.1029/2008JD009892, 2008.
 1101 Harris, N. R. P., Hassler, B., Tummon, F., Bodeker, G. E., Hubert, D., Petropavlovskikh, I., Steinbrecht,
 1102 W., Anderson, J., Bhartia, P. K., Boone, C. D., Bourassa, A., Davis, S. M., Degenstein, D., Delcloo, A.,
 1103 Frith, S. M., Froidevaux, L., Godin-Beekmann, S., Jones, N., Kurylo, M. J., Kyrölä, E., Laine, M.,
 1104 Leblanc, S. T., Lambert, J.-C., Liley, B., Mahieu, E., Maycock, A., de Maziere, M., Parrish, A., Querel,
 1105 R., Rosenlof, K. H., Roth, C., Sioris, C., Staehelin, J., Stolarski, R. S., Stubi, R., Tamminen, J.,
 1106 Vigouroux, C., Walker, K., Wang, H. J., Wild, J., and Zawodny, J. M.: Past changes in the vertical
 1107 distribution of ozone - Part 3: Analysis and interpretation of trends, *Atmos. Chem. Phys.*, in press, 2015.
 1108 Hassler, B., Bodeker, G. E., Solomon, S., and Young, P. J.: Changes in the polar vortex: Effects on
 1109 Antarctic total ozone observations at various stations, *Geophys. Res. Lett.*, 38, L01805,
 1110 doi:10.1029/2010GL045542, 2011.
 1111 Hegglin, M. I., Tegtmeier, S., Anderson, J., Froidevaux, L., Fuller, R., Funke, B., Jones, A., Lingenfelser,
 1112 G., Lumpe, J., Pendlebury, D., Remsberg, E., Rozanov, A., Toohey, M., Urban, J., von Clarmann, T.,
 1113 Walker, K. A., Wang, R., and Weigel, K.: SPARC Data Initiative: Comparison of water vapor
 1114 climatologies from international satellite limb sounders, *J. Geophys. Res. Atmos.*, 118, 11,824–11,846,
 1115 doi: 10.1002/jgrd.50752, 2013.
 1116 Hervig, M., and McHugh, M.: Cirrus detection using HALOE measurements, *Geophys. Res. Lett.*, 26,
 1117 No. 6, 719-722, 1999.
 1118 Huang, F. T., Mayr, H. G., Russell III, J. M., and Mlynczak, M. G.: Ozone diurnal variations in the
 1119 stratosphere and lower mesosphere, based on measurements from SABER on TIMED,
 1120 *J. Geophys. Res.*, 115, D24308, doi:10.1029/2010JD014484, 2010.
 1121 Hubert, D., et al., Ground-based assesment of the bias and long-term stability of fourteen limb and
 1122 occultation ozone profile data records, *Atmos. Meas. Tech.*, in review, 2015.
 1123 Hurst, D. F., Lambert, A., Read, W. G., Davis, S. M., Rosenlof, K. H., Hall, E. G., Jordan, A. F., and
 1124 Oltmans, S. J.: Validation of Aura Microwave Limb Sounder stratospheric water vapor measurements by

1125 the NOAA frost point hygrometer, *J. Geophys. Res. Atmos.*, 119, 1612-1625,
 1126 doi:10.1002/2013JD020757, 2014.

1127 Jiang, J. H., Su, H., Zhai, C., Perun, V. S., Del Genio, A., Nazarenko, L. S., Donner, L. J., Horowitz, L.,
 1128 Seman, C., Cole, J., Gettelman, A., Ringer, M. A., Rotstayn, L., Jeffrey, S., Wu, T., Brient, F., Dufresne,
 1129 J.-L., Kawai, H., Koshiro, T., Watanabe, M., L'Écuyer, T. S., Volodin, E. M., Iversen, T., Drange, H.,
 1130 Mesquita, M. D. S., Read, W. G., Waters, J. W., Tian, B., Teixeira, J., and Stephens, G. L.: Evaluation of
 1131 cloud and water vapor simulations in CMIP5 climate models using NASA "A-Train" satellite
 1132 observations, *J. Geophys. Res.*, 117, D14105, doi:10.1029/2011JD017237, 2012.

1133 Jones, A., Urban, J., Murtagh, D. P., Eriksson, P., Brohede, S., Haley, C., Degenstein, D., Bourassa, A.,
 1134 von. Savigny, C., Sonkaew, T., Rozanov, A., Bovensmann, H., and Burrows, J.: Evolution of
 1135 stratospheric ozone and water vapour time series studied with satellite measurements, *Atmos. Chem.*
 1136 *Phys.*, 9, 6055-6075, doi:10.5194/acp-9-6055-2009, 2009.

1137 Jones, A., Urban, J., Murtagh, D. P., Sanchez, C., Walker, K. A., Livesey, N. J., Froidevaux, L., and
 1138 Santee, M. L.: Analysis of HCl and ClO time series in the upper stratosphere using satellite data sets,
 1139 *Atmos. Chem. Phys.*, 11, 5321-5333, doi:10.5194/acp-11-5321-2011, 2011.

1140 Kirgis, G., Leblanc, T., McDermid, I. S., and Walsh, T. D.: Stratospheric ozone interannual variability
 1141 (1995–2011) as observed by Lidar and Satellite at Mauna Loa Observatory, HI and Table Mountain
 1142 Facility, CA, *Atmos. Chem. Phys.*, 13, 5033–5047, doi:10.5194/acp-13-5033-2013, 2013.
 1143

1144 Kley, D., Stone, E. J., Henderson, W. R., Drummond, J. W., Harrop, W. J., Schmeltekopf, A. L.,
 1145 Thompson, T. L., and Winkler, R. H.: In Situ Measurements of the Mixing Ratio of Water Vapor in the
 1146 Stratosphere, *J. Atmos. Sci.*, 36, 2513-2524, 1979.
 1147

1148 Kohlhepp, R., Ruhnke, R., Chipperfield, M. P., De Maziere M., Notholt, J., Barthlott, S., Batchelor, R. L.,
 1149 Blatherwick, R. D., Blumenstock, T., Coffey, M. T., Demoulin, P., Fast, H., Feng, W., Goldman, A.,
 1150 Griffith, D. W. T., Hamann, K., Hannigan, J. W., Hase, F., Jones, N. B., Kagawa, A., Kaiser, I., Kasai, Y.,
 1151 Kirner, O., Kouker, W., Lindenmaier, R., Mahieu, E., Mittermeier, R. L., Monge-Sanz, B., Morino, I.,
 1152 Murata, I., Nakajima, H., Palm, M., Paton-Walsh, C., Raffalski, U., Reddmann, T., Rettinger, M.,
 1153 Rinsland, C. P., Rozanov, E., Schneider, M., Senten, C., Servais, C., Sinnhuber, B.-M., Smale, D., Strong,
 1154 K., Sussmann, R., Taylor, J. R., Vanhaelewyn, G., Warneke, T., Whaley, C., Wiehle, M., and Wood, S.
 1155 W.: Observed and simulated time evolution of HCl, ClONO₂, and HF total column abundances, *Atmos.*

1156 Chem. Phys., 12, 3527–3557, doi:10.5194/acp-12-3527-2012, 2012.

1157

1158 Kuttippurath, J., Lefevre, F., Pommereau, J.-P., Roscoe, H. K., Goutail, F., Pazmino, A., and Shanklin, J.

1159 D.: Antarctic ozone loss in 1979–2010: first sign of ozone recovery, *Atmos. Chem. Phys.*, 13, 1625–1635,

1160 doi:10.5194/acp-13-1625-2013, 2013.

1161 Kyrölä, E., Laine, M., Sofieva, V., Tamminen, J., Päivärinta, S.-M., Tukiainen, S., Zawodny, J., and

1162 Thomason, L.: Combined SAGE II-GOMOS ozone profile data set for 1984-2011 and trend analysis of

1163 the vertical distribution of ozone, *Atmos. Chem. Phys.*, 13, 10,645-10,658, doi:10.5194/acp-13-10645-

1164 2013, 2013.

1165 Lambert, A., Read, W. G., Livesey, N. J., Santee, M. L., Manney, G. L., Froidevaux, L.,

1166 Wu, D. L., Schwartz, M. J., Pumphrey, H. C., Jimenez, C., Nedoluha, G. E., Cofield, R. E., Cuddy, D. T.,

1167 Daffer, W. H., Drouin, B. J., Fuller, R. A., Jarnot, R. F., Knosp, B. W., Pickett, H. M., Perun, V. S.,

1168 Snyder, W. V., Stek, P. C., Thurstans, R. P., Wagner, P. A., Waters, J. W., Jucks, K. W., Toon, G. C.,

1169 Stachnik, R. A., Bernath, P. F., Boone, C. D., Walker, K. A., Urban, J., Murtagh, D., Elkins, J. W., and

1170 Atlas, E.: Validation of the Aura Microwave Limb Sounder stratospheric water vapour and nitrous oxide

1171 measurements, *J. Geophys. Res.*, 112, D24S36, doi:10.1029/2007JD008724, 2007.

1172 Livesey, N. J., Read, W. J., Froidevaux, L., Waters, J. W., Santee, M. L., Pumphrey, H. C., Wu, D. L.,

1173 Shippony, Z., and Jarnot, R. F.: The UARS Microwave Limb Sounder version 5 dataset: Theory,

1174 characterization and validation, *J. Geophys. Res.*, 108 (D13), 4378, doi:10.1029/2002JD002273, 2003.

1175 Livesey, N. J., Read, W. G., Froidevaux, L., Lambert, A., Manney, G. L., Pumphrey, H. C., Santee, M.

1176 L., Schwartz, M. J., Wang, S., Cofield, R. E., Cuddy, D. T., Fuller, R. A., Jarnot, R. F., Jiang, J. H.,

1177 Knosp, B. W., Stek, P. C., Wagner, P. A., and Wu, D. L.: EOS MLS Version 3.3/3.4 Level 2 data quality

1178 and description document, Tech. rep., Jet Propulsion Laboratory, available from <http://mls.jpl.nasa.gov/>,

1179 2013.

1180 Mahieu, E., Duchatelet, P., Demoulin, P., Walker, K. A., Dupuy, E., Froidevaux, L., Randall, C., Catoire,

1181 V., Strong, K., Boone, C. D., Bernath, P. F., Blavier, J.-F., Blumenstock, T., Coffey, M., DeMaziere, M.,

1182 Griffith, D., Hannigan, J., Hase, F., Jones, N., Jucks, K. W., Kagawa, A., Kasai, Y., Mebarki, Y.,

1183 Mikuteit, S., Nassar, R., Notholt, J., Rinsland, C. P., Robert, C., Schrems, O., Senten, C., Smale, D.,

1184 Taylor, J., Tetard, C., Toon, G. C., Warneke, T., Wood, S. W., Zander, R., and Servais, C.: Validation of

1185 ACE-FTS v2.2 measurements of HCl, HF, CCl₃F and CCl₂F₂ using space-, balloon- and ground-based
 1186 instrument observations, *Atmos. Chem. Phys.*, 8, 6199-6221, doi:10.5194/acp-8-6199-2008, 2008.

1187 Mahieu, E., Zander, R., Bernath, P. F., Boone, C. D., and Walker, K. A.: Recent trend anomaly of
 1188 hydrogen chloride (HCl) at northern mid-latitudes derived from Jungfraujoch, HALOE, and ACE-FTS
 1189 infrared solar observations, in: *The Atmospheric Chemistry Experiment ACE at 10: a solar occultation*
 1190 *anthology*, Bernath, P. (Ed.), Deepak Publishing, Hampton, VA, 239-249, 2013.

1191 Mahieu, E., Chipperfield, M. P., Notholt, J., Reddmann, T., Anderson, J., Bernath, P. F., Blumenstock, T.,
 1192 Coffey, M. T., Dhomse, S. S., Feng, W., Franco, B., Froidevaux, L., Griffith, D. W. T., Hannigan, J. W.,
 1193 Hase, F., Hossaini, R., Jones, N. B., Morino, I., Murata, I., Nakajima, H., Palm, M., Paton-Walsh, C.,
 1194 Russell III, J. M., Schneider, M., Servais, C., Smale, D., and Walker, K. A.: Recent Northern Hemisphere
 1195 stratospheric HCl increase due to atmospheric circulation changes, *Nature*, 515, 104-107,
 1196 doi:10.1038/nature13857, 2014.

1197 McCormick, M. P., Zawodny, J. M., Veiga, R. E., Larsen, J. C., and Wang, P. H.: An overview of SAGE-
 1198 I and II ozone measurements, *Planetary and Space Science*, 37, No. 12, 1567-1586, 1989.

1199 McHugh, M., Hervig, M., Magill, B., Thompson, R. E., Remsberg, E., Wrotny, J., and
 1200 Russell, J. M.: Improved mesospheric temperature, water vapor, and polar mesospheric cloud extinctions
 1201 from HALOE, *Geophys. Res. Lett.*, 30, 8, doi: 10.1029/2002GL016859, 2003.

1202 McLinden, C. A., Tegtmeier, S., and Fioletov, V.: Technical Note: A SAGE-corrected SBUV zonal-mean
 1203 ozone data set, *Atmos. Chem. Phys.*, 9, 7963–7972, doi:10.5194/acp-9-7963-2009, 2009.

1204 McPeters, R. D., Bhartia, P. K., Haffner, D., Labow, G. J. and Flynn, L.: The v8.6 SBUV Ozone Data
 1205 Record: An Overview, *J. Geophys. Res.*, 118, 8032-8039, doi:10.1002/jgrd.50597, 2013.

1206 Molina, M. J., and Rowland, F. S.: Stratospheric sink for chlorofluoromethane: chlorine atom-catalyzed
 1207 destruction of ozone, *Nature*, 249, 810-812, 1974.

1208 Montzka, S. A., Butler, J. H., Elkins, J. W., Thompson, T. M., Clarke, A. D., and Lock, L. T.: Present
 1209 and future trends in the atmospheric burden of ozone-depleting halogens, *Nature*, 398, 690-694, 1999.

1210 Morris, G. A., Gleason, J. F., Russell III, J. M., Schoeberl, M. R., and McCormick, M. P.: A comparison
 1211 of HALOE V19 with SAGE II V6.00 ozone observations using trajectory mapping, *J. Geophys. Res.*,
 1212 107, D13, 4177, doi:10.1029/2001JD000847, 2002.

1213 Mote, P. W., Rosenlof, K. H., McIntyre, M. E., Carr, E. S., Gille, J. C., Holton, J. R., Kinnersley, J. S.,
 1214 Pumphrey, H. C., Russell III, J. M., and Waters, J. W.: An atmospheric tape recorder: The imprint of
 1215 tropical tropopause temperatures on stratospheric water vapor,
 1216 *J. Geophys. Res.*, 101, 3989–4006, 1996.

1217 Nair, P. J., Godin-Beekmann, S., Froidevaux, L., Flynn, L. E., Zawodny, J. M., Russell III, J. M.,
 1218 Pazmino, A., Ancellet, G., Steinbrecht, W., Claude, H., Leblanc, T., McDermid, S., van Gijssel, J. A. E.,
 1219 Johnson, B., Thomas, A., Hubert, D., Lambert, J.-C., Nakane, H., and Swart, D. P. J.: Relative drifts and
 1220 stability of satellite and ground-based stratospheric ozone profiles at NDACC lidar stations, *Atmos.*
 1221 *Meas. Tech.*, 5, 1301–1318, doi: 10.5194/amt-5-1301-2012, 2012.

1222 Nair, P. J., Godin-Beekmann, S., Kuttippurath, J., Ancellet, G., Goutail, F., Pazmiño, A., Froidevaux, L.,
 1223 Zawodny, J. M., Evans, R. D., Wang, H.-J., Anderson, A., and Pastel, M.: Ozone trends derived from the
 1224 total column and vertical profiles at a northern mid-latitude station, *Atmos. Chem. Phys.*, 13, 10373–
 1225 10384, doi:10.5194/acp-13-10373-2013, 2013.

1226

1227 Nair, P. J., Froidevaux, L., Kuttippurath, J., Zawodny, J. M., Russell III, J. M., Steinbrecht, W., Claude,
 1228 H., Leblanc, T., van Gijssel, J. A. E., Johnson, B., Swart, D. P. J., Thomas, A., Querel, R., Wang, R., and
 1229 Anderson, J.: Subtropical and midlatitude ozone trends in the stratosphere: Implications for recovery, *J.*
 1230 *Geophys. Res.*, 120, 7247–7257, doi:10.1002/2014JD022371, 2015.

1231 Nazaryan, H., McCormick, M. P., and Russell III, J. M.: New studies of SAGE II and HALOE ozone
 1232 profile and long-term change comparisons, *J. Geophys. Res.*, 110, D09305, doi:10.1029/2004JD005425,
 1233 2005.

1234 Nedoluha, G. E., Gomez, R. M., Hicks, B. C., Bevilacqua, R. M., Russell III, J. M.,
 1235 Connor, B. J., and Lambert, A.: A comparison of middle atmospheric water vapor as measured by
 1236 WVMS, EOS-MLS, and HALOE, *J. Geophys. Res.*, 112, D24S39, doi:10.1029/2007JD008757, 2007.

1237

1238 Nedoluha, G. E., Gomez, R. M., Hicks, B. C., Wrotny, J. E., Boone, C., and Lambert, A.: Water vapor
 1239 measurements in the mesosphere from Mauna Loa over solar cycle 23, *J. Geophys. Res.*, 114, D23303,
 1240 doi:10.1029/2009JD012504, 2009.

1241

1242 Nedoluha, G., Gomez, R. M., Hicks, B. C., Helmboldt, J., Bevilacqua, R. M., and Lambert, A.: Ground-
 1243 based microwave measurements of water vapor from the midstratosphere to the mesosphere, *J. Geophys.*

1244 Res., 116, D02309, doi:10.1029/2010JD014728., 2011.

1245

1246 Newchurch, M. J., Yang, E. S., Cunnold, D. M., Reinsel, G. C., Zawodny, J. M., and
 1247 Russell III, J. M.: Evidence for slowdown in stratospheric ozone loss: First stage of ozone recovery, J.
 1248 Geophys. Res., 108, D16, doi:10.1029/2003JD003471, 2003.

1249 Parrish, A., Boyd, I. S., Nedoluha, G. E., Bhartia, P. K., Frith, S. M., Kramarova, N. A.,
 1250 Connor, B. J., Bodeker, G. E., Froidevaux, L., Shiotani, M., and Sakazaki, T.: Diurnal variations of
 1251 stratospheric ozone measured by ground-based microwave remote sensing at the Mauna Loa NDACC
 1252 site: measurement validation and GEOSCCM model comparison, Atmos. Chem. Phys., 7255-7272,
 1253 doi:10.5194/acp-14-7255-2014, 2014.

1254 Perliski, L. M., Solomon, S., and London, J.: On the interpretation of seasonal variations of stratospheric
 1255 ozone, Planet. Space Sci., 37, 12, 1527-1538, 1989.

1256 Pumphrey, H. C.: Validation of a new prototype water vapor retrieval for UARS MLS,
 1257 J. Geophys. Res., 104 (D8), 9399-9412, 1999.

1258 Pumphrey, H. C., Clark, H. L., and Harwood, R. S.: Lower stratospheric water vapor as measured by
 1259 UARS MLS, Geophys. Res. Lett., 27, 1691-1694, 2000.

1260 Randel, W. J., Wu, F., Oltmans, S. J., Rosenlof, K., and Nedoluha, G. E.: Interannual changes of
 1261 stratospheric water vapor and correlations with tropical tropopause temperatures, J. Atmos. Sci., 61,
 1262 2133-2148, 2004.

1263

1264 Read, W. G., Lambert, A., Bacmeister, J., Cofield, R. E., Christensen, L. E., Cuddy, D. T., Daffer, W.
 1265 H., Drouin, B. J., Fetzer, E., Froidevaux, L., Fuller, R., Herman, R., Jarnot, R. F., Jiang, J. H., Jiang, Y.
 1266 B., Kelly, K., Knosp, B. W., Kovalenko, L. J., Livesey, N. J., Liu, H.-C., Manney, G. L., Pickett, H. M.,
 1267 Pumphrey, H. C., Rosenlof, K. H., Sabouchi, X., Santee, M. L., Schwartz, M. J., Snyder, W. V., Stek, P.
 1268 C., Su, H., Takacs, L. L., Thurstans, R. P., Voemel, H., Wagner, P. A., Waters, J. W., Webster, C. R.,
 1269 Weinstock, E. M., and Wu, D. L.: Aura Microwave Limb Sounder upper tropospheric and lower
 1270 stratospheric H₂O and relative humidity with respect to ice validation, J. Geophys. Res., 112, D24S35,
 1271 doi:10.1029/2007JD008752, 2007.

1272

1273 Read, W. G., Schwartz, M. J., Lambert, A., Su, H., Livesey, N. J., Daffer, W. H., and
 1274 Booe, C. D.: The roles of convection, extratropical mixing, and in-situ freeze-drying in the Tropical

1275 Tropopause Layer, *Atmos. Chem. Phys.*, 8, 6051–6067, doi:10.5194/acp-8-6051-2008, 2008.

1276

1277 Remsberg, E.: Observed seasonal to decadal scale responses in mesospheric water vapor,

1278 *J. Geophys. Res.*, 115, D06306, doi:10.1029/2009JD012904, 2010.

1279

1280 Ricaud, P., de La Noë, J., Connor, B. J., Froidevaux, L., Waters, J. W., Harwood, R. S., MacKenzie, I. A.,

1281 and Peckham, G. E.: Diurnal variability of mesospheric ozone as measured by the UARS microwave limb

1282 sounder instrument: Theoretical and ground-based validations, *J. Geophys. Res.*, 101 (D6), 10,077–

1283 10,089, doi:10.1029/95JD02841, 1996.

1284

1285 Rienecker, M., Suarez, M. J., Gelaro, R., Todling, R., Bacmeister, J., Liu, E., Bosilovich, M. G.,

1286 Schubert, S. D., Takacs, L., Kim, G.-K., Bloom, S., Chen, J., Collins, D., Conaty, A.,

1287 da Silva, A., Gu, W., Joiner, J., Koster, R. D., Lucchesi, R., Molod, A., Owens, T., Pawson, S., Pegion,

1288 P., Redder, C. R., Reichle, R., Robertson, J., F. R., Ruddick, A. G., Sienkiewicz, M., and Woollen, J.:

1289 MERRA: NASA’s Modern-Era Retrospective Analysis for Research and Applications, *J. Climate*, 24,

1290 3624–3648, doi:10.1175/JCLI-D-11-00015.1, 2011.

1291

1292 Russell III, J. M., Gordley, L. L., Park, J. H., Drayson, S. R., Hesketh, D. H., Cicerone, R. J., Tuck, A. F.,

1293 Frederick, J. E., Harries, J. E., and Crutzen, P.: The Halogen Occultation Experiment, *J. Geophys. Res.*,

1294 98, 10777-10797, 1993.

1295 Russell III, J. M., Deaver, L. E., Luo, M., Park, J. H., Gordley, L. L., Tuck, A. F., Toon, G. C., Gunson ,

1296 M. R., Traub, W. A., Johnson, D. G., Jucks, K. W., Murcray, D. G., Zander, R.,

1297 Nolt, I. G., and Webster, C. R.: Validation of hydrogen chloride measurements made by the Halogen

1298 Occultation Experiment from the UARS platform, *J. Geophys. Res.*, 101 (D6), 10,151– 10,162, 1996.

1299 Sakazaki, T., Fujiwara, M., Mitsuda, C., Imai, K., Manago, N., Naito, Y., Nakamura, T., Akiyoshi, H.,

1300 Kinnison, D., Sano, T., Suzuki, M., and Shiotani, M.: Diurnal ozone variations in the stratosphere

1301 revealed in observations from the Superconducting Submillimeter-Wave Lime-Emission Sounder

1302 (SMILES) on board the International Space Station (ISS), *J. Geophys. Res. Atmos.*, 118, 2991-3006,

1303 doi:10.1002/jgrd.50220, 2013.

1304 Santee, M. L., Lambert, A., Read, W. G., Livesey, N. J., Cofield, R. E., Cuddy, D. T.,

1305 Daffer, W. H., Drouin, B. J., Froidevaux, L., Fuller, R. A., Jarnot, R. F., Knosp, B. W.,

1306 Manney, G. L., Perun, V. S., Snyder, W. V., Stek, P. C., Thurstans, R. P., Wagner, P. A.,
 1307 Waters, J. W., Muscari, G., de Zafra, R. L., Dibb, J. E., Fahey, D. W., Popp, P. J., Marcy, T. P., Jucks, K.
 1308 W., Toon, G. C., Stachnik, R. A., Bernath, P. F., Boone, C. D., Walker, K. A.,
 1309
 1310 Urban, J., and Murtagh, D.: Validation of the Aura Microwave Limb Sounder HNO₃ measurements, *J.*
 1311 *Geophys. Res.*, 112, D24S40, doi:10.1029/2007JD008, 2007.
 1312 Salby, M., Titova, E., and Deschamps, L.: Rebound of Antarctic ozone, *Geophys. Res. Lett.*, 38, L09702,
 1313 doi:10.1029/2011GL047266, 2011.
 1314 Salby, M. L., Titova, E. A., and Deschamps, L.: Changes of the Antarctic ozone hole: Controlling
 1315 mechanisms, seasonal predictability, and evolution, *J. Geophys. Res.*, 117, D10111,
 1316 doi:10.1029/2011JD016285, 2012.
 1317 Schwartz, M. J., Froidevaux, L., Fuller, R. A., and Pawson, S.: GOZCARDS Merged Data for
 1318 Temperature Monthly Zonal Means on a Geodetic Latitude and Pressure Grid, version 1.01, Greenbelt,
 1319 MD, USA: NASA Goddard Earth Science Data and Information Services Center, accessible from
 1320 doi:10.5067/MEASURES/GOZCARDS/DATA3023, 2013.
 1321 Shepherd, T. G., Plummer, D. A., Scinocca, J. F., Hegglin, M. I., Fioletov, V. E., Reader, M. C., Remsberg,
 1322 E., von Clarmann, T., and Wang, H. J.: Reconciliation of halogen-induced ozone loss with the total-
 1323 column ozone record, *Nature Geoscience*, 7, 443-449, doi:10.1038/NCEO2155, 2014.
 1324
 1325 Solomon P. M., Barrett, J., Mooney, T., Connor, B., Parrish, A., and Siskind, D. E.: Rise and decline of
 1326 active chlorine in the stratosphere, *Geophys. Res. Lett.*, 33, L18807, doi:10.1029/2006GL027029, 2006.
 1327 Sofieva, V. F., Kalakoski, N., Päiväranta, S.-M., Tamminen, J., Laine, M., and Froidevaux, L.: On
 1328 sampling uncertainty of satellite profile ozone measurements, *Atmos. Meas. Tech.*, 7, 1891–1900,
 1329 doi:10.5194/amt-7-1891-2014, 2014.
 1330 Solomon, S.: Stratospheric ozone depletion: A review of concepts and history, *Rev. Geophys.*, 37, 275–
 1331 316, doi:10.1029/1999RG900008, 1999.

1332 Solomon, S., Rosenlof, K., Portmann, R., Daniel, J., Davis, S., Sanford, T., and Plattner, G.-K.:
 1333 Contributions of Stratospheric Water Vapor to Decadal Changes in the Rate of Global Warming, *Science*,
 1334 237, 1219-1223, 2010.

1335 SPARC: Assessment of Trends in the Vertical Distribution of Ozone, edited by N. Harris, R. Hudson and
 1336 C. Phillips, SPARC/IOC/GAW, SPARC Rep. 1, WMO Ozone Res. Monit. Project Rep. 43, 1998.

1337 SPARC WAVAS: Assessment of upper tropospheric and stratospheric water vapour, World Climate
 1338 Research Programme, WCRP-113, WMO/TD-No.1043, 261-264, 2000.

1339 Steinbrecht, W., Koehler, U., Claude, H., Weber, M., Burrows, J. P., and van der A, R. J.: Very high
 1340 ozone columns at northern mid latitudes in 2010, *Geophys. Res. Lett.*, 38, L06803,
 1341 doi:10.1029/2010GL046634, 2011.

1342 Strong, K., Wolff, M. A., Kerzenmacher, T. E., Walker, K. A., Bernath, P. F., Blumenstock, T., Boone,
 1343 C., Catoire, V., Coffey, M., De Maziere, M., Demoulin, P., Duchatelet, P., Dupuy, E., Hannigan, J.,
 1344 Hopfner, M., Glatthor, N., Griffith, D. W. T., Jin, J. J., Jones, N., Jucks, K., Kuellmann, H., Kuttippurath,
 1345 J., Lambert, A., Mahieu, E., McConnell, J. C., Mellqvist, J., Mikuteit, S., Murtagh, D. P., Notholt, J.,
 1346 Piccolo, C., Raspollini, P., Ridolfi, M., Robert, C., Schneider, M., Schrems, O., Semeniuk, K., Senten, C.,
 1347 Stiller, G. P., Strandberg, A., Taylor, J., Tetard, C., Toohey, M., Urban, J., Warneke, T., and Wood, S.:
 1348 Validation of ACE-FTS N₂O measurements, *Atmos. Chem. Phys.*, 8, 4759-4786, doi:10.5194/acp-8-
 1349 4759-2008, 2008.

1350 Tegtmeier, S., Hegglin, M. I., Anderson, J., Bourassa, A., Brohede, S., Degenstein, D., Froidevaux, L.,
 1351 Fuller, R., Funke, B., Gille, J., Jones, A., Kasai, Y., Krüger, K., Kyrölä, E., Lingenfelser, G., Lumpe, J.,
 1352 Nardi, B., Neu, J., Pendlebury, D., Remsberg, E., Rozanov, A., Smith, L., Toohey, M., Urban, J., von
 1353 Clarmann, T., Walker, K. A., and Wang, H. J.: The SPARC Data Initiative: A comparison of ozone
 1354 climatologies from international satellite limb sounders, *J. Geophys. Res. Atmos.*, 118, 12,229–12,247,
 1355 doi: 10.1002/2013JD019877, 2013.

1356 Toohey, M., Hegglin, M. I., Tegtmeier, S., Anderson, J., Añel, J. A., Bourassa, A., Brohede, S.,
 1357 Degenstein, D., Froidevaux, L., Fuller, R., Funke, B., Gille, J., Jones, A., Kasai, Y., Krüger, K., Kyrölä,
 1358 E., Neu, J. L., Rozanov, A., Smith, L., Urban, J., von Clarmann, T., Walker, K. A., and Wang, R.:
 1359 Characterizing sampling bias in the trace gas climatologies of the SPARC Data Initiative, *J. Geophys.*
 1360 *Res. Atmos.*, 118, 11,847–11,862, doi: 10.1002/jgrd.5087, 2013.

1361 Tummon, F., Hassler, B., Harris, N. R. P., Staehelin, J., Steinbrecht, W., Anderson, J.,
 1362 Bodeker, G. E., Bourassa, A., Davis, S. M., Degenstein, D., Frith, S. M., Froidevaux, L.,
 1363 Kyrölä, E., Laine, M., Long, C., Penckwitt, A. A., Sioris, C. E., Rosenlof, K. H., Roth, C.,
 1364 Wang, H.-J., and Wild, J.: Intercomparison of vertically resolved merged satellite ozone data sets:
 1365 interannual variability and long-term trends, *Atmos. Chem. Phys.*, 15, 3021-3043, doi: 10.5194/acp-15-
 1366 3021-2015, 2015.

1367 Urban, J., Lantié, N., Murtagh, D. P., Eriksson, P., Kasai, Y., Lossow, S., Dupuy, E.,
 1368 de LaNoë, J., Frisk, U., Olberg, M., Flochmoën, E. Le., and Ricaud, P.: Global observations of middle
 1369 atmospheric water vapour by the Odin satellite: An overview, *Planet. Space Sci.*, 55, 9, 1093-1102, 2007.

1370 Urban, J., Lossow, S., Stiller, G., and Read, W.: Another drop in water vapor, *EOS Transactions,*
 1371 *American Geophysical Union*, 95, 27, 245-252, doi:10.1002/2014EO270001, 2014.

1372 Veiga, R.E., Cunnold, D. M., Chu, W. P., and McCormick, M. P.: Stratospheric Aerosol and Gas
 1373 Experiments I and II comparisons with ozonesondes. *J. Geophys. Res.*, 100 (D5), 9073-9090, 1995.

1374 Voemel, H., Barnes, J. E., Forno, R. N., Fujiwara, M., Hasebe, F., Iwasaki, S., Kivi, R., Komala, N.,
 1375 Kyrölä, E., Leblanc, T., Morel, B., Ogino, S.-Y., Read, W. G., Ryan, S. C., Saraspriya, S., Selkirk, H.,
 1376 Shiotani, M., Valverde Canossa, J., and Whiteman, D. N.: Validation of Aura Microwave Limb Sounder
 1377 water vapor by balloon-borne Cryogenic Frost point Hygrometer measurements, *J. Geophys. Res.*, 112,
 1378 D24S37, doi:10.1029/2007JD008698, 2007.

1379 Wang, H. J., Cunnold, D. M., and Bao, X.: A critical analysis of Stratospheric Aerosol and Gas
 1380 Experiment ozone trends *J. Geophys. Res.*, 101 (D7), 12495-12514, 1996.

1381 Wang, H. J., Cunnold, D. M., Thomason, L. W., Zawodny, J. M., and Bodeker, G. E.: Assessment of
 1382 SAGE version 6.1 ozone data quality, *J. Geophys. Res.*, 107 (D23),
 1383 doi: 10.1029/2002JD002418, 2002.

1384 Wang, H. J., Cunnold, D. M., Trepte, C., Thomason, L. W., and Zawodny, J. M.: SAGE III solar ozone
 1385 measurements: Initial results, *Geophys. Res. Lett.*, 33, L03805, doi:10.1029/2005GL025099, 2006.

1386 Wang, R., Froidevaux, L., Anderson, J., Fuller, R. A., Bernath, P. F., McCormick, M. P., Livesey, N. J.,
 1387 Russell III, J. M., Walker, K. A., and Zawodny, J. M.: GOZCARDS Merged Data for Ozone Monthly
 1388 Zonal Means on a Geodetic Latitude and Pressure Grid, version 1.01, Greenbelt, MD, USA: NASA
 1389 Goddard Earth Science Data and Information Services Center, accessible from
 1390 doi:10.5067/MEASURES/GOZCARDS/DATA3006, 2013.

1391 Waters, J. W., Microwave limb sounding, in *Atmospheric Remote Sensing by Microwave Radiometry*,
1392 ed. by M. Janssen, chap. 8, John Wiley, New York, 1993.

1393 Waters, J. W., Froidevaux, L., Read, W. G., Manney, G. L., Eslon, L. S., Flower, D. A., Jarnot, R. F., and
1394 Harwood, R. S.: Stratospheric ClO and ozone from the Microwave Limb Sounder on the Upper
1395 Atmosphere Research Satellite, *Nature*, 362, 597-602, 1993.

1396 Waters, J. W., Froidevaux, L., Harwood, R. S., Jarnot, R. F., Pickett, H. M., Read, W. G., Siegel, P. H.,
1397 Cofield, R. E., Filipiak, M. J., Flower, D. A., Holden, J. R., Lau, G. K., Livesey, N. J., Manney, G. L.,
1398 Pumphrey, H. C., Santee, M. L., Wu, D. L., Cuddy, D. T., Lay, R. R., Loo, M. S., Perun, V. S., Schwartz,
1399 M. J., Stek, P. C., Thurstans, R. P., Boyles, M. A., Chandra, S., Chavez, M. C., Chen, G.-S., Chudasama,
1400 B. V., Dodge, R., Fuller, R. A., Girard, M. A., Jiang, J. H., Jiang, Y., Knosp, B. W., LaBelle, R. C., Lam,
1401 J. C., Lee, K. A., Miller, M., Oswald, J. E., Patel, N. C., Pukala, D. M., Quintero, O., Scaff, D. M.,
1402 Snyder, W. V., Tope, M. C., Wagner, P. A., and Walch, M. J.: The Earth Observing System Microwave
1403 Limb Sounder (EOS MLS) on the Aura satellite, *IEEE Trans. Geosci. Remote Sens.*, 44 (5), 1075–1092,
1404 doi:10.1109/TGRS.2006.873771, 2006.

1405 Waugh, D. W., Considine, D. B., and Fleming, E. L.: Is Upper Stratospheric Chlorine Decreasing as
1406 Expected?, *Geophys. Res. Lett.*, 28(7), 1187–1190, 2001.

1407 WMO (World Meteorological Organization): Scientific Assessment of Ozone Depletion: 2002, Global
1408 Ozone Research and Monitoring Project – Report No. 47, Geneva, Switzerland, 2003.

1409 WMO (World Meteorological Organization), Scientific Assessment of Ozone Depletion: 2010, Global
1410 Ozone Research and Monitoring Project – Report No. 52, Geneva, Switzerland, 2011.

1411 WMO (World Meteorological Organization), Scientific Assessment of Ozone Depletion: 2014, Global
1412 Ozone Research and Monitoring Project – Report No. 55, Geneva, Switzerland, 2014.

1413 Wohltmann, I., Lehmann, R., Rex, M., Brunner, D., and Mader, J.A.: A process-oriented regression
1414 model for column ozone, *J. Geophys. Res.*, 112, D12304, doi:10.1029/2006JD007573, 2007.

1415 Wolff, M. A., Kerzenmacher, T., Strong, K., Walker, K. A., Toohey, M., Dupuy, E., Bernath, P. F.,
1416 Boone, C. D., Brohede, S., Catoire, V., von Clarmann, T., Coffey, M., Daffer, W. H., De Maziere, M.,
1417 Duchatelet, P., Glatthor, N., Griffith, D. W. T., Hannigan, J., Hase, F., Hopfner, M., Huret, N., Jones, N.,
1418 Jucks, K., Kagawa, A., Kasai, Y., Kramer, I., Kullmann, H., Kuttippurath, J., Mahieu, E., Manney, G.,
1419 McElroy, C. T., McLinden, C., Mebarki, Y., Mikuteit, S., Murtagh, D., Piccolo, C., Raspollini, P.,
1420 Ridolfi, M., Ruhnke, R., Santee, M., Senten, C., Smale, D., Tetard, C., Urban, J., and Wood, S.:

1421 Validation of HNO_3 , ClONO_2 , and N_2O_5 from the Atmospheric Chemistry Experiment Fourier Transform
 1422 Spectrometer (ACE-FTS), *Atmos. Chem. Phys.*, 8, 3529–3562, doi:10.5194/acp-8-3529-2008, 2008.
 1423 Yang, E.-S., Cunnold, D. M., Newchurch, M. J., Salawitch, R., McCormick, J. M. P., Russell III, J. M.,
 1424 Zawodny, J. M., and Oltmans, S. J.: First stage of Antarctic ozone recovery, *J. Geophys. Res.*, 113,
 1425 D20308, doi:10.1029/2007JD009675, 2008.
 1426 Ziemke, J. R., and Chandra, S.: Development of a climate record of tropospheric and stratospheric
 1427 column ozone from satellite remote sensing: evidence of an early recovery of global stratospheric ozone,
 1428 *Atmos. Chem. Phys.*, 12, 5737-5753, doi:10.5194/acp-12-5737-2012, 2012.
 1429 Ziemke, J. R., Chandra, S., and Bhartia, P. K.: A 25-year data record of atmospheric ozone from TOMS
 1430 Cloud Slicing: Implications for trends in stratospheric and tropospheric ozone, *J. Geophys. Res.*, 110,
 1431 D15105, doi:10.1029/2004JD005687, 2005.
 1432

1433 **Appendix A**

1434 **A.1. GOZCARDS data provenance**

1435 The general origin of the datasets is summarized here. Data coverage from limb sounders
1436 (including the instruments used here) is displayed nicely in the work by Toohey et al. (2013).

1437 ***SAGE I***

1438 SAGE I was launched February 18, 1979, aboard the Applications Explorer Mission-B
1439 (AEM-B) satellite. SAGE I was a sun photometer using solar occultation (Chu and McCormick,
1440 1979), and it collected a global database for nearly three years on stratospheric aerosol, O₃, and
1441 NO₂. For more information, the reader is referred to <http://sage.nasa.gov/SAGE1>.

1442 ***SAGE II***

1443 SAGE II was launched aboard the Earth Radiation Budget Satellite (ERBS) in October 1984
1444 and its data gathering period ended in August 2005. During each sunrise and sunset, SAGE II
1445 measured stratospheric aerosols, O₃, NO₂, and H₂O via solar occultation. This long dataset has
1446 proven very valuable in determining past ozone trends. For more information on and data access
1447 to the (V6.2) dataset used for GOZCARDS, the reader is referred to <http://sage.nasa.gov/SAGE2>.

1448 ***HALOE***

1449 Since its launch on September 12, 1991 from the Space Shuttle Discovery until November
1450 2005, UARS HALOE collected profiles of atmospheric composition and temperature. HALOE
1451 (Russell et al., 1993) used solar occultation to measure vertical profiles of O₃, HCl, HF, CH₄,
1452 H₂O, NO, NO₂, temperature, aerosol extinction, and aerosol composition and size distribution.
1453 More information and access to the HALOE data can be obtained from <http://haloe.gats-inc.com>
1454 and <http://disc.sci.gsfc.nasa.gov/UARS/data-holdings/HALOE>. For GOZCARDS purposes, we
1455 have used Version 19 HALOE netCDF data files available at <http://haloe.gats-inc.com>.

1456 ***UARS MLS***

1457 This instrument observed the Earth's limb in microwave emission using three radiometers, at
1458 frequencies near 63, 183 and 205 GHz (Waters, 1993; Barath et al., 1993), providing unique

daily global information on stratospheric ClO, along with other profiles, including O₃, H₂O, HNO₃, temperature, and cloud ice water content. The stratospheric H₂O data ceased on April 15, 1993, after the failure of the 183 GHz radiometer. After March 15, 1994, measurements became increasingly sparse in order to conserve the life of the MLS antenna scan mechanism and UARS power. Data exist until July 28, 1999, although for GOZCARDS, only data through mid-June 1997 are used, as data sparseness and degradation of the 63 GHz radiometer led to less ‘trend-quality’ data after this. Sampling patterns follow the alternating yaw cycles imposed on MLS by the precessing UARS orbit; MLS measurements were obtained continuously for all latitudes between 34°S and 34°N, with higher latitudes covered in either the northern or southern hemisphere with a roughly 36-day cycle. Livesey et al. (2003) provide more information on the UARS MLS instrument, retrievals, and results. For data access, the reader is directed to the relevant Goddard Earth Sciences and Information Services Center (GES DISC) data holdings at <http://disc.sci.gsfc.nasa.gov/UARS/data-holdings/MLS>. L3AT data files were used as the basis for the production of the GOZCARDS UARS MLS monthly source datasets.

ACE-FTS

ACE-FTS is the primary instrument onboard the SCISAT satellite, launched on August 12, 2003. It is a high spectral resolution (0.02 cm⁻¹) Michelson interferometer operating from 2.2 to 13.3 μm (750-4400 cm⁻¹); see Bernath et al. (2005) for an overview of the ACE mission. The instrument can simultaneously measure temperature and many trace gases (including all the species mentioned here for GOZCARDS), thin clouds, and aerosols, using the solar occultation technique. ACE-FTS data version 2.2, along with the version 2.2 update for ozone, were used here for GOZCARDS. For access to the public ACE-FTS datasets, with a routine measurement start date of March 2004, the reader is directed to <http://www.ace.uwaterloo.ca>.

Aura MLS

MLS is one of four instruments on NASA's Aura satellite, launched on July 15th 2004. Aura MLS is a greatly enhanced version of the UARS MLS experiment, providing better spatial coverage, vertical resolution, and vertical range, along with more continuous data over its lifetime (and with ongoing measurements at the time of writing). The instrument includes

radiometers at 118, 190, 240, and 640 GHz, and a 2.5 THz module (Waters et al., 2006). Aura MLS provides measurements of many chemical species, cloud ice, temperature and geopotential height. Continuous measurements have been obtained since August 2004, with the exception of OH, for which sparser measurements exist since August 2010, in order to preserve the life of the THz module. For more information and access to the Aura MLS datasets, the reader is referred to <http://disc.sci.gsfc.nasa.gov/Aura/data-holdings/MLS>. For GOZCARDS, we use the currently recommended Aura MLS data versions (version 2.2/2.3 for ozone and 3.3/3.4 for other species).

A.2. Calculation details for the iterative merging procedure

Given three time series, the merging procedure that we use first combines two out of the three time series, $y_1(i)$ and $y_2(i)$ (where index i represents time for each monthly mean value in a given latitude/pressure bin). We first obtain the temporary merged series $m_1(i)$ via:

$$m_1(i) = (1/2) (y_1(i) + y_2(i)) \quad (1)$$

with the average offsets for $y_1(i)$ and $y_2(i)$ being $(1/(2 n_{12})) \sum (y_1(i) - y_2(i))$ and -1 times this value, respectively; n_{12} is the number of overlapping data points between the two time series. Then, we merge together the time series $m_1(i)$ and $y_3(i)$, keeping the weightings equal for all 3 time series (1/3 for each), so that we calculate the new merged time series $m(i)$ via:

$$m(i) = w_m m_1(i) + w_3 y_3(i) = (1/3) (y_1(i) + y_2(i) + y_3(i)) \quad (2)$$

which will hold if the weights are $w_m = 2/3$ and $w_3 = 1/3$ (given equation (1) for $m_1(i)$). The average reference value (to which the adjustments of $m_1(i)$ and $y_3(i)$ in the 2nd step are made) is given by $(1/n_m) \sum ((2/3) m_1(i) + (1/3) y_3(i))$, where n_m represents the number of (overlapping pairs of) data values used in step 2. For the HCl and H₂O data merging procedure, we always use the Aura MLS time series as one of the first two series involved in the initial merging step, for example as $y_1(i)$, in order to maximize the overlap between the first two series and obtain more robust offset values. Then, we use the 3rd time series; the order used for HALOE and ACE-FTS (i.e., whether we use HALOE or ACE-FTS for y_2 or y_3) makes very little difference.

Calculation of the standard deviation for the merged data values

The average and standard deviation (square root of variance) for each y_k value (i.e. for each monthly zonal mean in a particular lat/p bin) are calculated from equations (3) and (4) below:

$$\bar{y}_k = \frac{1}{n_{yk}} \sum_j y_{kj} \quad (3)$$

and, for the variance,

$$\sigma_{yk}^2 = \frac{1}{n_{yk} - 1} \sum_j (y_{kj} - \bar{y}_k)^2 \quad (4)$$

where index “ j ” corresponds to individual data values within a month, index k represents a given instrument (data source), and n is the total number of data values for a given bin and source (instrument) time series point in time (or month). Each value \bar{y}_k above is a monthly average (although we also use instead the simpler notation y_k), with standard deviation about the mean σ_{yk} . Now, given the merged series $u(i)$ (where index i runs over a large number of months), the standard deviation of each merged data point (for a given month) can be obtained by considering the original datasets y_{kj} that were used to construct u . Specifically, we have the variance for the merged dataset

$$\sigma_u^2 = \frac{1}{n_u - 1} \sum_j (u_j - u_{ref})^2 \quad (5)$$

where u_{ref} is the merged value (which is not necessarily chosen to be the average value \bar{u}) and the u_j values represent the union of adjusted data values that make up the merged product, with the index j for this combined dataset covering all values (up to the total n_u) obtained from the original source values y_{kj} . In practice, we do not keep track of the individual data values that went into making the averages for the series y_k that are being merged, and we need to obtain σ_u based solely on the values \bar{y}_k , σ_{yk} , and the original number of points for each dataset y_k , namely n_{yk} . If we consider all the original values, we have a combined dataset with n_u points, such that $n_u = \sum_k n_{yk}$. Now, expanding equation (5), we get

$$(n_u - 1) \sigma_u^2 = \sum_j (u_j^2 + u_{ref}^2 - 2u_{ref} u_j) \quad (6)$$

or

$$(n_u - 1) \sigma_u^2 = \sum_j u_j^2 + n_u u_{ref}^2 - 2u_{ref} \sum_j u_j \quad (7)$$

Expanding (4) for each individual dataset y_k , we get

$$(n_{yk} - 1) \sigma_{yk}^2 = \sum_j y_{kj}^2 + \bar{y}_k^2 - 2\bar{y}_k \sum_j y_{kj} \quad (8)$$

which leads to

$$\sum_j u_j^2 = \sum_{k,j} y_{kj}^2 = \sum_k (n_{yk} - 1) \sigma_{yk}^2 + \sum_k n_{yk} \bar{y}_k^2, \quad (9)$$

so that extracting the variance from equation (7) now leads to

$$\sigma_u^2 = \frac{1}{(n_u - 1)} \left(\sum_k (n_{yk} - 1) \sigma_{yk}^2 + \sum_k n_{yk} \bar{y}_k^2 + n_u u_{ref}^2 - 2u_{ref} \sum_k n_{yk} \bar{y}_k \right) \quad (10)$$

The adjusted time series are obtained from the original series y_k as Y_k , and we can write

Equation (4) in the same manner for the Y_k data values, namely

$$\sigma_{Yk}^2 = \frac{1}{n_{yk} - 1} \sum_j (Y_{kj} - \bar{Y}_k)^2 \quad (11)$$

with $\sigma_{Yk} = \sigma_{yk}$ as the adjustments (offsets) are performed in an additive manner; if these adjustments were performed using multiplicative factors, those factors would also have to be considered in a multiplicative way to get the new σ_{Yk} values. We can thus write (10) for the adjusted datasets as:

$$\sigma_u^2 = \frac{1}{(n_u - 1)} \left(\sum_k (n_{yk} - 1) \sigma_{yk}^2 + \sum_k n_{yk} \bar{Y}_k^2 + n_u U_{ref}^2 - 2U_{ref} \sum_k n_{yk} \bar{Y}_k \right) \quad (12)$$

Equation (12) for the standard deviation of the merged dataset simplifies if the original datasets are adjusted to exactly the same reference value ref ($\bar{Y}_k = ref$) and the merged value U_{ref} is also equal to that value, as the sum of the last 3 terms in Eq. (10) (with Y_k replacing y_k) then reduces to $n_u ref^2 + n_u ref^2 - 2n_u ref^2$, which is zero. In this case, one obtains

$$\sigma_u^2 = \frac{1}{(n_u - 1)} \left(\sum_k (n_{yk} - 1) \sigma_{yk}^2 \right) \quad (13)$$

However, in general, one should use equation (12) for the standard deviation of the merged dataset, given the adjusted datasets \overline{Y}_k and the merged (or reference) value U_{ref} . Also, we often use a merged value equal to the average of the original data (over a given overlap period), so that

$$U_{ref} = \frac{1}{n_y} \sum_k \overline{y}_k \quad (14)$$

where n_y is the total number of datasets (y_k), as opposed to having the merged value place more weight on the larger datasets (e.g., for emission-type measurements versus occultation-type), in which case one would consider using $U_{ref} = \frac{1}{n_u} \sum_k n_{yk} \overline{y}_k$. For ozone, we use a particular dataset (SAGE II ozone) as the primary reference, but equation (12) can be used to obtain the standard deviation for the merged dataset (about the SAGE II reference) in that case also. While it is useful to have the formalism above for obtaining the merged dataset standard deviation σ_u , we often find significant differences between the standard deviations of various datasets, so that this effect will have the greatest influence on the results, as opposed to the impact of the last 3 terms in the summation (in (12)). Finally, it is easy to test equation (12) (and we have done so) by using synthetic series and calculating the standard deviation of the combined set. In reality, the standard deviations of the time series monthly mean values are typically larger for MLS than for ACE-FTS, mainly because of the more complete sampling of variability from the daily global measurements acquired by MLS. Sample plots for standard deviations and standard errors in the case of HCl are shown in Fig. A1. As expected, merged standard deviations follow the standard deviations from HALOE HCl before Aug. 2004 and those from MLS HCl after this time. However, the merged standard errors for the MLS time period follow the smaller MLS standard errors, because these values vary inversely with the square root of the number of values sampled, and are therefore made smaller by the significantly larger daily and monthly MLS sampling rate and coverage.

A.3. Procedural details for GOZCARDS HCl, H₂O, and O₃

Data screening procedures for the GOZCARDS source datasets, following previously described methods, are provided (with references) in Table A1, along with certain species-related specifics. Other GOZCARDS data characteristics and details are provided below for each species.

A.3.1. HCl

- The vertical data range for valid HCl merged values is between 0.46 hPa and 147 hPa (inclusive), as a result of data sparseness or data quality issues outside these ranges.
- At 147 hPa, no merged HCl values exist for latitude bins from 35°S to 35°N inclusive, because of unrealistically large Aura MLS HCl values in this region; also, there is not enough data at this level to provide a meaningful product from HALOE and ACE-FTS data alone.
- Because of occasional small negative merged values during southern hemisphere polar winter, we did not apply HCl data offsets in the lower stratosphere for the 65°S through 85°S bins from June through September and for pressures larger than or equal to 15 hPa. For vertical continuity purposes, we applied this method to all lower stratospheric pressure levels, although the small negative merged values only occurred in a small fraction of cases.
- As Aura MLS and ACE-FTS data exist in the 85°N and 85°S bins, but there are no HALOE measurements, we simply extended the offsets from the adjacent bins (at 75°N and 75°S) to these two bins to obtain a merged record after 2004 that exhibits continuity versus latitude.
- At 100 hPa, we used HCl offsets from the 5°S bin for the 5°N bin, as there was insufficient data from the combined data in the latter bin to calculate meaningful offsets. This procedure seems reasonable, given that the time series in these two adjacent tropical latitude bins (during years outside the 2004/2005 overlap period) look continuous and stable enough to justify identical adjustments in both bins and to avoid a data gap in the merged series at 5°N.

A.3.2. H₂O

- The vertical data range for valid H₂O merged values is between 0.01 hPa and 147 hPa (inclusive). While H₂O data exist at 147 hPa for low latitudes, more careful work would be needed to extend the merged data globally in such a region.

- Users should keep in mind the PMC-related caveats mentioned in Sect. 4 for summer at high latitudes in the upper mesosphere, prior to the end of the HALOE dataset (Nov. 2005).
- As for HCl, we could not use our standard merging procedure at the two most poleward latitude bins; we simply extended the offsets from the adjacent bins (at 75°N and 75°S) to these polar bins to obtain a merged record after 2004 that exhibits continuity versus latitude.
- Also as for HCl, at 100 hPa, we used H₂O offsets from the 5°S bin for the 5°N bin, as there was insufficient data from the combined datasets in the latter bin to calculate meaningful offsets and merge the datasets. This procedure avoids a data gap in the merged series at 5°N.

A.3.3. O₃

- The vertical range for valid O₃ merged data is from 0.2 hPa to 215 hPa (inclusive), with the lower altitude bound varying with latitude; the merged product at 147 and 215 hPa has valid data only for the 35° to 85° latitude bins, with values mostly larger than ~ 0.1 ppmv. The upper troposphere is more of a merging challenge, given smaller abundances, more difficult measurements, and a larger impact from different instrument resolutions. Also, while we suggest (see main text) that GOZCARDS merged ozone data should not be subject to a large impact from diurnal variations, the highest altitude region should be treated with caution.
- SAGE I monthly mean source data are used for the merged dataset in the tropical bins (25°S to 25°N) from 1 through 68 hPa only and, at higher latitudes, from 1 through 100 hPa only.
- We omitted the use of UARS MLS at 100 hPa for low latitudes (from 25°S to 25°N), as these monthly values are biased quite high and also exhibit too large a seasonal cycle amplitude, in comparison to HALOE and SAGE II data; this appears to relate to a UARS MLS artifact.
- Since there is no (monthly) overlap between SAGE II and HALOE versus UARS MLS or Aura MLS in the 85°N and 85°S latitude bins, the same offsets as for 75°N and 75°S (respectively) are applied for these bins, in order to minimize discontinuities.
- Because of discontinuities that appeared in merged O₃ at high latitudes above the stratopause, particularly in the 75°S bin, we flagged merged values for 75° and 85° (N and S) as bad, for pressures less than 1 hPa. This issue could be the result of a few bad data points or not enough data overlap. To minimize artifacts, we left the resolution of this issue for future investigations; also, the reduced amount of occultation data at these high latitudes makes the

1638 usefulness of a merged product with poorly sampled seasonal changes somewhat marginal
1639 (for certain years at least, the number of monthly values drops significantly at high latitudes).

1640

1641

1642 **Table 1.** Characteristics of instrument datasets used to create GOZCARDS ESDRs (version ev1.01).

Instrument and Data Versions	Platform	Type of measurement	Time period (GOZCARDS source files)	Vertical Resolution (km)	Retrieved quantity and stratospheric vertical grid spacing
SAGE I V5.9_rev O ₃	AEM-2	Solar occultation VIS/UV and near-IR	Feb. 1979 - Nov. 1981	1	Density on altitude grid 1 km spacing
SAGE II V6.2 O ₃	ERBS	Solar occultation VIS/UV and near-IR	Oct. 1984 - Aug. 2005	0.5 - 1	Density on altitude grid 0.5 km spacing
HALOE V19	UARS	Solar occultation mid-IR	Oct. 1991 - Nov. 2005	2.5	Volume Mixing Ratio on pressure grid with 30 levels per decade (LPD) change in p
MLS V5 O ₃ V6 H ₂ O	UARS	Limb emission microwave / sub-mm	Oct. 1991 - June 1997 (May 1993 end for strat. H ₂ O)	H₂O 3 - 4 (strat.) 5 - 12 (mes.) O₃ 3.5 - 5 (strat.) 5 - 8 (mes.)	Volume Mixing Ratio on pressure grid with 6 LPD in stratosphere 6 LPD in stratosphere
ACE-FTS V2.2 (V2.2 update for O ₃)	SCISAT	Solar occultation mid-IR	Mar. 2004 through Sep. 2010 (2009 for O ₃)	3 - 4	Volume Mixing Ratio on 1 km grid spacing (height and p provided)
MLS V3.3 V2.2 O ₃	Aura	Limb emission microwave / sub-mm	Aug. 2004 through 2012	HCl 3 - 5 H₂O 3 - 4 (p > 0.1 hPa) 5 - 9 (0.1-0.01 hPa) O₃ 3	Volume Mixing Ratio on pressure grid with 6 LPD 12 LPD 6 LPD

1644 **Table 2.** Products and instrument source data making up the available GOZCARDS data records.

Merged Products and pressure range	Source Datasets (and years used)
HCl 147 – 0.5 hPa	HALOE (1991-2005), ACE-FTS (2004-2010), Aura MLS (2004 onward) Note: MLS data for p < 10 hPa not used for merged time series
H₂O 147 – 0.01 hPa	HALOE (1991-2005), UARS MLS (1991-1993), ACE-FTS (2004-2010), Aura MLS (2004 onward)
O₃ 215 – 0.2 hPa	SAGE I (1979-1981), SAGE II (1984-2005), HALOE (1991-2005), UARS MLS (1991-1997), ACE-FTS (2004-2009), Aura MLS (2004 onward)
HNO₃ 215 – 1 hPa	ACE-FTS (2004-2010), Aura MLS (2004 onward)
N₂O 100 – 0.5 hPa	ACE-FTS (2004-2010), Aura MLS (2004 onward)
Temperature 1000 – 0.015 hPa	GMAO MERRA (1979 onward)

1645

1646

1647

1648

1649

1650

1651

1652

1653 **Table A1.** Data screening procedures and related references used for the source dataset generation.

Instrument	Data Screening Issue / Method	Reference
SAGE I (O ₃)	Aerosol interference issue: Remove values at altitudes below which the 1 μm extinction $> 10^{-3} \text{ km}^{-1}$.	L. Thomason (personal communication, 2012)
SAGE II (O ₃)	Remove entire profile if any error error value exceeds 10% of VMR (for 30 to 50 km altitude); this occurred mainly in 1993 & 1994 ("short events"). Use aerosol extinctions and extinction ratios to remove data affected by clouds or by aerosols (from Mt. Pinatubo). Remove anomalously low values resulting from very small SAGE II transmittances (errors are capped at 300% as a flag). Remove profiles under high beta angle conditions.	Wang et al. (2002) See also Wang et al. (1996)
HALOE	Remove cloud-contaminated values. Also remove profiles that may contain artifacts from faulty trip angle or constant lockdown angle registration. Remove aerosol contamination (O ₃ and HCl).	Hervig and McHugh (1999) haloe.gats-inc.com/user_docs/index.php Bhatt et al. (1999)
UARS MLS	Use screening guidelines based on instrument status, retrieval quality flags, and sign of precision values.	Livesey et al. (2003)
Aura MLS	Use screening guidelines based on instrument status, retrieval quality and convergence flags, and sign of precision values.	Livesey et al. (2013)
ACE-FTS	Remove occultations listed as bad. Remove data when error value $> \text{VMR}$ or error value $< 10^{-4} \times \text{VMR}$. Use a data screening procedure (see Sect. 2.1) to identify and remove the largest outliers. V2.2 data after Sep. 2010 (2009 for ozone) are not used because of a data processing issue.	databace.scisat.ca/validation/data_issues.php K. Walker (personal communication, 2012)

Fig. 1. Merging procedure illustration for HCl. Top left panel shows the HCl monthly mean source data during the overlap period (Aug. 2004 - Nov. 2005) for HALOE, ACE-FTS, and Aura MLS. Top right panel illustrates step 1 in the merging procedure, with the temporary merged data values (orange) resulting from the adjustment of ACE-FTS and Aura MLS values to the mean reference indicated by the black dashed line (time mean of co-located ACE-FTS/Aura MLS points). Also, the cyan dashed line is the mean of the ACE-FTS points and the red dashed line is the mean of MLS points co-located with ACE-FTS. Middle left panel shows step 2 results, namely the merged values arising from merging HALOE data with the temporary merged data; the black dashed line is the new average reference value, obtained from a 2/3 and 1/3 weighting of the dashed orange (mean of orange points co-located with HALOE) and dashed blue line (mean of HALOE) values, respectively. Middle right panel shows all the source data and the final merged values during the overlap period. Bottom panel shows the source and merged time series from 1991 through 2012 after the calculated additive offsets are applied to the whole source datasets, which are then merged (averaged) together wherever overlap between instruments exists.

Fig. 2. Offsets applied to the HCl source datasets (top panels for HALOE, middle panels for ACE-FTS, bottom panels for Aura MLS) as a function of latitude and pressure. The left column gives offsets in ppbv and the right column provides offsets as a percent of the zonal average merged mixing ratios during the overlap period (Aug. 2004 – Nov. 2005) used here to compute the average offsets.

Fig. 3. Example of HCl time series analyses for 50°N-60°N and 32 hPa. (a) HCl monthly mean source data from ACE-FTS and Aura MLS; the MLS dots are filled when there is time overlap with ACE-FTS, and open if no such overlap exists. Simple linear fits are shown as colored lines for ACE-FTS and for Aura MLS (orange line for all red dots and red line for filled red dots only). Correlation coefficient values (R values) for the two time series are provided in the title. (b) Deseasonalized anomalies for both ACE-FTS and Aura MLS, with corresponding linear fits (and R values). (c) Difference of deseasonalized anomalies (ACE-FTS minus Aura MLS), with linear fit.

Fig. 4. Latitude/pressure contours of time series diagnostics obtained from analyses illustrated in Fig. 3 for HCl from Aura MLS and ACE-FTS. Top panel: Correlation coefficient for the deseasonalized time series. Bottom panel: Ratio of the slope of the difference between deseasonalized series over the error in this slope.

Fig. 5. Illustration of GOZCARDS HCl monthly averages with systematic error estimates (grey shading) at 46 hPa for 30°S-40°S; see text for the meaning of this shaded region. The source data from HALOE, Aura MLS, and ACE-FTS are shown in different colors (see legend), along with the merged values.

Fig. 6. Systematic error estimates for GOZCARDS HCl. One error (left panels) is relevant for values lower than (below) the merged values, and one (right panels) for values larger than the merged values; the

top panels give the error estimates in ppbv, and the bottom panel errors are expressed as percent of the average merged values over the relevant time periods (see text). These error bars provide a range within which 95% of the source data values lie.

Fig. 7. Time series of the GOZCARDS monthly-averaged merged HCl abundance for 3 different latitude bin averages (see color legend in panel (a)) for (a) 0.7 hPa, (b) 10 hPa, (c) 32 hPa, and (d) 68 hPa.

Fig. 8. The average rate of change (percent per year) for HCl as a function of pressure for different latitude bin averages (see legend) for time periods corresponding to the appropriate GOZCARDS HCl values (see text) in the upper stratosphere (Jan. 1997 - Sep. 2010) and lower stratosphere (Jan. 1997 - Dec. 2012). Deseasonalized monthly data were used to obtain a long-term trend for these time periods; two-sigma error bars are shown.

Fig. 9. Rates of change for GOZCARDS HCl (connected open circles) are given as a function of latitude in 10° latitude bins for sliding 6-year periods centered on Jan. 1 of each year (e.g., the 1998 point is an average for data from 1995 through 2000, and the 2011 point is for data from 2008 through 2013). (a) is for changes in upper stratospheric HCl at 0.7 hPa and (b) is for the change in the integrated HCl column between 68 hPa and 10 hPa. The two additional curves in (a) represent the rates of change in the estimated surface total chlorine from NOAA data (green is for a 6-year time shift, and purple for a 7-year time shift, to account for transport time to the upper stratosphere); see text for more details. Error bars indicate twice the standard errors in the means.

Fig. 10. Offsets applied to the H₂O source datasets as a function of latitude and pressure, similar to Fig. 2 for HCl.

Fig. 11. Latitude/pressure contours of time series diagnostics for H₂O from Aura MLS and ACE-FTS; this is similar to Fig. 4 for HCl.

Fig. 12. A depiction of the “tape recorder” evolution for tropical water vapor abundances from 147 to 10 hPa for October 1991 through December 2013. This plot was produced from GOZCARDS merged H₂O time series anomalies (differences from the long-term means) for the average of the 4 tropical bins covering 20°S to 20°N.

Fig. 13. Systematic error estimates for GOZCARDS H₂O (similar to Fig. 6 for HCl).

Fig. 14. Variations in stratospheric water vapor from the GOZCARDS H₂O merged data records (1992 through 2013) averaged from (a) 60°S to 60°N and (b) 20°S to 20°N. Monthly average values and annual averages are shown by thin and thick lines (connecting similarly-colored dots), respectively, for the pressure levels indicated in the plot legend.

Fig. 15. Stratospheric water vapor variability on decadal timescales for 1992 through 2013 for tropical (20°S-20°N in black) and mid-latitude (20°N-60°N in red and 20°S-60°S in blue) zonal means, based on the GOZCARDS merged H₂O data record. The variability is expressed here as the difference between maximum and minimum annual average abundances, from 100 to 1 hPa, in ppmv (left panel) and percent (right panel).

Fig. 16. (a) Variations in upper mesospheric (0.01 hPa) water vapor mixing ratios averaged from 60°S to 60°N for Oct. 1991 through Dec. 2013, based on the GOZCARDS merged H₂O data records. Monthly average values and annual averages are shown by connected brown dots and connected black dots, respectively. (b) GOZCARDS merged H₂O annual averages (connected filled symbols) from 60°S to 60°N for 1992 through 2013 at pressure levels between 0.1 and 0.01 hPa. A time series of annually-averaged Lyman α solar flux values (open circles), scaled to arbitrary units, is also displayed (see text).

Fig. 17. Time series of monthly zonal mean O₃ for 10°S - 20°S between 1 hPa and 6.8 hPa (with pressure values given by "pre") from SAGE I, SAGE II, HALOE, UARS MLS, Aura MLS, and ACE-FTS, all color-coded following the legend in top left panel.

Fig. 18. Schematic diagram describing the creation of the merged GOZCARDS monthly zonal mean ozone data record from various satellite datasets. Instruments represented in red inside the boxes are used as a reference. Instruments whose measurements have already been adjusted to a reference are indicated with a "*" superscript. AMLS refers to Aura MLS and UMLS to UARS MLS. See text for more details.

Fig. 19. Offsets applied to the O₃ source datasets, similar to Fig. 2 for HCl.

Fig. 20. Latitude/pressure contours of time series diagnostics for O₃ from Aura MLS and ACE-FTS; this is similar to Fig. 4 for HCl. The correlation coefficients (R values) and slope trend diagnostics are provided for HALOE versus SAGE II in the top two panels (for 1993-1999 as the trend issue for converted SAGE II data occurs after mid-2000 and to avoid Pinatubo-related data gaps before 1993) and for ACE-FTS versus Aura MLS in the bottom two panels (for 2005-2009).

Fig. 21. Systematic error estimates for GOZCARDS O₃ (similar to Fig. 6 for HCl).

Fig. 22. Near-global (60°S to 60°N) results for average column ozone (total and stratospheric, from *Ziemke and Chandra, 2012*) compared to GOZCARDS O₃ columns above 68 hPa. Stratospheric columns are offset to better match the total column values, in order to more easily compare relative variations versus time; the black dots and red crosses are referenced to the 1980 total column values, while the cyan

curves are referenced to 2007 to better illustrate the fits in the later years. Also shown (as purple open circles) are yearly-averaged total column data (60°S to 60°N) from the SBUV Merged Ozone (V8.6) Dataset (see text); these values were adjusted upward slightly (by 0.8 DU) to match the ZC12 total column values in 1980.

Fig. 23. Time evolution (Aug. 2004 through 2012) versus latitude of GOZCARDS merged N₂O (ppbv) at (a) 6.8 hPa and (b) 100 hPa.

Fig. 24. Sample results display the time evolution of satellite-retrieved HNO₃ (ppbv) for two different periods, 1992-1997 in (a) and (c) versus 2004-2013 in (b) and (d). Panels (a) and (b) are contour plots at 46 hPa from UARS MLS global data and the merged GOZCARDS global data after 2004, respectively; (c) and (d) show time series at 32 hPa and for the 40°N-50°N latitude bin, with (a) from UARS MLS data, and (d) from ACE-FTS, Aura MLS, and the merged combination (between the two source data sets).

Fig. A1. Illustration of the standard deviations (in (a)) and standard errors (in (b)) for monthly mean GOZCARDS HCl (source and merged records) at 46 hPa for 30°S-40°S. Source data from HALOE, Aura MLS, and ACE-FTS are given by the filled colored dots (see legend); each standard deviation is simply obtained from the range of values measured during the month. The large open brown circles give standard deviations for the merged HCl product; this Appendix provides the formulae to calculate these quantities.

Fig. S1: Illustration of the latitudinal dependence of the HCl offsets for HALOE, ACE-FTS, and Aura MLS at two pressure levels (top panel for 0.46 hPa, bottom panel for 46 hPa). Error bars represent twice the standard error in the derived offsets (based on variability during the overlapping period). Larger standard error values indicate that there were either fewer points of overlap or larger offset variability (standard deviations); we found that both of these factors contribute.

Fig. S2: Latitude/pressure contours of the fitted mean annual amplitudes (ppbv) from HCl time series for HALOE, ACE-FTS, and Aura MLS, based on their respective measurement periods (see text).

Fig. S3: Time evolution (Oct. 1991 through 2013) versus latitude of GOZCARDS merged HCl (ppbv) at 46 hPa.

Fig. S4: HALOE sunrise measurements of H₂O versus the 3.46 μ m extinction coefficient for 1992, 1993, and 1999 at 22 hPa. The green vertical line represents the aerosol extinction value ($5 \times 10^{-4} \text{ km}^{-1}$) used to screen anomalous HALOE H₂O values. It is apparent that anomalously low H₂O values occurred in 1992 when the 3.46 μ m aerosol extinction exceeded about $5 \times 10^{-4} \text{ km}^{-1}$. These artifacts were confined to 1991

and 1992; for these years, and for pressure levels at and below 22 hPa, the corresponding H₂O data values were excluded. This screening method eliminates about 10% of the global (lower stratospheric) measurements in 1992.

Fig. S5: Merging procedure illustration for H₂O at 5°N and 22hPa. This is similar to Fig. 2 (for HCl), but an additional step is illustrated for the end of this procedure, whereby stratospheric H₂O data from UARS MLS are adjusted to the early portion of the merged time series that was obtained after the 2nd step; this adds more coverage (more brown dots in the bottom panel for 1991-1993).

Fig. S6: Latitude/pressure contours of the fitted mean annual amplitudes (ppmv) from H₂O time series for HALOE, ACE-FTS, and Aura MLS, based on their respective measurement periods.

Fig. S7: Time evolution (Oct. 1991 through 2013) versus latitude of GOZCARDS merged H₂O (ppmv) at 3.2 hPa (top panel) and 68 hPa (bottom panel).

Fig. S8: Monthly zonal mean ozone differences (%) between SAGE II and (a) HALOE, (b) UARS MLS (UMLS for short), (c) Aura MLS (AMLS for short), and (d) ACE-FTS during their respective overlap periods. Differences are expressed (in percent) as $100 \times [(SAGE\ II - Other) / (Other)]$. Shaded areas indicate negative values.

Fig. S9: Monthly zonal mean temperature differences between NCEP (used by SAGE II) and HALOE temperatures relative to MERRA for 10°S - 20°S between 1 and 6.8 hPa, per color-coding indicated in bottom left panel; “pre” represents the pressure value. From 1 to 2.1 hPa, differences between NCEP and MERRA are generally within ± 4 K before mid-2000. After that time, NCEP temperatures show a sharp increase and are systematically higher than MERRA values by 5 to 10K. However, this divergence and trend are not seen in HALOE temperatures. NCEP temperatures between 3.2 and 6.8 hPa are smaller than MERRA after mid-2000; negative trends (versus MERRA) also occur in the HALOE data at these levels.

Fig. S10: Relative trends (K/decade) in zonal mean temperature differences for NCEP – MERRA and HALOE – MERRA (color-coded as in Fig. S9) in the upper stratosphere. NCEP temperatures show positive trends versus MERRA of ~ 2 -5 K/decade between 2.1 and 1 hPa for all latitudes. However, HALOE temperatures show no significant trends versus MERRA, except at 1.5 hPa in the southern hemisphere. For pressures between 3.2 and 6.8 hPa, the temperature analyses are not conclusive; although NCEP values show negative trends of ~ 2 -3 K/decade versus MERRA, they agree with HALOE.

Fig. S11: Mean differences and standard deviations (horizontal bars) between SAGE II and Aura MLS ozone in three different latitude bins: 20°S to 60°S (left panel), 20°S to 20°N (middle panel), and 20°N to 60°N (right panel). Results based on monthly zonal mean and coincident profiles (see text for coincidence

criteria) during overlap periods are shown in red and blue, respectively. To choose collocated profiles, coincidence criteria of $\pm 1^\circ$ in latitude and $\pm 8^\circ$ in longitude were used; the time difference criterion was chosen as 12 hours, but only nighttime measurements from Aura MLS were used.

Fig. S12: Latitude/pressure contours of the fitted mean annual amplitudes (ppmv) from O₃ time series for SAGE II, HALOE, ACE-FTS, and Aura MLS, based on their respective measurement periods.

Fig. S13: Illustration of the time evolution of the GOZCARDS merged O₃ data field versus latitude at 68 hPa (top panel) and versus pressure for the 40°N-50°N latitude bin (bottom panel).

Fig. S14: Offsets applied to the N₂O source datasets (top panels for ACE-FTS, bottom panels for Aura MLS) as a function of latitude and pressure. The left column gives offsets in ppbv and the right column provides offsets as a percent of the zonal average merged mixing ratios during the overlap period (Aug. 2004 – Sep. 2010) used here to compute the average offsets.

Fig. S15: Latitude/pressure contours of time series diagnostics derived from Aura MLS and ACE-FTS N₂O data comparisons (and obtained from analyses similar to those illustrated in Fig. 6 for HCl). Top panel: Correlation coefficient for the deseasonalized time series. Bottom panel: Ratio of the slope of the difference between deseasonalized series over the error in this slope.

Fig. S16: Offsets applied to the HNO₃ source datasets (top panels for ACE-FTS, bottom panels for Aura MLS) as a function of latitude and pressure. The left column gives offsets in ppbv and the right column provides offsets as a percent of the zonal average merged mixing ratios during the overlap period (Aug. 2004 – Sep. 2010) used here to compute the average offsets.

Fig. S17: Latitude/pressure contours of time series diagnostics derived from Aura MLS and ACE-FTS HNO₃ data comparisons (and obtained from analyses similar to those illustrated in Fig. 6 for HCl). Top panel: Correlation coefficient for the deseasonalized time series. Bottom panel: Ratio of the slope of the difference between deseasonalized series over the error in this slope.

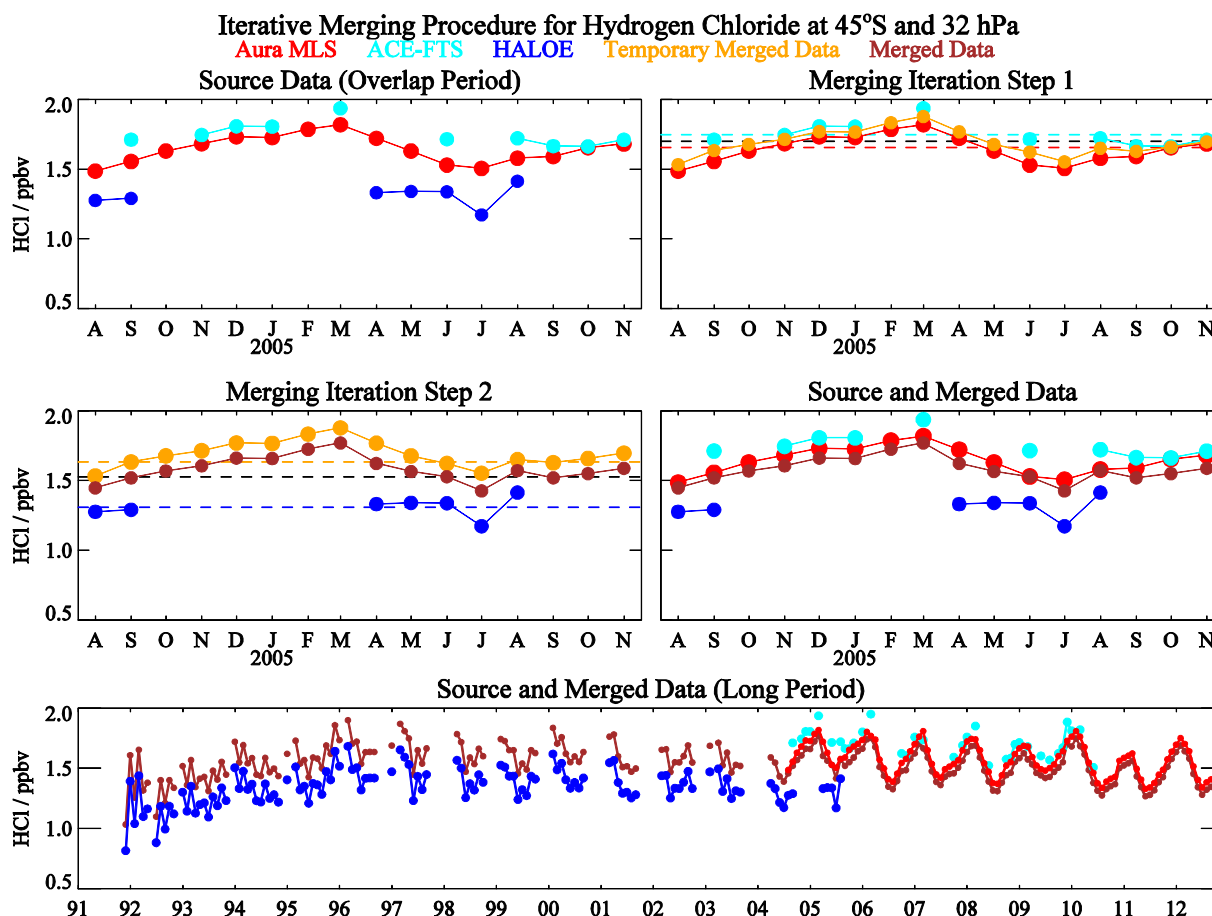


Fig. 1. Merging procedure illustration for HCl. Top left panel shows the HCl monthly mean source data during the overlap period (Aug. 2004 - Nov. 2005) for HALOE, ACE-FTS, and Aura MLS. Top right panel illustrates step 1 in the merging procedure, with the temporary merged data values (orange) resulting from the adjustment of ACE-FTS and Aura MLS values to the mean reference indicated by the black dashed line (time mean of co-located ACE-FTS/Aura MLS points). Also, the cyan dashed line is the mean of the ACE-FTS points and the red dashed line is the mean of MLS points co-located with ACE-FTS. Middle left panel shows step 2 results, namely the merged values arising from merging HALOE data with the temporary merged data; the black dashed line is the new average reference value, obtained from a 2/3 and 1/3 weighting of the dashed orange (mean of orange points co-located with HALOE) and dashed blue line (mean of HALOE) values, respectively. Middle right panel shows all the source data and the final merged values during the overlap period. Bottom panel shows the source and merged time series from 1991 through 2012 after the calculated additive offsets are applied to the whole source datasets, which are then merged (averaged) together wherever overlap between instruments exists.

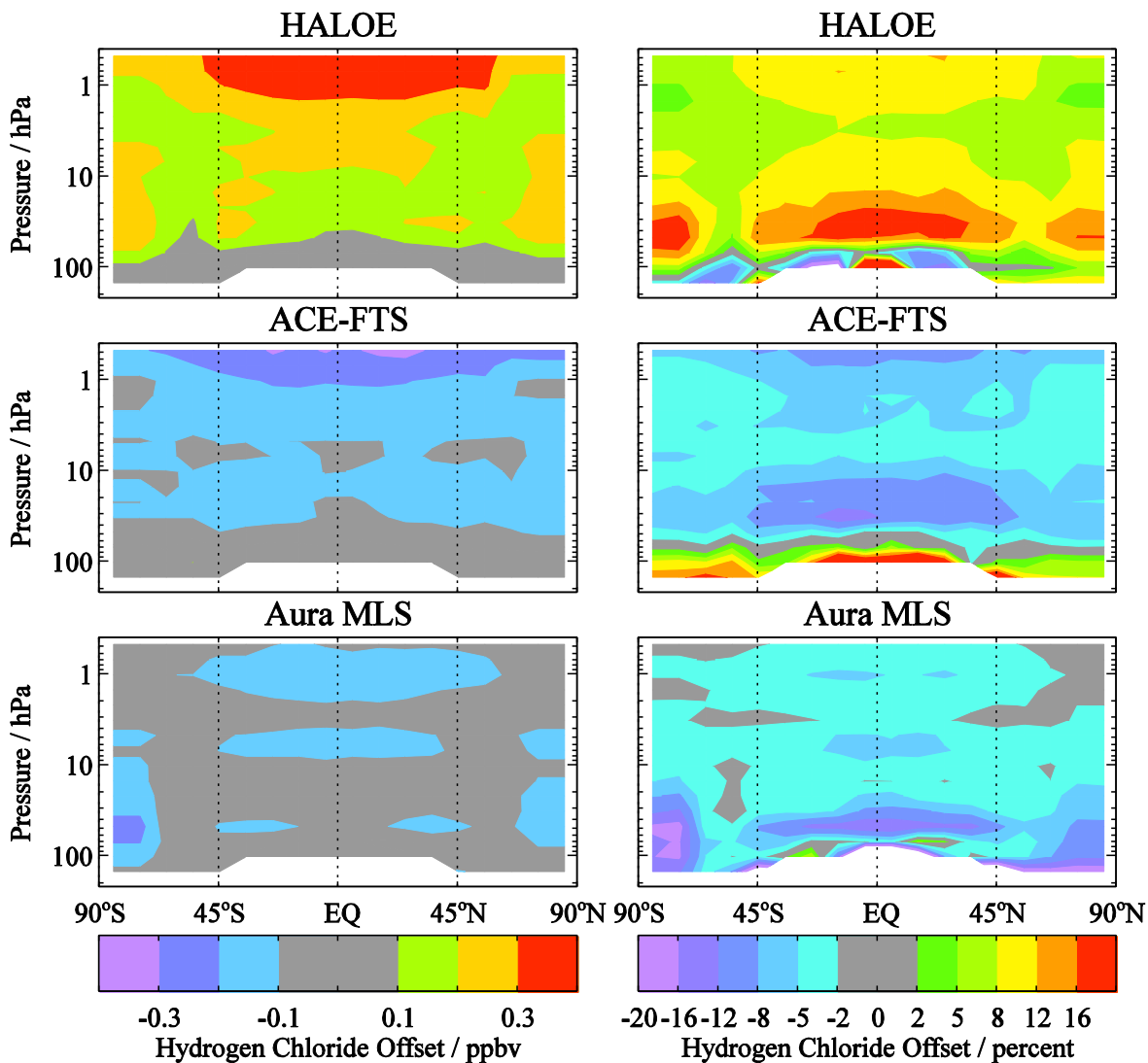


Fig. 2. Offsets applied to the HCl source datasets (top panels for HALOE, middle panels for ACE-FTS, bottom panels for Aura MLS) as a function of latitude and pressure. The left column gives offsets in ppbv and the right column provides offsets as a percent of the zonal average merged mixing ratios during the overlap period (Aug. 2004 – Nov. 2005) used here to compute the average offsets.

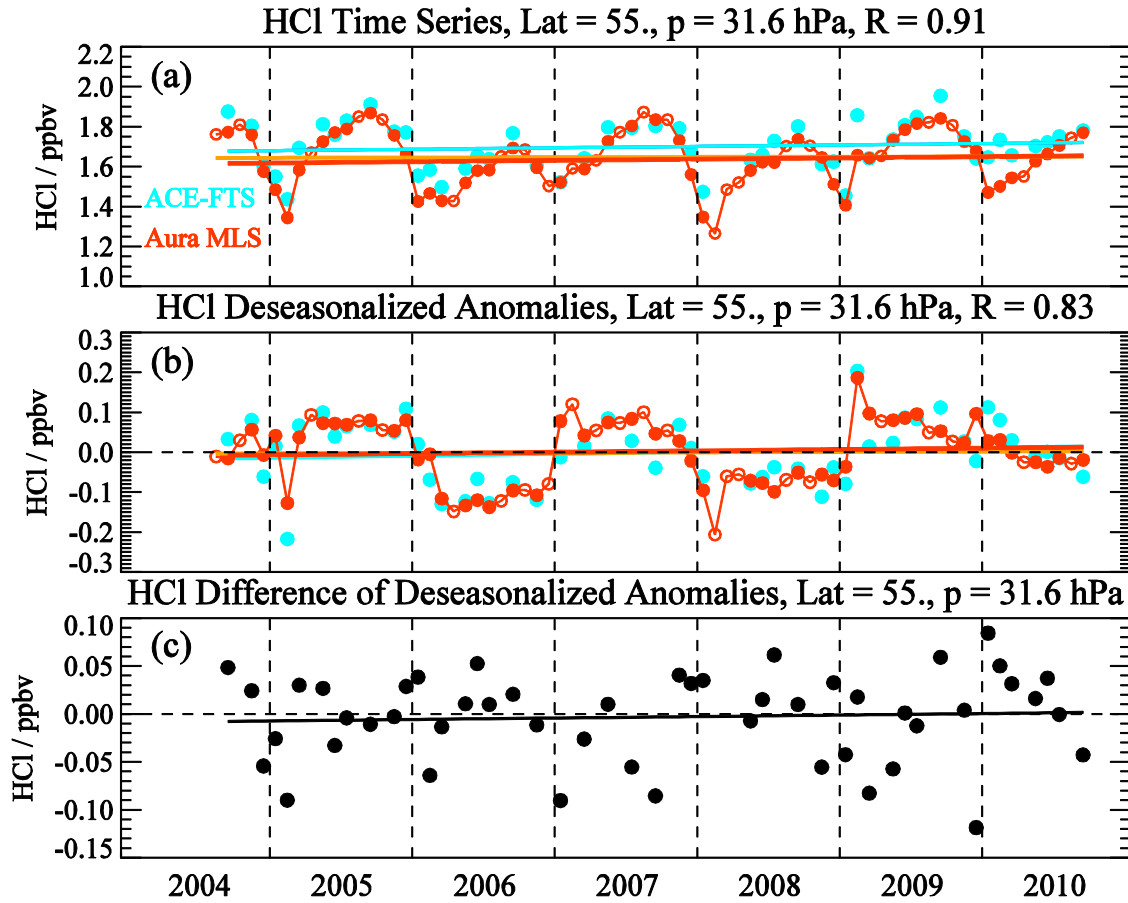


Fig. 3. Example of HCl time series analyses for 50°N-60°N and 32 hPa. (a) HCl monthly mean source data from ACE-FTS and Aura MLS; the MLS dots are filled when there is time overlap with ACE-FTS, and open if no such overlap exists. Simple linear fits are shown as colored lines for ACE-FTS and for Aura MLS (orange line for all red dots and red line for filled red dots only). Correlation coefficient values (R values) for the two time series are provided in the title. (b) Deseasonalized anomalies for both ACE-FTS and Aura MLS, with corresponding linear fits (and R values). (c) Difference of deseasonalized anomalies (ACE-FTS minus Aura MLS), with linear fit.

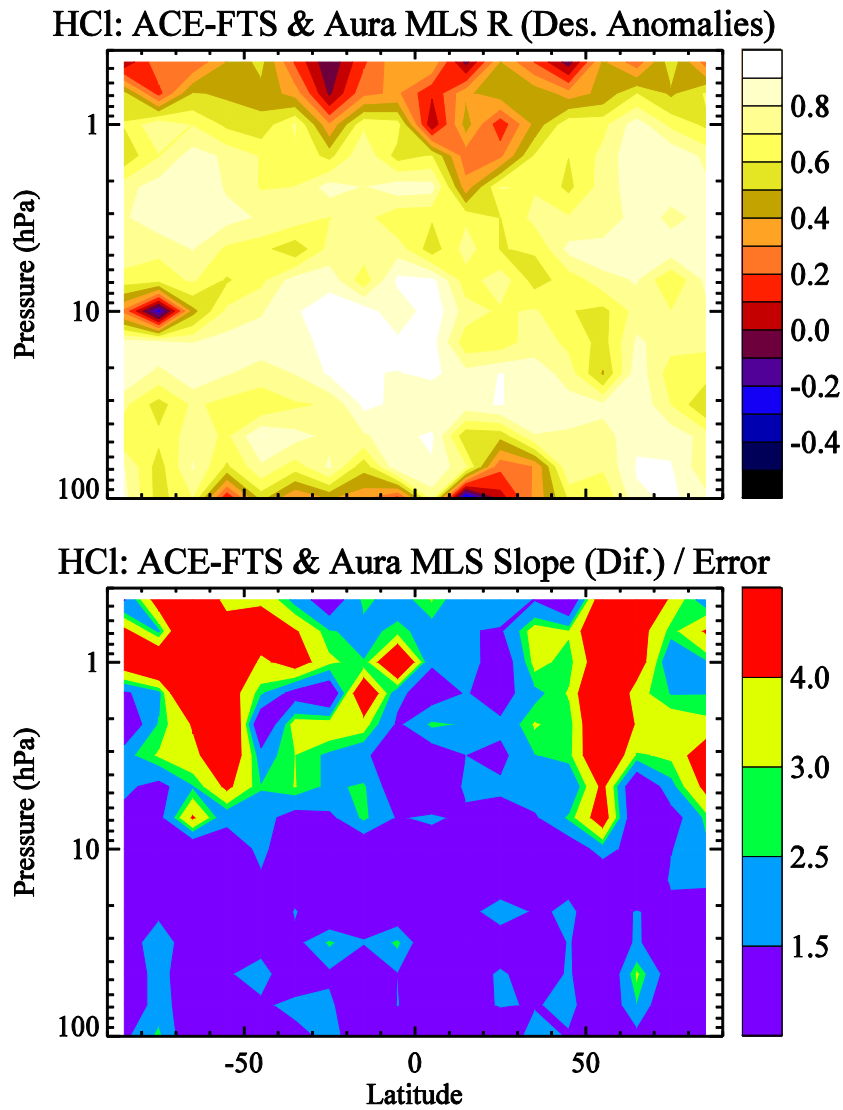


Fig. 4. Latitude/pressure contours of time series diagnostics obtained from analyses illustrated in Fig. 3 for HCl from Aura MLS and ACE-FTS. Top panel: Correlation coefficient for the deseasonalized time series. Bottom panel: Ratio of the slope of the difference between deseasonalized series over the error in this slope.

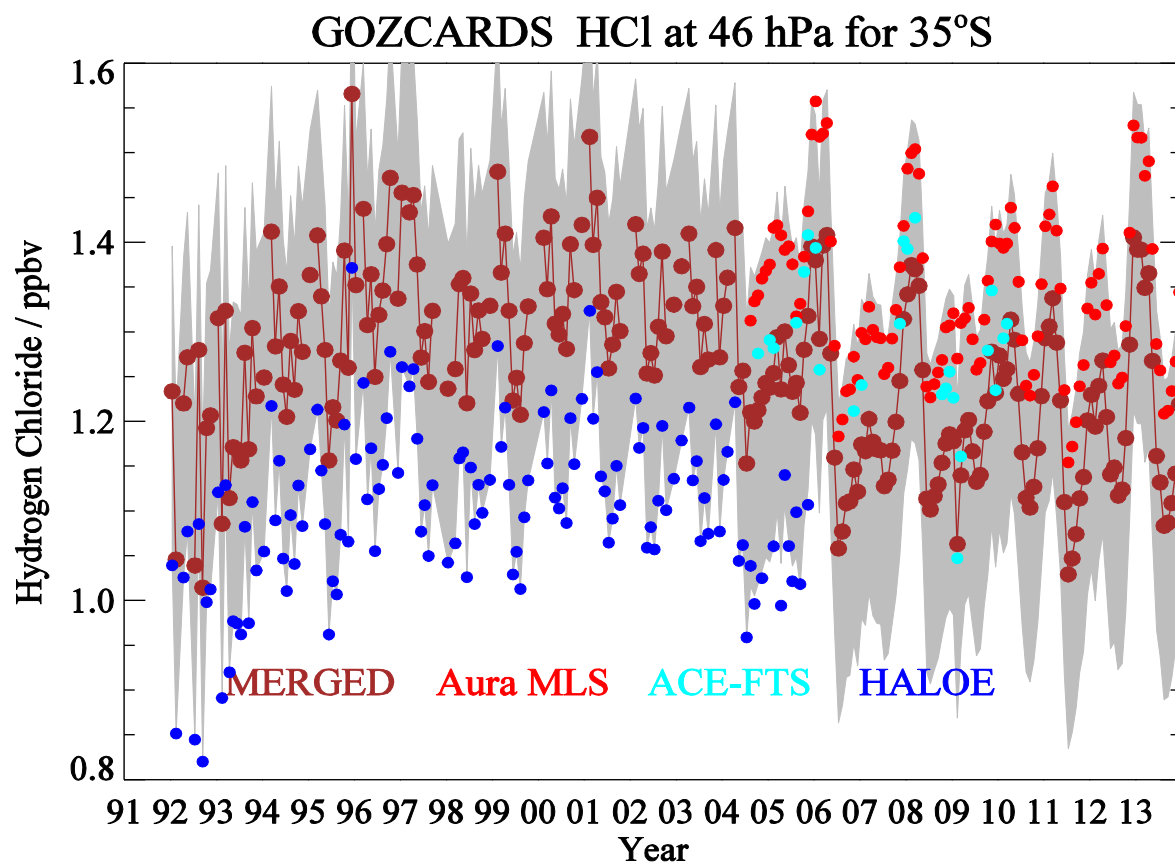


Fig. 5. Illustration of GOZCARDS HCl monthly averages with systematic error estimates (shown as grey shading) at 46 hPa for 30°S-40°S; see text for the meaning of this shaded region. The source data from HALOE, Aura MLS, and ACE-FTS are shown in different colors (see legend), along with the merged values.

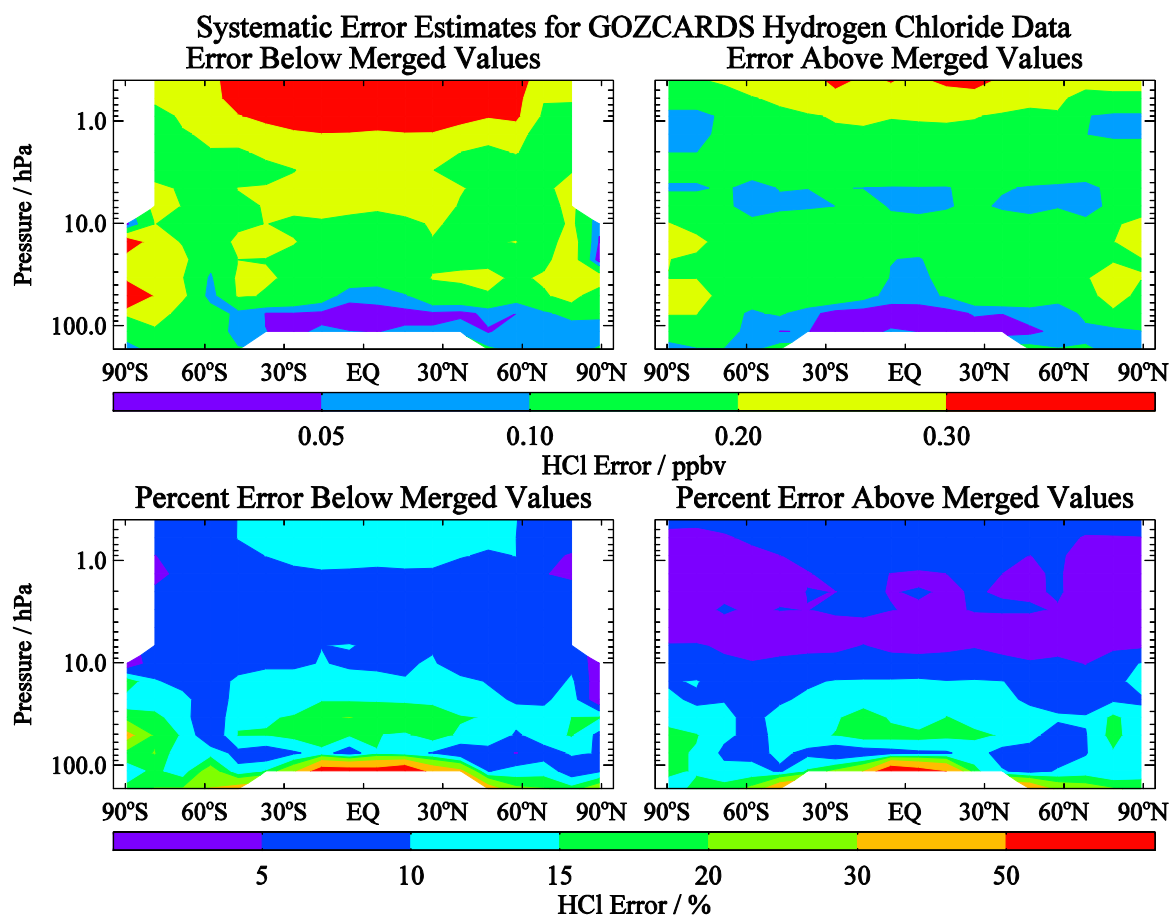
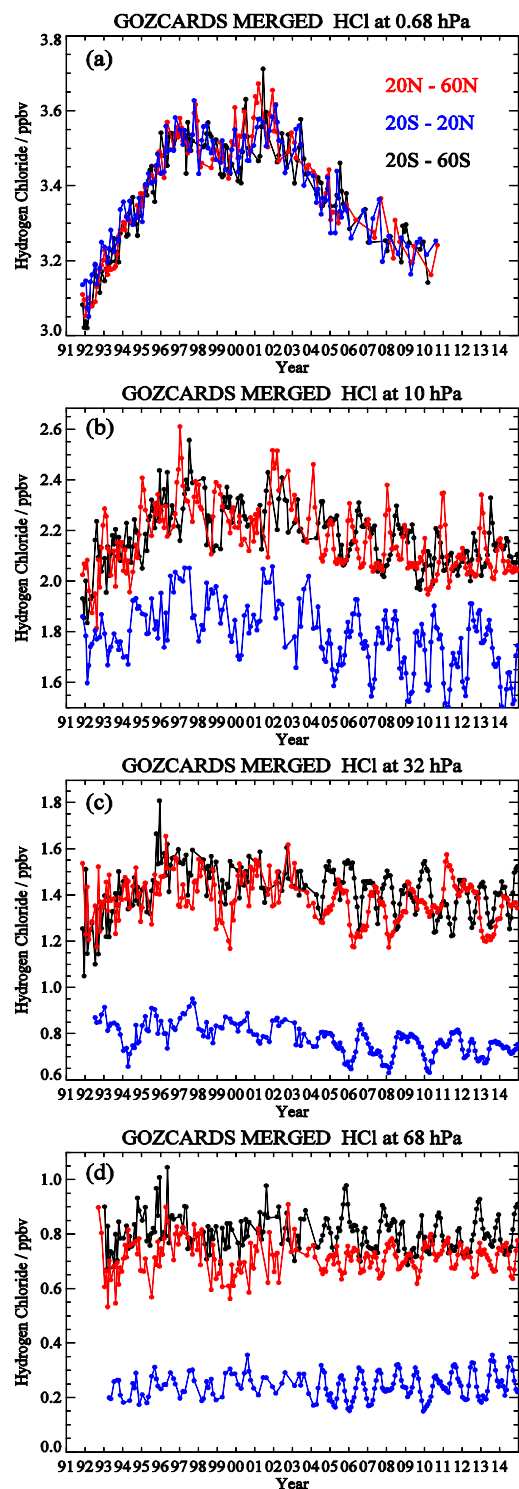


Fig. 6. Systematic error estimates for GOZCARDS HCl. One error (left panels) is relevant for values lower than (below) the merged values, and one (right panels) for values larger than the merged values; the top panels give the error estimates in ppbv, and the bottom panel errors are expressed as percent of the average merged values over the relevant time periods (see text). These error bars provide a range within which 95% of the source data values lie.



71

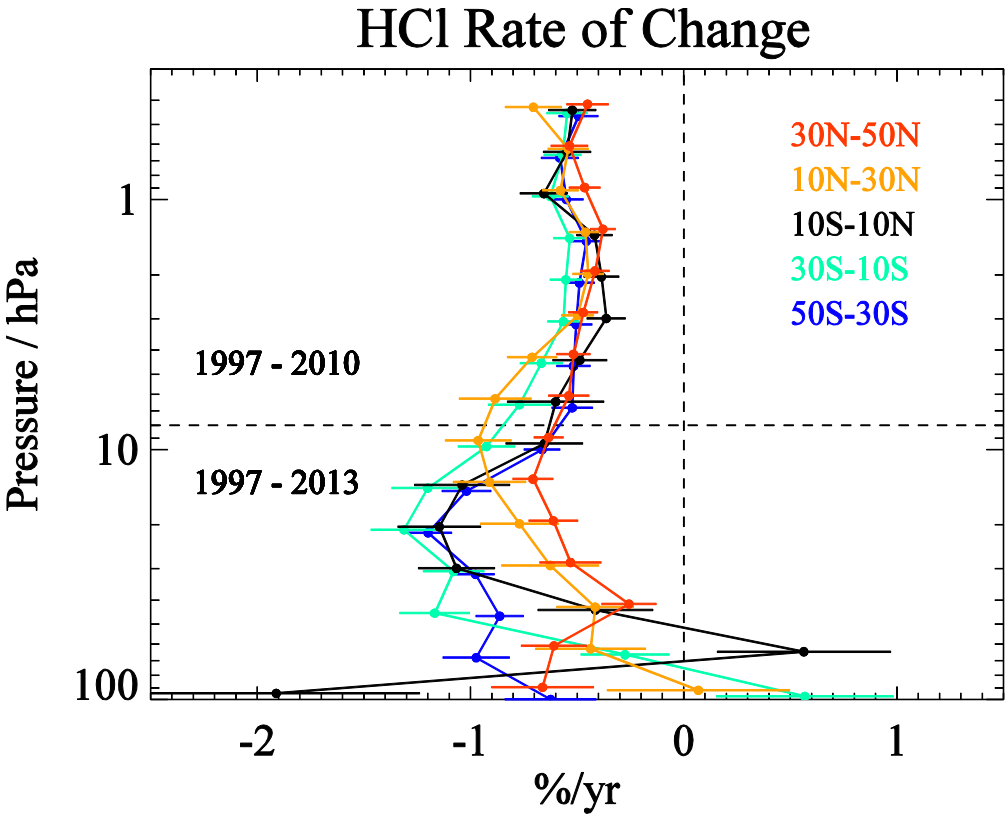
72

73

74

Fig. 7. Time series of the GOZCARDS monthly-averaged merged HCl abundance for 3 different latitude bin averages (see color legend in panel (a)) for (a) 0.7 hPa, (b) 10 hPa, (c) 32 hPa, and (d) 68 hPa.

75



76

77

78

79

80

81

82

83

84

85

86

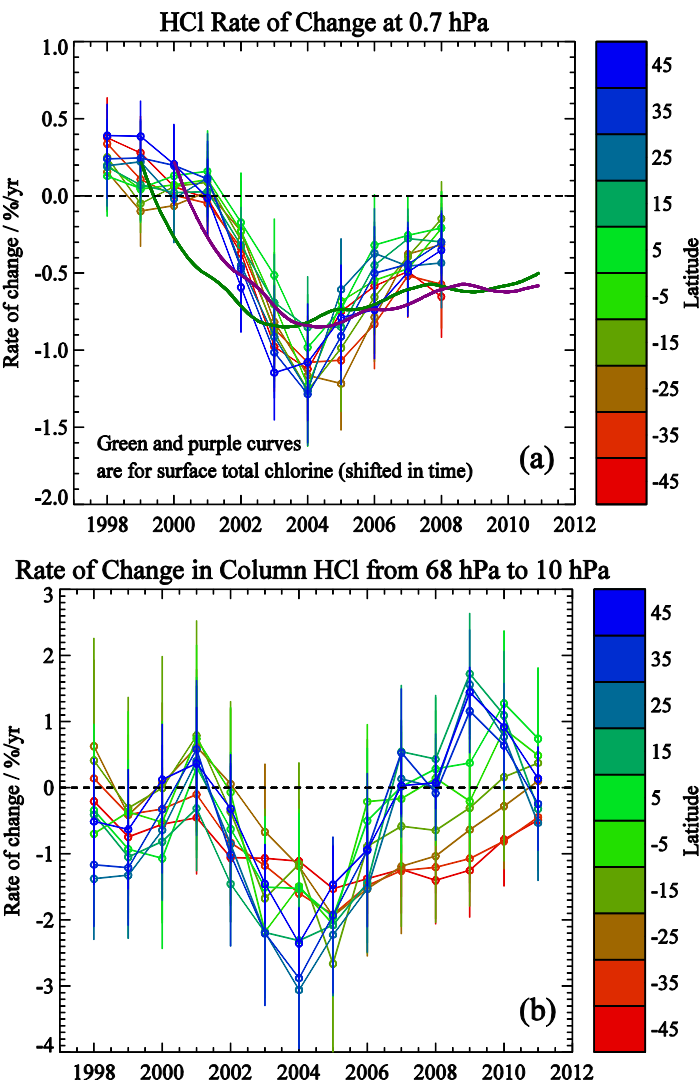
87

88

89

90

Fig. 8. The average rate of change (percent per year) for HCl as a function of pressure for different latitude bin averages (see legend) for time periods corresponding to the appropriate GOZCARDS HCl values (see text) in the upper stratosphere (Jan. 1997 - Sep. 2010) and lower stratosphere (Jan. 1997 - Dec. 2012). Deseasonalized monthly data were used to obtain a long-term trend for these time periods; two-sigma error bars are shown.



92

93

94

95

96

97

98

99

100

101

Fig. 9. Rates of change for GOZCARDS HCl (connected open circles) are given as a function of latitude in 10° latitude bins for sliding 6-year periods centered on Jan. 1 of each year (e.g., the 1998 point is an average for data from 1995 through 2000, and the 2011 point is for data from 2008 through 2013). (a) is for changes in upper stratospheric HCl at 0.7 hPa and (b) is for the change in the integrated HCl column between 68 hPa and 10 hPa. The two additional curves in (a) represent the rates of change in the estimated surface total chlorine from NOAA data (green is for a 6-year time shift, and purple for a 7-year time shift, to account for transport time to the upper stratosphere); see text for more details. Error bars indicate twice the standard errors in the means.

102

103

104

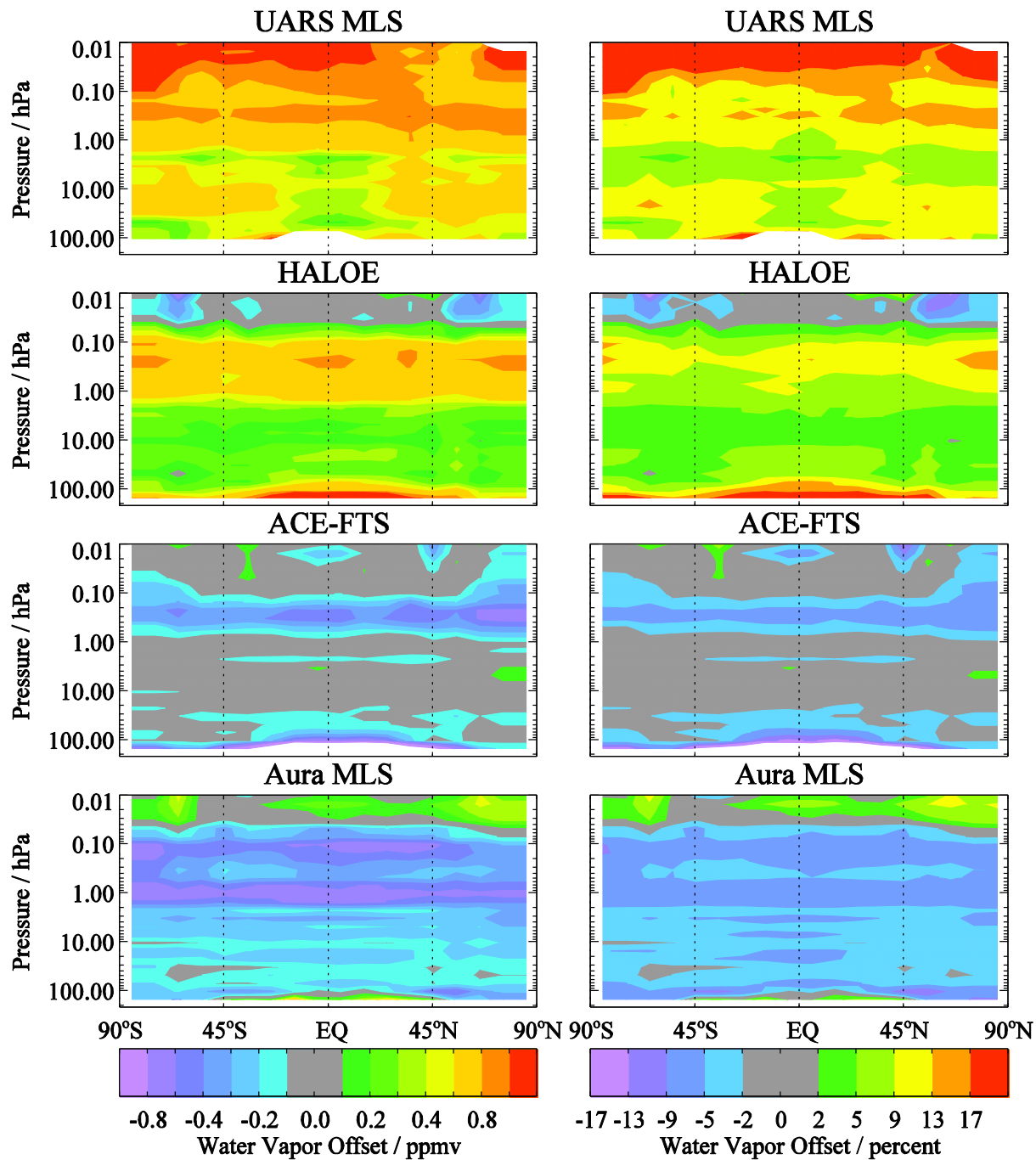
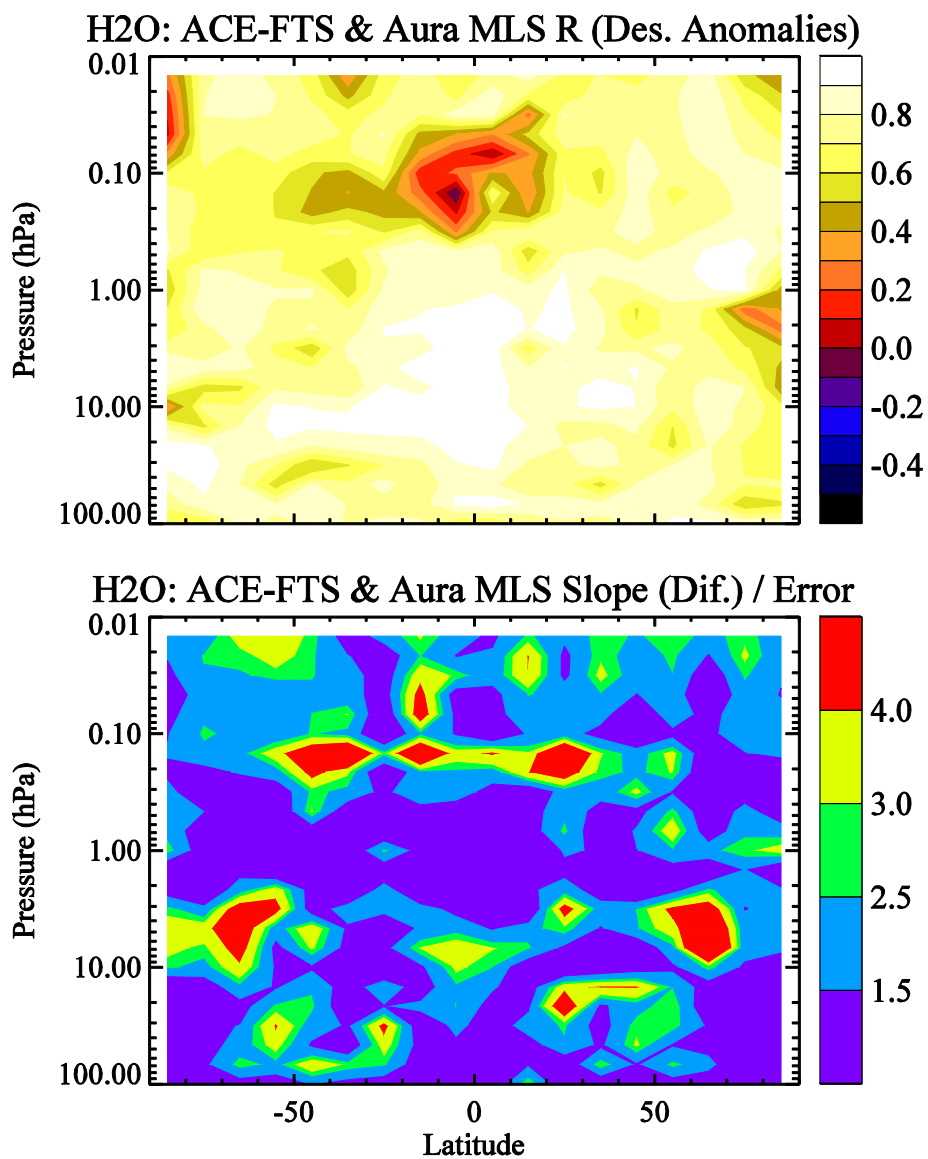


Fig. 10. Offsets applied to the H₂O source datasets as a function of latitude and pressure, similar to Fig. 2 for HCl.

111
112
113



114
115 **Fig. 11.** Latitude/pressure contours of time series diagnostics for H₂O from Aura MLS and ACE-FTS;
116 this is similar to Fig. 4 for HCl.

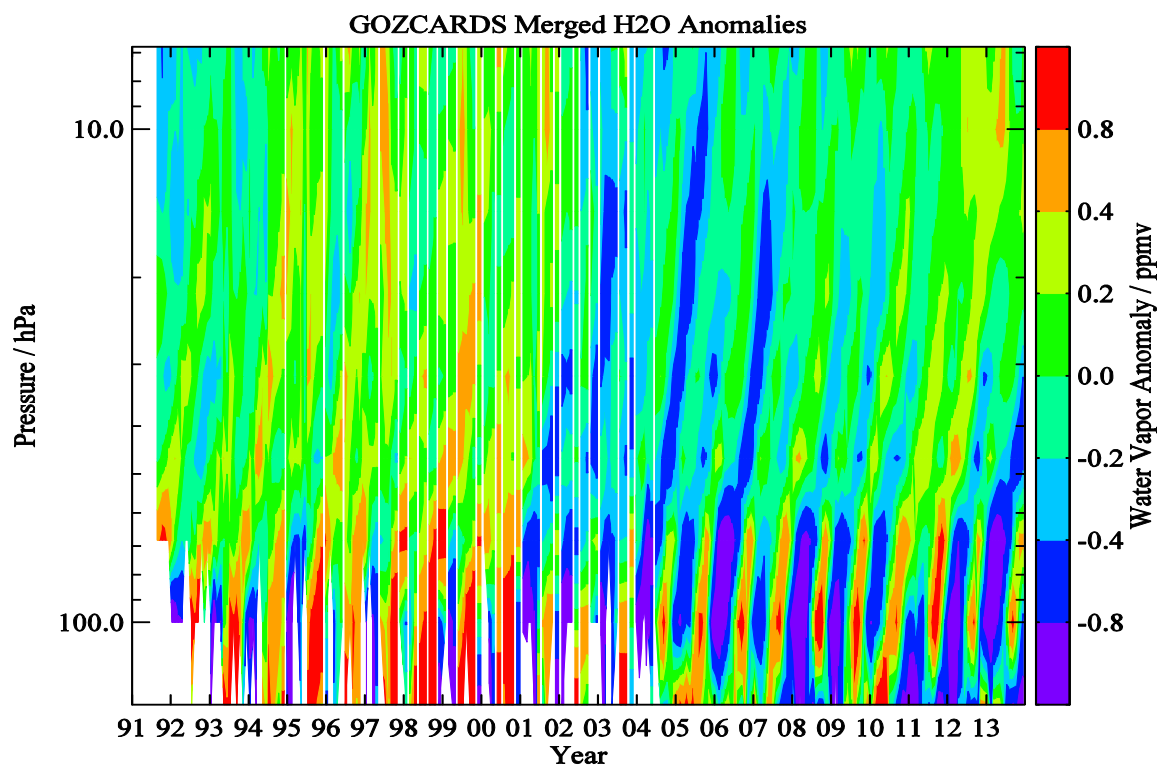


Fig. 12. A depiction of the “tape recorder” evolution for tropical water vapor abundances from 147 to 10 hPa for October 1991 through December 2013. This plot was produced from GOZCARDS merged H₂O time series anomalies (differences from the long-term means) for the average of the 4 tropical bins covering 20°S to 20°N.

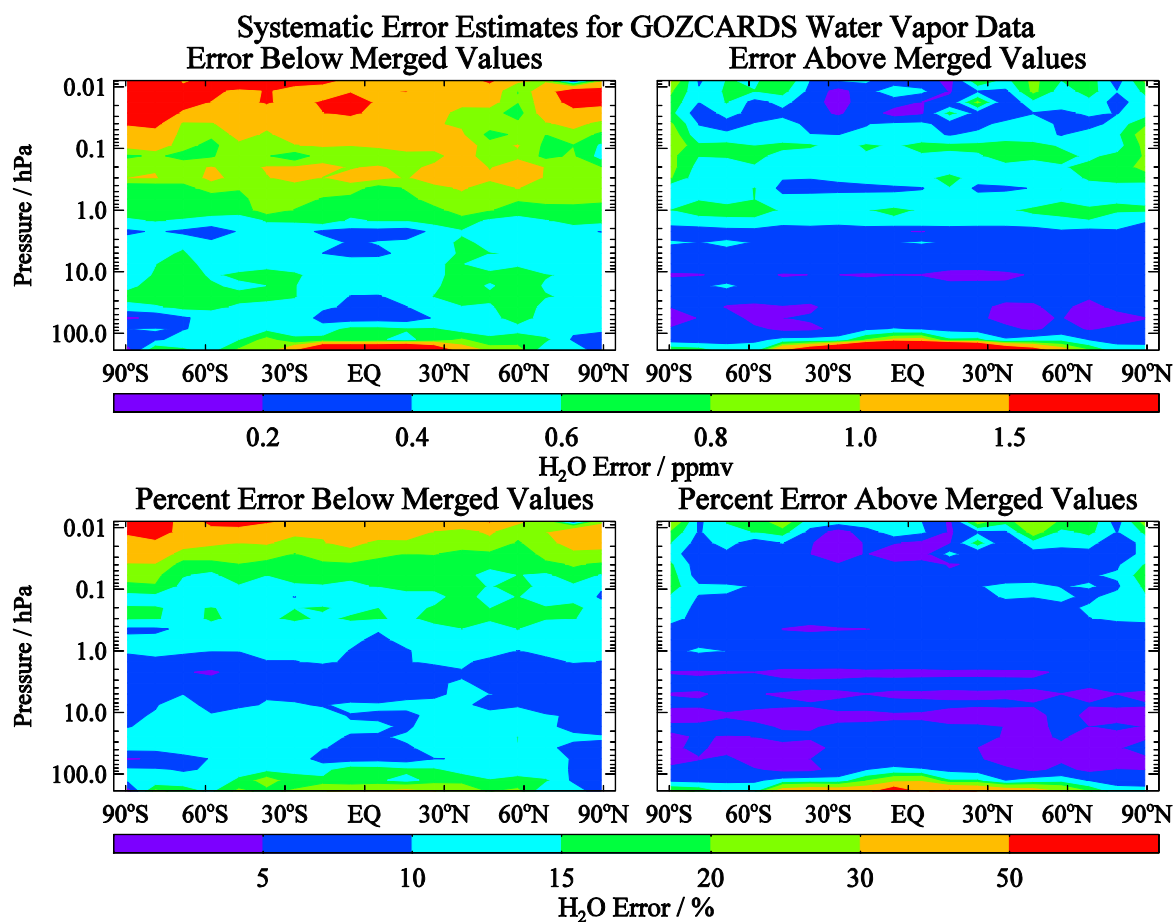
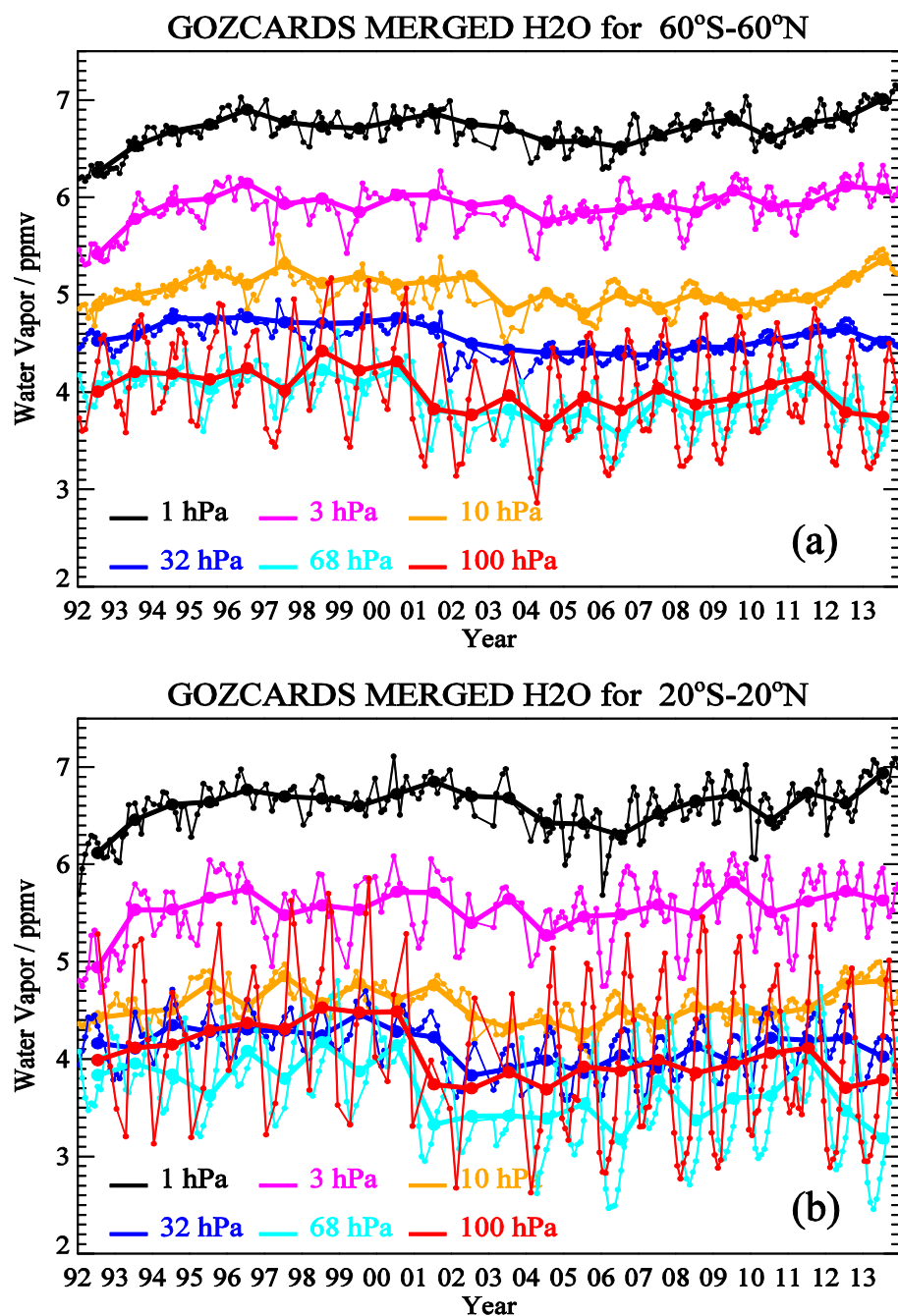


Fig. 13. Systematic error estimates for GOZCARDS H₂O (similar to Fig. 6 for HCl).



133

134 **Fig. 14.** Variations in stratospheric water vapor from the GOZCARDS H₂O merged data records (1992
 135 through 2013) averaged from (a) 60°S to 60°N and (b) 20°S to 20°N. Monthly average values and annual
 136 averages are shown by thin and thick lines (connecting similarly-colored dots), respectively, for the
 137 pressure levels indicated in the plot legend.

138

139

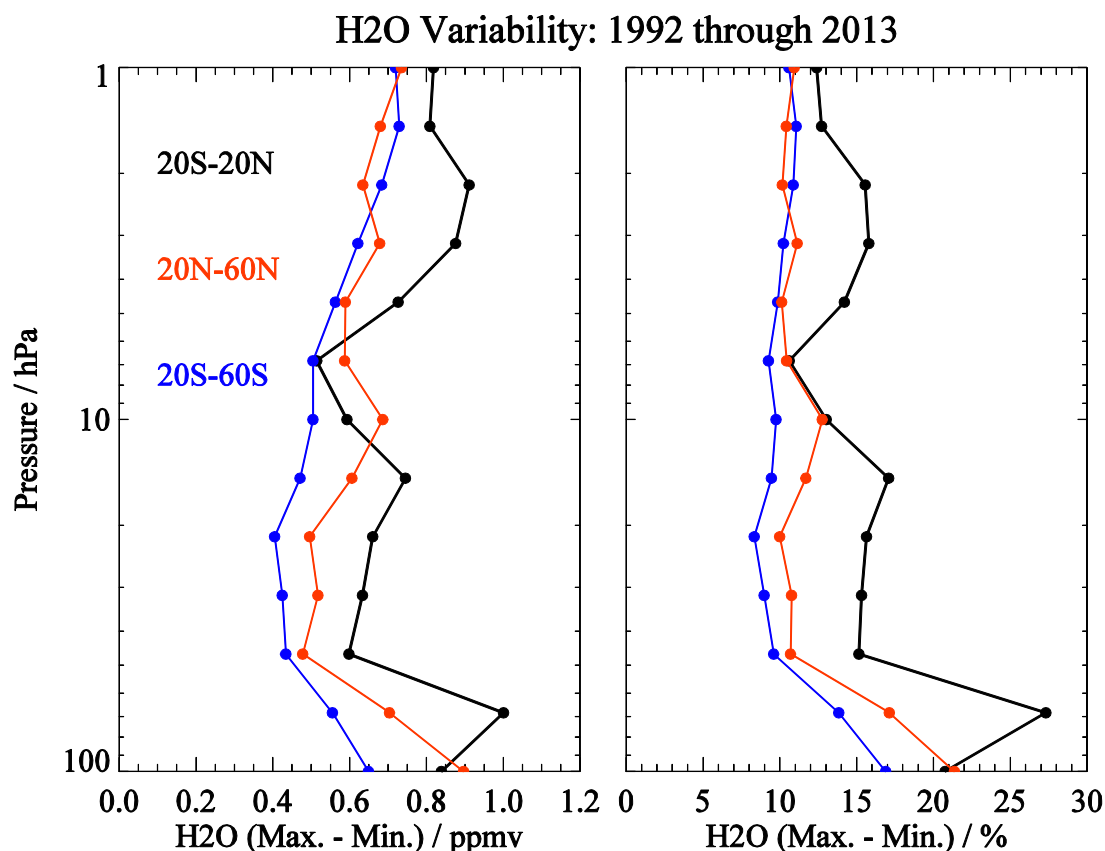


Fig. 15. Stratospheric water vapor variability on decadal timescales for 1992 through 2013 for tropical (20°S-20°N in black) and mid-latitude (20°N-60°N in red and 20°S-60°S in blue) zonal means, based on the GOZCARDS merged H₂O data record. The variability is expressed here as the difference between maximum and minimum annual average abundances, from 100 to 1 hPa, in ppmv (left panel) and percent (right panel).

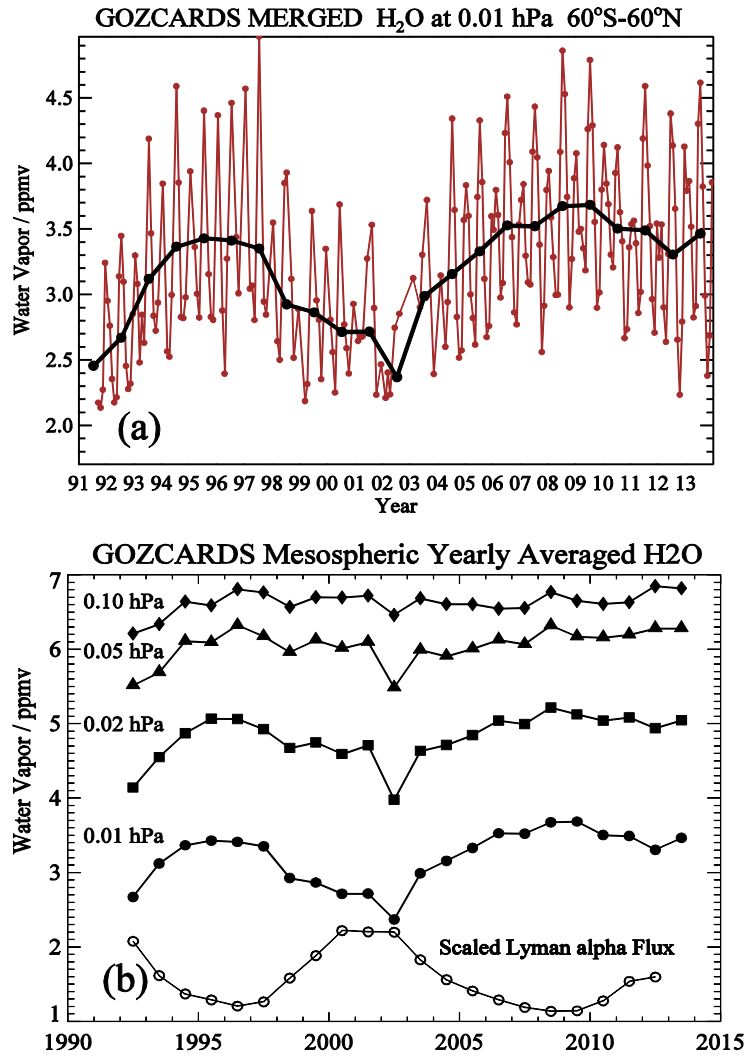


Fig. 16. (a) Variations in upper mesospheric (0.01 hPa) water vapor mixing ratios averaged from 60°S to 60°N for Oct. 1991 through Dec. 2013, based on the GOZCARDS merged H₂O data records. Monthly average values and annual averages are shown by connected brown dots and connected black dots, respectively. (b) GOZCARDS merged H₂O annual averages (connected filled symbols) from 60°S to 60°N for 1992 through 2013 at pressure levels between 0.1 and 0.01 hPa. A time series of annually-averaged Lyman α solar flux values (open circles), scaled to arbitrary units, is also displayed (see text).

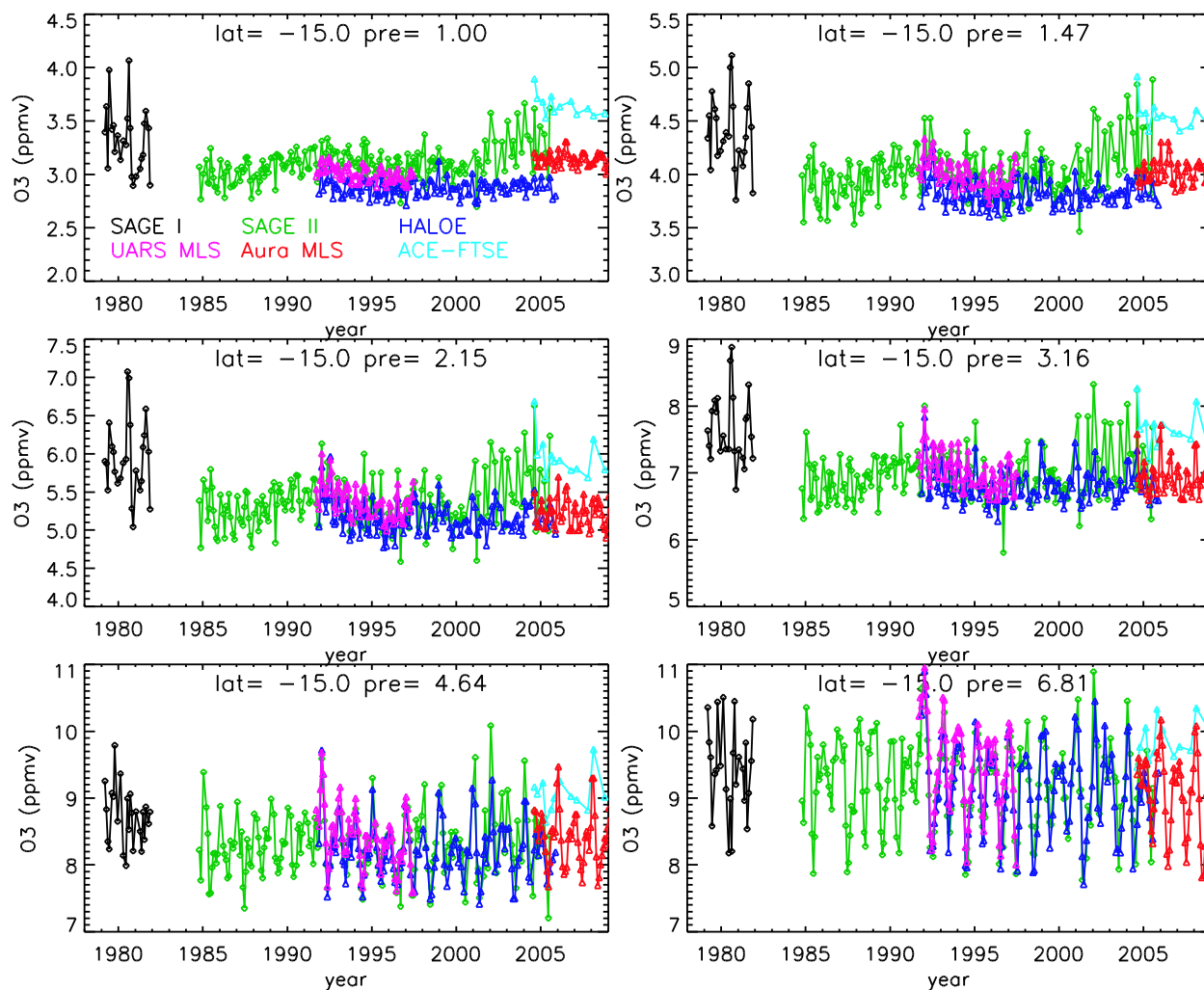


Fig. 17. Time series of monthly zonal mean O_3 for $10^{\circ}S - 20^{\circ}S$ between 1 hPa and 6.8 hPa (with pressure values given by "pre") from SAGE I, SAGE II, HALOE, UARS MLS, Aura MLS, and ACE-FTS, all color-coded following the legend in top left panel.

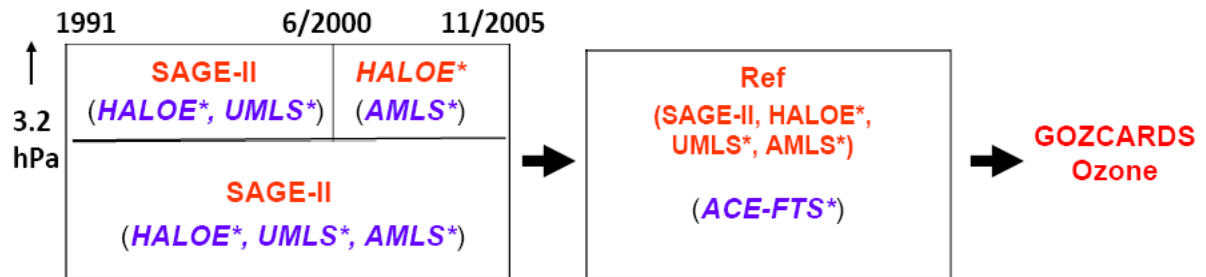


Fig. 18. Schematic diagram describing the creation of the merged GOZCARDS monthly zonal mean ozone data record from various satellite datasets. Instruments represented in red inside the boxes are used as a reference. Instruments whose measurements have already been adjusted to a reference are indicated with a “*” superscript. AMLS refers to Aura MLS and UMLS to UARS MLS. See text for more details.

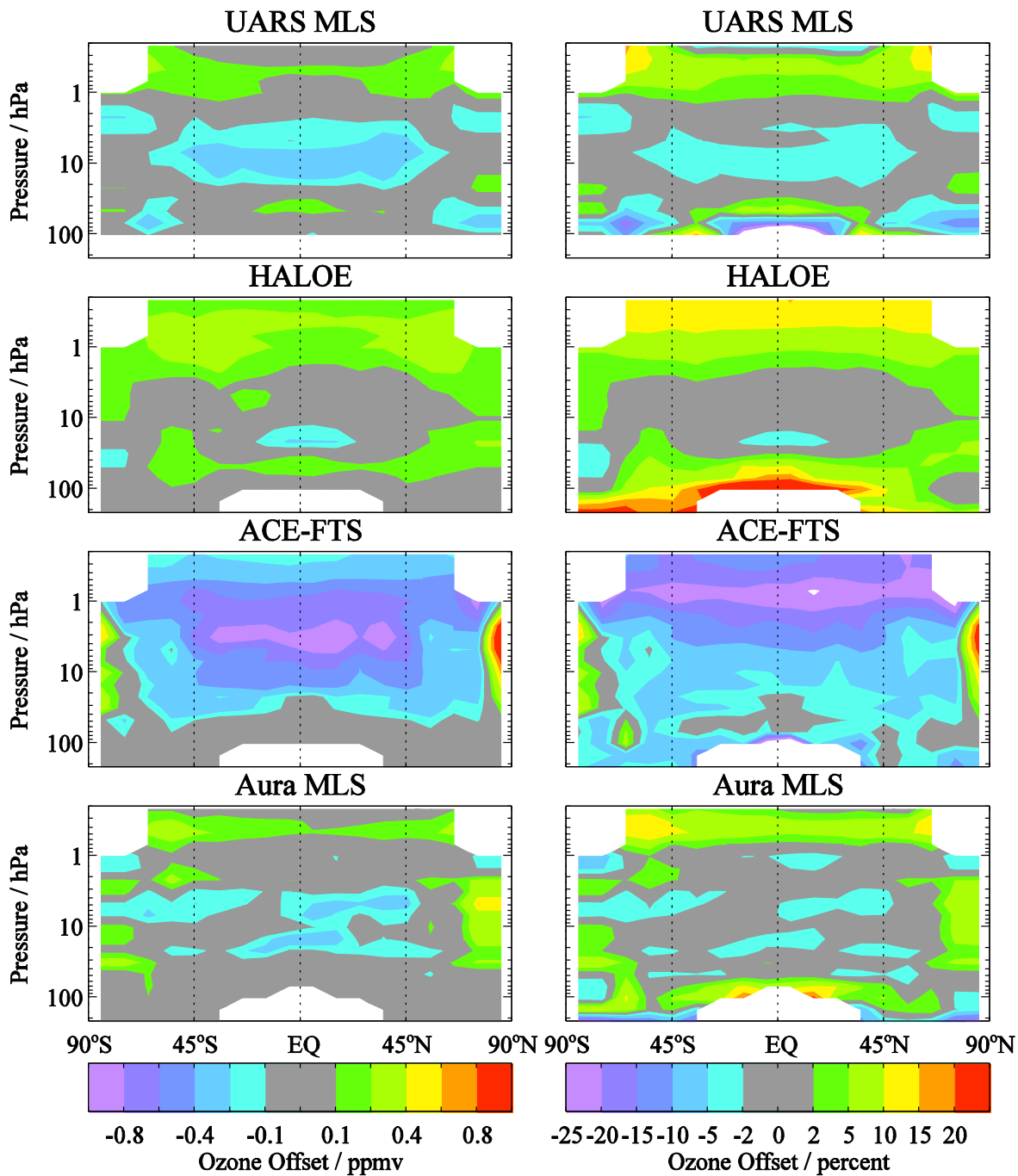
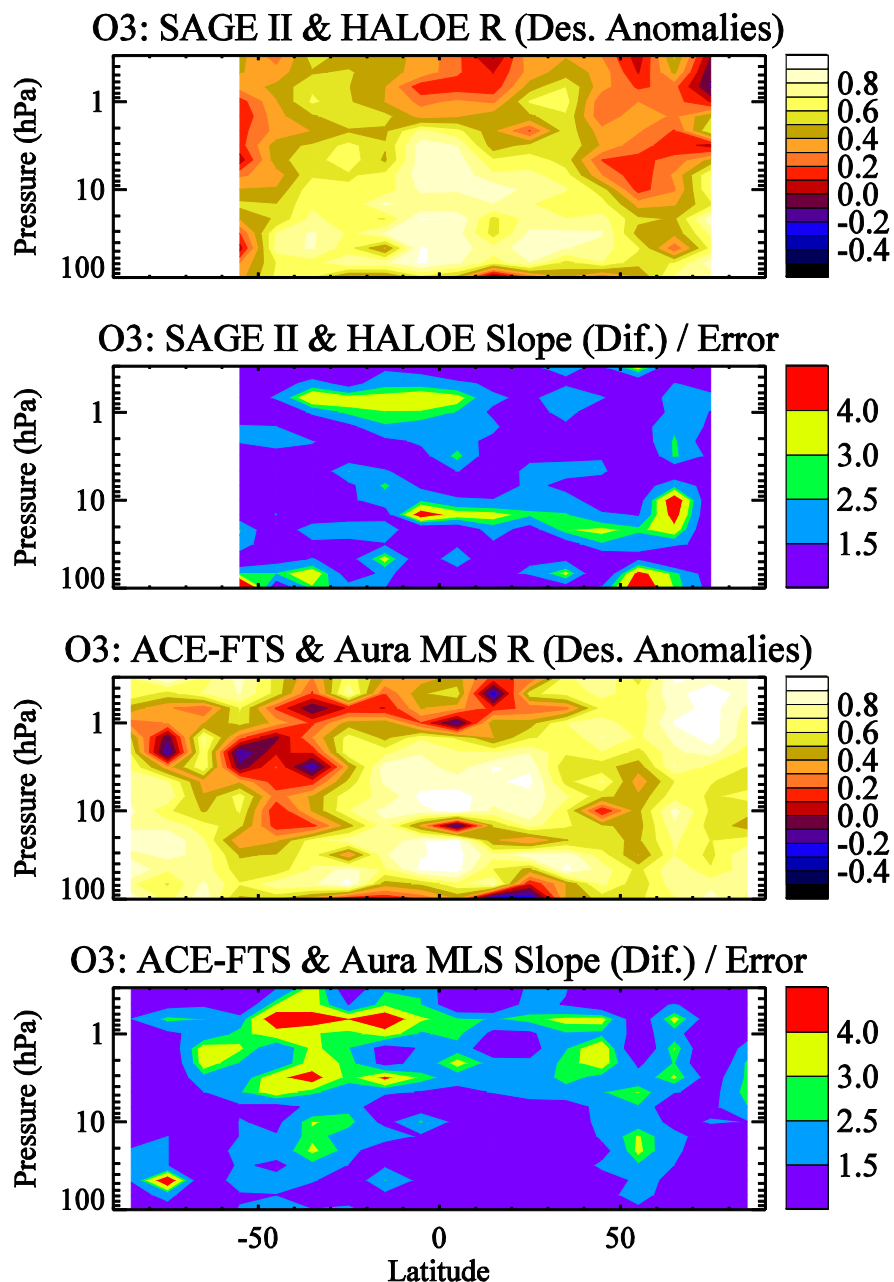


Fig. 19. Offsets applied to the O₃ source datasets, similar to Fig. 2 for HCl.



190

191 **Fig. 20.** Latitude/pressure contours of time series diagnostics for O₃ from Aura MLS and ACE-FTS; this
 192 is similar to Fig. 4 for HCl. The correlation coefficients (R values) and slope trend diagnostics are
 193 provided for HALOE versus SAGE II in the top two panels (for 1993-1999 as the trend issue for
 194 converted SAGE II data occurs after mid-2000 and to avoid Pinatubo-related data gaps before 1993) and
 195 for ACE-FTS versus Aura MLS in the bottom two panels (for 2005-2009).

196

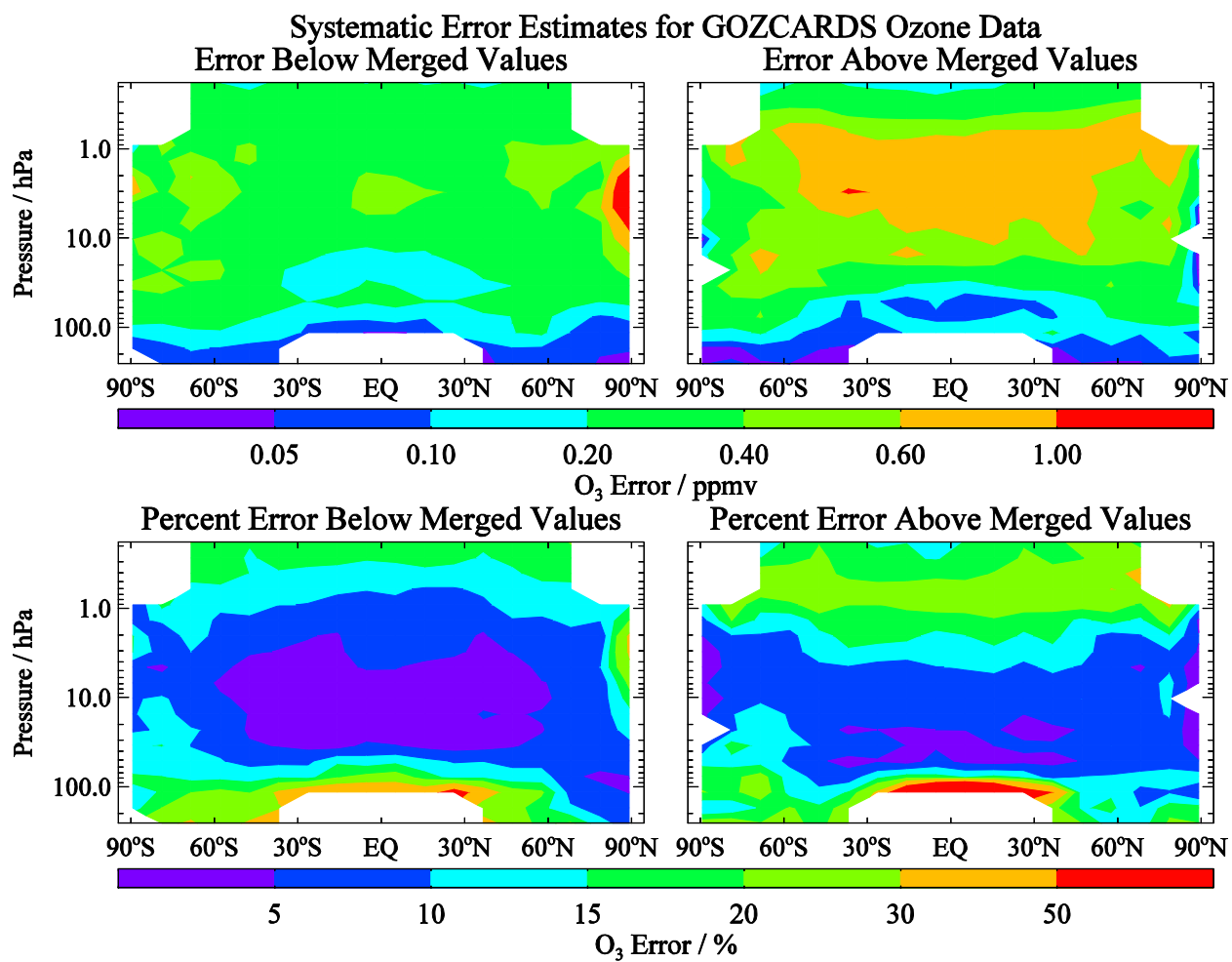


Fig. 21. Systematic error estimates for GOZCARDS O₃ (similar to Fig. 6 for HCl).

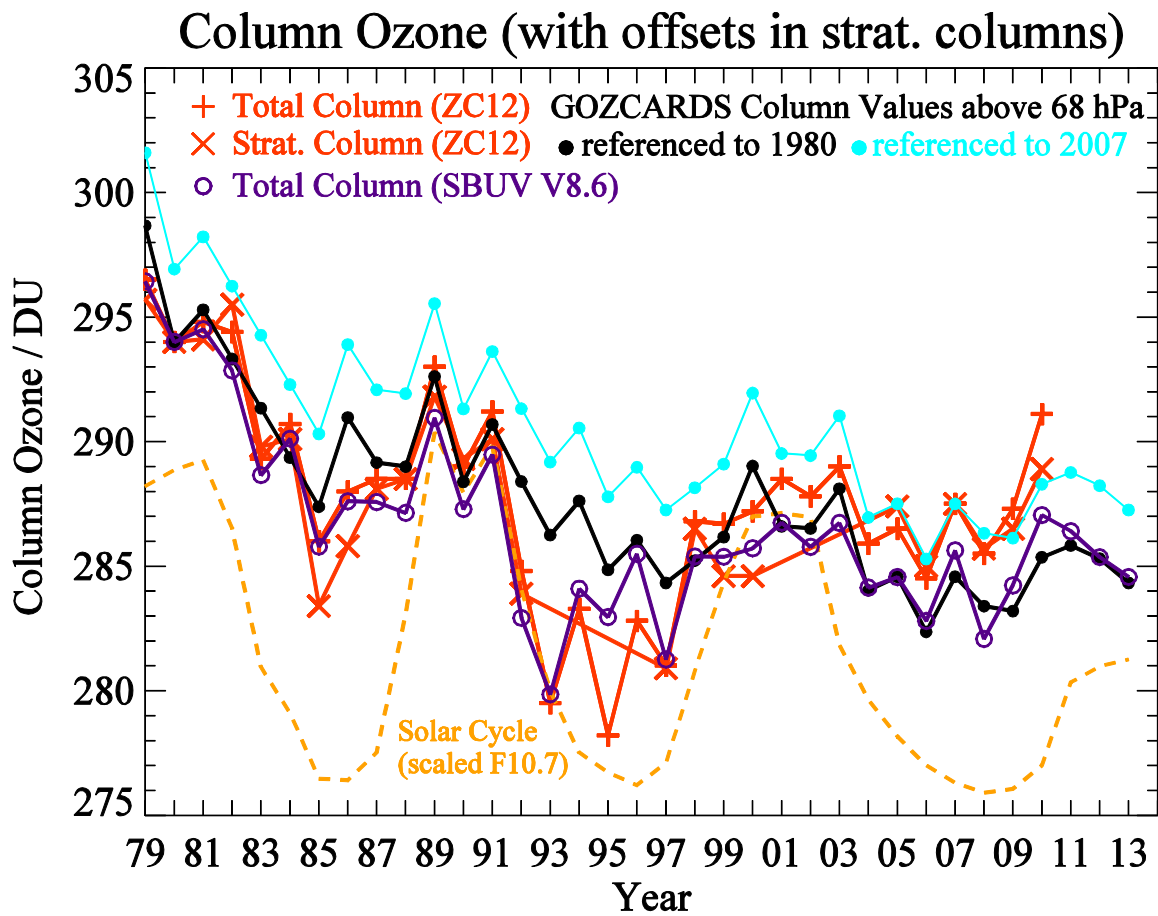


Fig. 22. Near-global (60°S to 60°N) results for average column ozone (total and stratospheric, from Ziemke and Chandra, 2012) compared to GOZCARDS O₃ columns above 68 hPa. Stratospheric columns are offset to better match the total column values, in order to more easily compare relative variations versus time; the black dots and red crosses are referenced to the 1980 total column values, while the cyan curves are referenced to 2007 to better illustrate the fits in the later years. Also shown (as purple open circles) are yearly-averaged total column data (60°S to 60°N) from the SBUV Merged Ozone (V8.6) Dataset (see text); these values were adjusted upward slightly (by 0.8 DU) to match the ZC12 total column values in 1980.

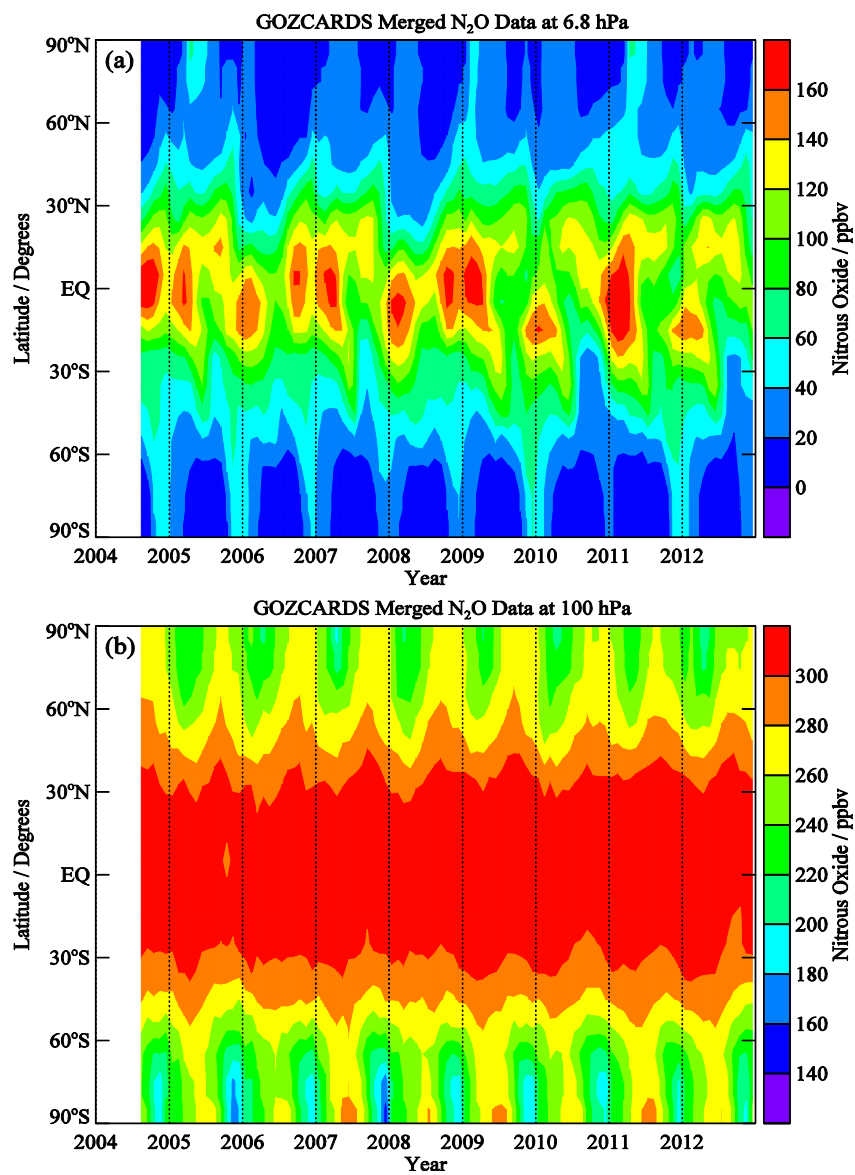


Fig. 23. Time evolution (Aug. 2004 through 2012) versus latitude of GOZCARDS merged N₂O (ppbv) at (a) 6.8 hPa and (b) 100 hPa.

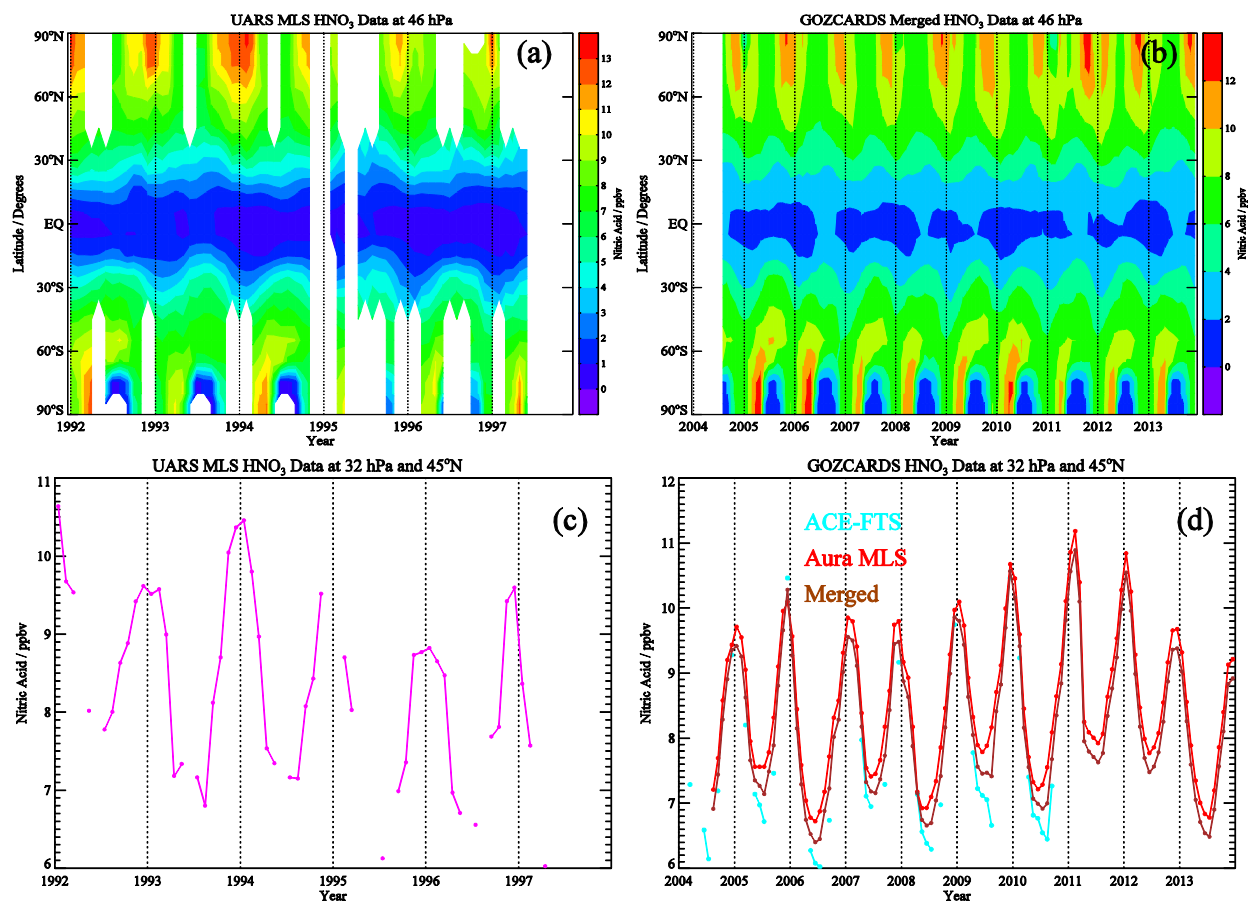


Fig. 24. Sample results display the time evolution of satellite-retrieved HNO₃ (ppbv) for two different periods, 1992-1997 in (a) and (c) versus 2004-2013 in (b) and (d). Panels (a) and (b) are contour plots at 46 hPa from UARS MLS global data and the merged GOZCARDS global data after 2004, respectively; (c) and (d) show time series at 32 hPa and for the 40°N-50°N latitude bin, with (a) from UARS MLS data, and (d) from ACE-FTS, Aura MLS, and the merged combination (between the two source data sets).